

AD610037

RADC-TDR-64-334  
Final Report



DESIGN OF METAL SPACE FRAME RADOMES

COPY <u>2</u> OF <u>3</u> <i>Ymc</i>	
HARD COPY	\$ .4.00
MICROFICHE	\$ .1.00

TECHNICAL DOCUMENTARY REPORT NO. RADC-TDR-64-334

November 1964

Development Engineering Branch  
Rome Air Development Center  
Research and Technology Division  
Air Force Systems Command  
Griffiss Air Force Base, New York

Project No. 5579 , Task No. 557901

(Prepared under Contract AF 39(602)-2937 by TRG,  
Incorporated , East Boston, Massachusetts. Authors:  
Alan F. Kay and Donald Paterson.)

D D C

JAN 21 1965

ARCHIVE COPY

When US Government drawings, specifications, or other data are used for any purpose other than a definitely related government procurement operation, the government thereby incurs no responsibility nor any obligation whatsoever; and the fact that the government may have formulated, furnished, or in any way supplied the said drawings, specifications, or other data is not to be regarded by implication or otherwise, as in any manner licensing the holder or any other person or corporation, or conveying any rights or permission to manufacture, use, or sell any patented invention that may in any way be related thereto.

Qualified requesters may obtain copies from Defense Documentation Center.

Defense Documentation Center release to Office of Technical Services is authorized.

Do not return this copy. Retain or destroy.

## UNCLASSIFIED

RADC-TDR-64-334

November 1964

## ERRATA - JANUARY 1965

The following errors have been noted in the derivations of the formulas appearing in Part II of RADC-TDR-64-334, "Design of Metal Space Frame Radomes," dated November 1964. Since they occur in the derivations their influence is reflected throughout Part II and their correction will require substantial rewriting. The revision will hopefully be available by May 1965.

Page 75, Equation (3). This equation,  $4\pi R^2 t_s = 1/2wd \sum_1^N L_i$  should

read  $4\pi R^2 k t_s = 1/2wd \sum_1^N L_i$  to account for truncation of the sphere.

Page 75, Equation (5). This equation  $t_s = \sqrt{\mu} d$  should read

$$t_s = \sqrt{1-\mu^2} d.$$

Page 82, Equation (31). The term  $\rho$  should be twice the density of the actual material used in the radome members since  $t_s$  is representative of half the actual volume of material in the members.

Page 86, Equation (41). The  $R^2$  in the denominator of the second term of this equation should be  $\pi^2$ .

Page 86, Equation (41). This equation is based upon an Euler buckling stress for a fixed ended column. Since you cannot achieve complete fixity at the ends of the radome members this is considered too liberal an assumption. The more conservative approach would be to assume the members as pin ended.

Development Engineering Branch  
Rome Air Development Center  
Research and Technology Division  
Air Force Systems Command  
Griffiss Air Force Base, New York

UNCLASSIFIED

## Evaluation

This contractual effort resulted in the development of two classes of theoretical tools heretofore not available to the radome designer -

1. Simplified formulas, charts and graphs for computing the insertion loss, side lobe perturbation, and boresight shift caused by a metal space frame radome. Whereas these computations formerly required extensive time and computer services, they now may be performed in a timely fashion by ordinary desk computational techniques. This allows us to make analytical checks on radome performance which until this time, have not been possible on a practical working basis.

2. An integrated electromagnetic - structural design procedure for metal space frame radomes. The design is conducted within simultaneous structural and electromagnetic constraints resulting in a prescribed electrical transmission loss coupled with a prescribed level of structural integrity at minimum practical weight. Previous radome design procedure has been an iterative process of structural design v.s. electromagnetic checks until an acceptable design was achieved.

The two techniques described above represent a large step in a long range program to convert ground radome design to a practical engineering procedure which is not dependent upon extensive computer programs and electromagnetic testing.

This information will be made available, through distribution of the final report, to those agencies and firms involved in the design and/or application of rigid ground radomes.

*Robert B. Curtis*  
ROBERT B. CURTIS  
Project Engineer

## ABSTRACT

PART I - Design graphs, formulas and procedures for the design and evaluation of the electrical performance of metal space frame radomes is presented covering specifically transmission loss, boresight error, and side-lobe variation. The relative merits of metal and dielectric elements is analyzed.

PART II - The study consists of developing a straight forward simple procedure for the optimum sizing of solid beam elements for large space frame radomes. Equations were derived expressing the relationship between the element dimensions necessary to satisfy a prescribed electrical transmission loss and the structural integrity of the space frame. These equations, considered as design constraints, were utilized in the selection of the element size which satisfied a defined optimum criterion. Two optimization criteria were adopted: first, the minimization of the transmission loss subject to a constraint of structural integrity and, second, the reduction of the total structural weight of the elements which simultaneously satisfy the transmission loss and structural constraint.

A sample design computation was conducted as an example of the procedure. The second optimization criterion was applied to a 150 foot diameter radome which was required to sustain 150 mph winds. A procedure for implementing the first optimization criterion employing the method of Lagrangian multipliers was presented resulting in four equations to be solved simultaneously.

## PUBLICATION REVIEW

This report has been reviewed and is approved. For further technical information on this project, contact Mr. Robert B. Curtis, EMEA, Ext. 6210

Approved: Robert B. Curtis  
ROBERT B. CURTIS  
Development Engineering Branch

Approved: Joseph Mauskay  
WILLIAM F. BETHKE  
Chief, Engineering Division

FOR THE COMMANDER: Irving J. Gabelman  
IRVING J. GABELMAN  
Chief, Advanced Studies Group

## TABLE OF CONTENTS

	Page No.
<u>PART I</u>	
INTRODUCTION	1
LOSS DUE TO SPACE FRAME ELEMENTS	1
LOSS DUE TO HUBS	17
LOSS DUE TO DIELECTRIC SKINS	35
BORESIGHT ERROR	36
EXPECTED SIDELobe LEVELS DUE TO THE SPACE FRAME	55
COMPARISON OF DIELECTRIC AND METAL STIFFENING RIBS	64
<u>PART II</u>	
SUMMARY	69
ELECTRICAL CONSTRAINT ON THE ELEMENT	71
STRUCTURAL ANALYSIS OF SPACE FRAME	72
A. External Loads	72
B. Structural Analysis	73
OPTIMUM DESIGN CRITERION	90
SAMPLE RADOME DESIGN	100
MECHANICAL DESIGN OBJECTIVES	112
REFERENCES	115-116
APPENDIX	117

## PART I

### SYMBOLS

(also used in Appendix)

1.  $G$  - relative power loss due to space frame radome
2.  $\rho$  - blocking area ratio of space frame radome, i. e. ratio of projected area of space frame to area of reflector
3.  $g$  - the induced field ratio of a scatterer, i. e., the field strength in the projected blocking area of the scatterer which would produce the actual scattered far field produced by the scatterer, divided by the incident field strength
4.  $W$  - width of scattering element
5.  $d$  - depth of scattering element
6.  $L$  - average length of scattering element
7.  $g_l, g_t$  - values of  $g$  when the polarization of the incident field is respectively longitudinal and transverse to the length of the element
8.  $\lambda$  - free space wavelength
9.  $f$  - frequency of electromagnetic radiation
10.  $c$  - parameter depending on curvature of radome
11.  $D$  - hub diameter also, in context, the dish aperture diameter
12.  $\rho_1$  - blocking area ratio of the hubs
13.  $\epsilon, \delta$  - dielectric constant relative to free space value and thickness, respectively, of skins
14.  $r, \eta$  - polar coordinates in the antenna aperture
15.  $\psi(r, \eta)$  - phase error at  $(r, \eta)$
16.  $\theta, \theta'$  - boresight shift in radians due to a phase error
17.  $\theta_{rms}$  - rms boresight shift
18.  $a$  - radius of dish aperture
19.  $f(r)$  - illumination of circularly symmetric aperture
20.  $\Delta g, \Delta W, \Delta L, \Delta d, \Delta \epsilon, \Delta \delta$  - variations in these quantities
21.  $\left\{ \begin{array}{l} \mu \\ n \end{array} \right\} = \left\{ \begin{array}{l} \text{fraction} \\ \text{number} \end{array} \right\}$  of elements, hubs, or windows having a specified tolerance or design variation
22.  $g_{av} = (g_l + g_t)/2$
23.  $c_0, c_1, c_1', c_2, c_3, c_4, c_5, c_6$  - functions of aperture illumination defined in context
24.  $A$  - area of a part of the radome

SYMBOLS (cont'd)

25. R - radius of radome
26.  $\theta, t$  - defined in Figure 38
27.  $\theta_g$  - angle at which grating lobe occurs
28.  $t_0$  - defined in eq(34)
29. P - defined in eq(37)
30.  $A_e, A_o$  - defined in eq(36)
31. subscript m - metal
32. " d - dielectric
33. E - Young's modulus
34. S',  $\alpha, \sigma_m, \sigma_d$  - quantities defined in [3]

## PART II SYMBOLS

1. A - area
2. C - constant
3. D - constant
4. d - element depth
5. E - modulus of elasticity
6. F - total force
7. f - unit force
8. H - constant
9. I - moment of inertia
10. k - surface area coefficient
11. K - Tsien-Von Karman coefficient
12. L - element length
13. M - moment or number of panels
14. N - stress resultant or number of elements
15.  $P_0$  - pressure at wind stagnation point
16. q - distributed transverse load
17. Q - equivalent shell weight density
18. R - radius of radome
19. S - effective spacing of elements
20. t - thickness
21. u - circumferential displacement
22. V - velocity of wind
23. v - meridional displacement
24. W - weight of elements
25. w - element width
26. x - coordinate
27. y - coordinate
28. z - coordinate
29.  $\alpha$  - meridional angle from base
30.  $\mathcal{A}$  - exponent coefficient
31.  $\theta$  - circumferential shell coordinate
32.  $\lambda$  - Lagrangian Multiplier
33.  $\mu$  - Poisson's ratio
34.  $\rho$  - weight density
35.  $\sigma$  - normal stress
36.  $\phi$  - meridional shell coordinate
37. w - normal displacement
38. subscript 1 - boundary condition one
39. " 2 - boundary condition two
40. " R - radome
41. " r - reinforcement
42. " s - shell

SYMBOLS (cont'd)

- 43. subscript e - external
- 44. " i - internal
- 45. " cr - critical
- 46. " yp - yield point
- 47. " b - base of radome
- 48. "  $\phi$  - direction of meridian coordinate
- 49. "  $\theta$  - direction of circumferential coordinate
- 50. "  $\phi\theta$  - direction of  $\phi$  in plane normal to  $\theta$
- 51. " n - direction normal to surface of radome

# DESIGN OF METAL SPACE FRAME RADOMES

## PART I - ELECTRICAL DESIGN

### INTRODUCTION

"Electrical Design of Metal Space Frame Radomes. ' [1] by Alan F. Kay, was prepared and submitted for publication on August 20, 1963. A revised version dated March 23, 1964 has been accepted for publication in the Transactions of the IEEE, Professional Technical Group on Antennas and Propagation. This paper contains the fundamental theory on which most of this present report is based. The present report gives design graphs, formulas, and procedures for specific radomes in the .1 to 10 gc/s. band, as well as considerably more design data than included in [1]. This data pertains to the three most critical electrical properties of the radome: loss, boresight error, and sidelobe increase. A section on the relative merits of metal and dielectric ribs is included.

### LOSS DUE TO SPACE FRAME ELEMENTS

Equation(22) of [1] is the fundamental approximate formula for the loss due to the space frame itself. In the Appendix, p.120, a brief derivation is given of this expression:

$$(1) \quad G = |1 + \rho g|^2$$

where  $G$  is the relative power loss as measured at (or near) the peak of the antenna beam due to the presence of the radome space frame,  $\rho$  is the blocking area ratio of the space frame and  $g$  is the induced field ratio of the space

frame elements. Equation(1) neglects the loss due to hubs and dielectric skin. We give here simple formulas and graphs by which  $G$  may be computed in most cases.

Consider the space frame to be comprised of triangles of elements of average length  $L$  from hub center to hub center and of width  $W$ . Consider any one triangle as extending to the midline of each of the three elements comprising it. If the triangles were exactly equilateral then  $\rho$  would equal

$$2\sqrt{3} \frac{W}{L} = 3.46 \frac{W}{L} .$$

If the triangles were right isosceles then  $\rho = 3.56 \frac{W}{L}$ .  $\rho$  generally increases the further from equilateral the triangles depart or the greater the standard deviation of the element lengths from the average value  $L$ . For a well designed radome geometry the element lengths should all be close to the average  $L$  and the triangles all reasonably close to equilateral. A reasonable approximate value of  $\rho$  has been found to be

$$(2) \quad \rho = 3.5 \frac{W}{L} .$$

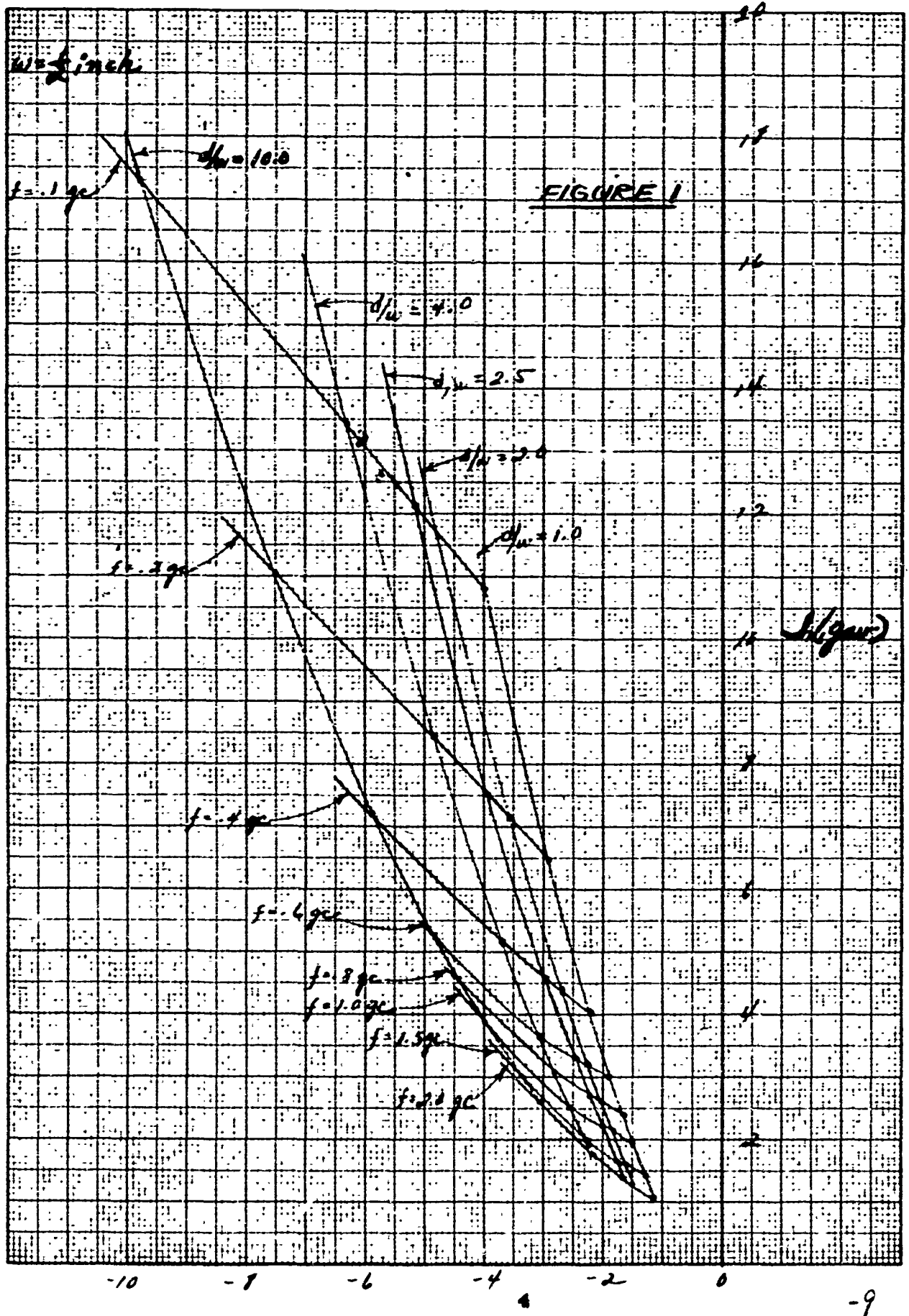
This value is also approximately corrected for a quadrilateral geometry.

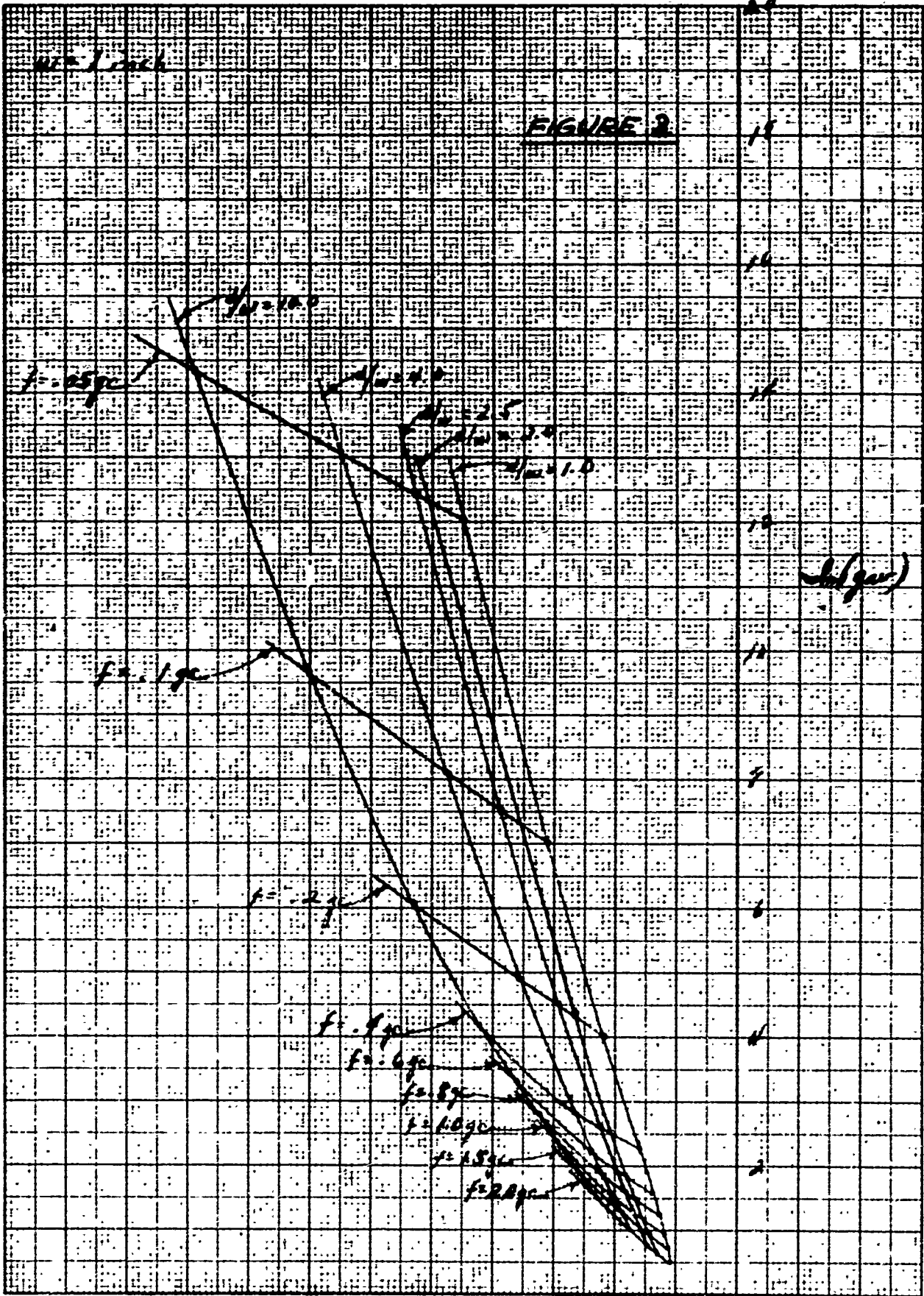
The value of  $g$  depends on the element cross-section, the average incidence angle  $\theta$  of the radiation from the dish to the curved radome, and the polarization. When the projection of the elements into the aperture plane are all parallel to  $E$ , the appropriate value of  $g$  is  $g_0$ . When the projection

of the elements into the aperture plane are all transverse to E, the appropriate value of  $g$  is  $g_t$ .<sup>[1]</sup> In the case of a triangular geometry with  $L \ll D$ , where  $D$  is the dish diameter, the appropriate value of  $g$  is

$$(3) \quad g_{av} = \frac{g_l + g_t}{2} .$$

Values of  $g_{av}$  for various rectangular cross sections,  $W \times d$ , and frequencies are shown in Figures 1 to 3 for  $\theta = 0$ . These values were obtained by the computer program described in [1]. At sufficiently high frequencies  $f$ ,  $R(g_{av})$  approaches -1 and  $Y_v(g_{av})$  approaches zero. However, the manner of approach is such that each of the curves  $d/W = \text{constant}$  spirals an infinite number of times before reaching the terminal point  $(-1, 0)$ . If the graphs were extended into the regime where this spiraling takes place, they would be difficult to read and interpolation either in  $f$  or  $d/W$  would be virtually impossible. It is also in this regime where shaping of the element<sup>[1]</sup> can effectively reduce loss and consideration of purely rectangular elements becomes less significant. Figures 4 to 6 are transparent overlays for three values of  $\rho$  which give  $G$  directly in db, according to equation(1) if any of these are placed over one of the Figures 1-3 with the axes coincident. In any case where values of  $\rho$ ,  $W$ , and  $d$  imply that  $L < \lambda$ , then multiple scattering becomes important<sup>[1]</sup> and equation(1) is inaccurate. These cases occur at low  $f$  when the apparent values of  $G$  obtained from (1) seem to increase above unity (negative db)





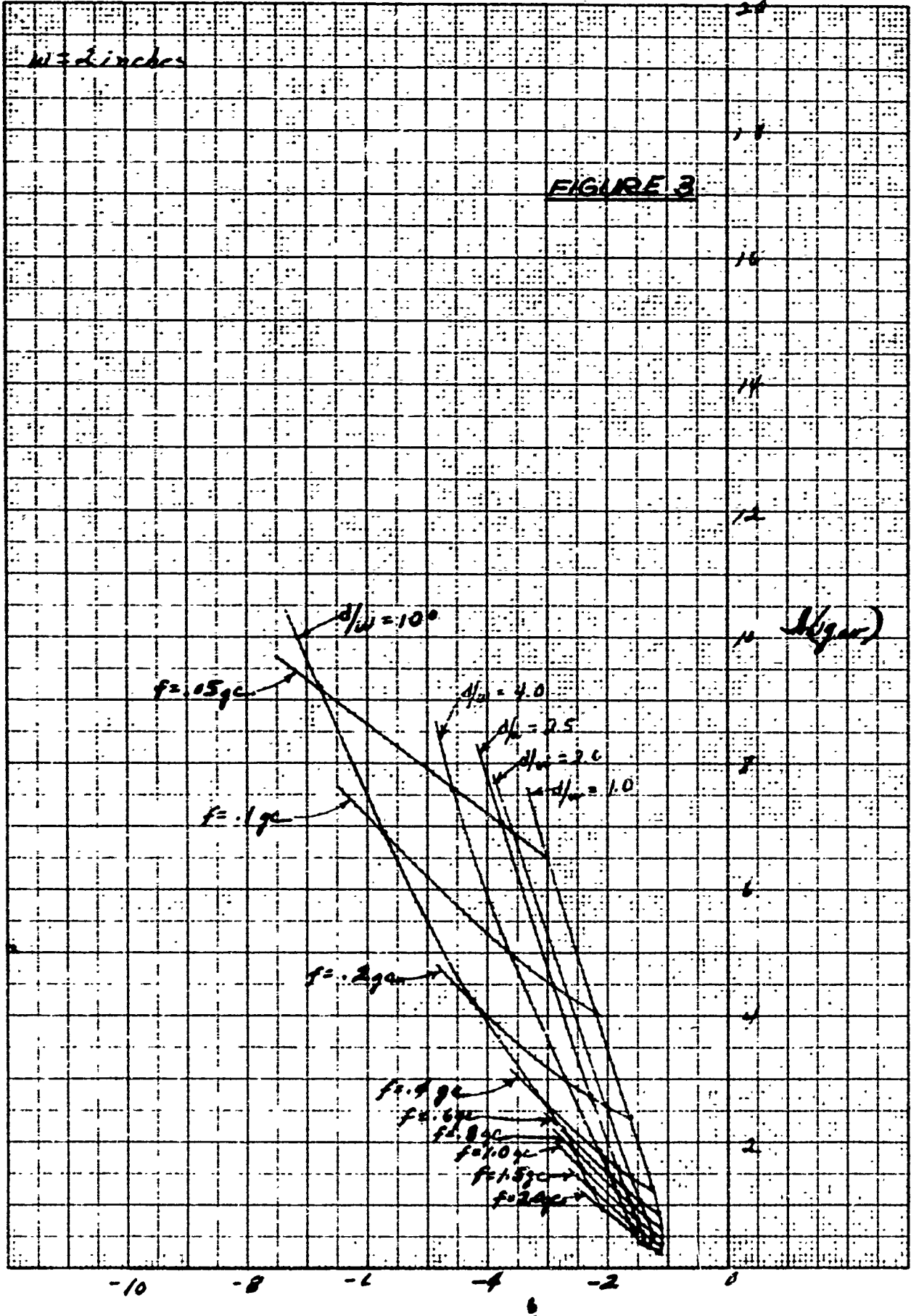
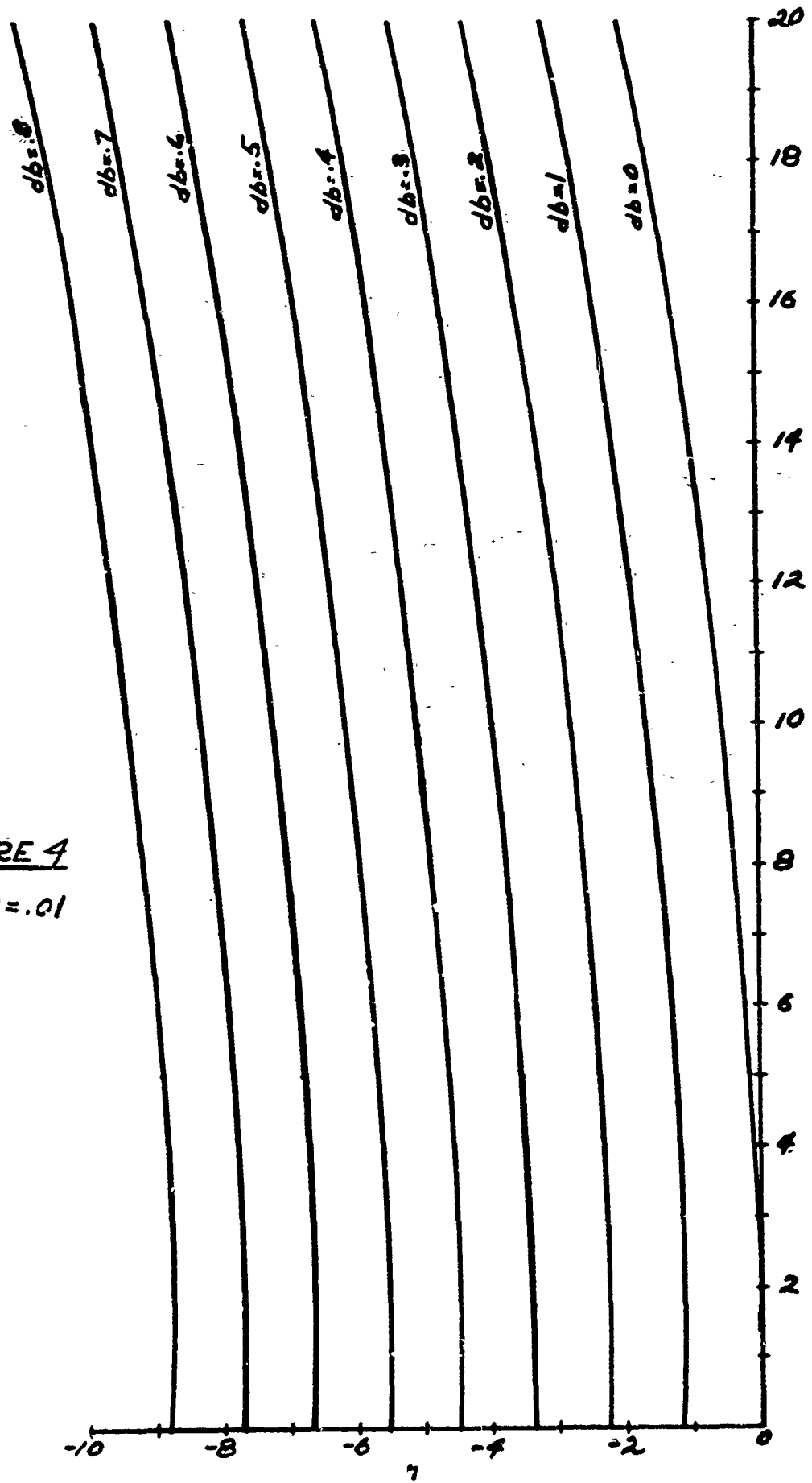


FIGURE 4

$P = .01$



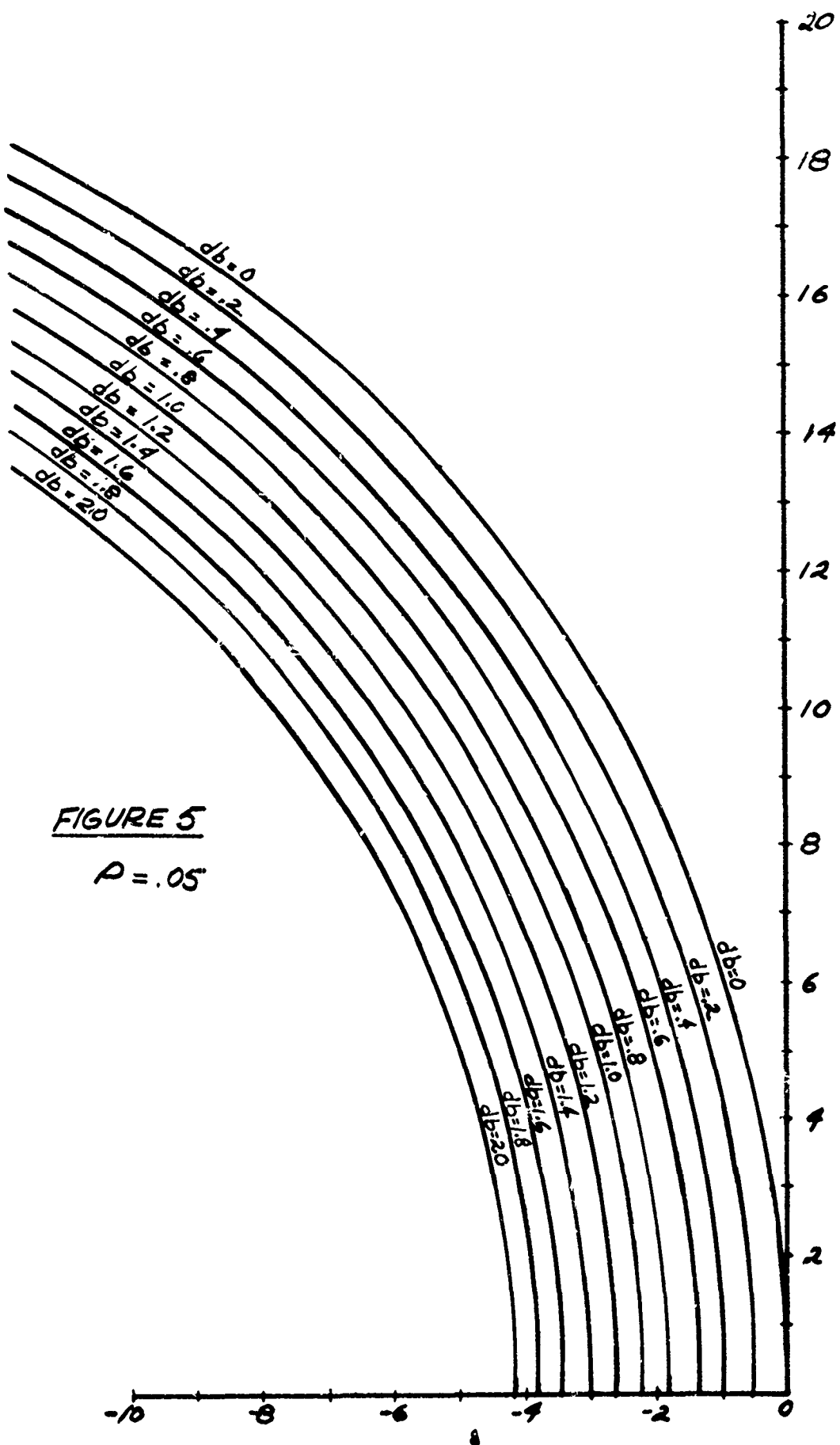


FIGURE 5

$P = .05$

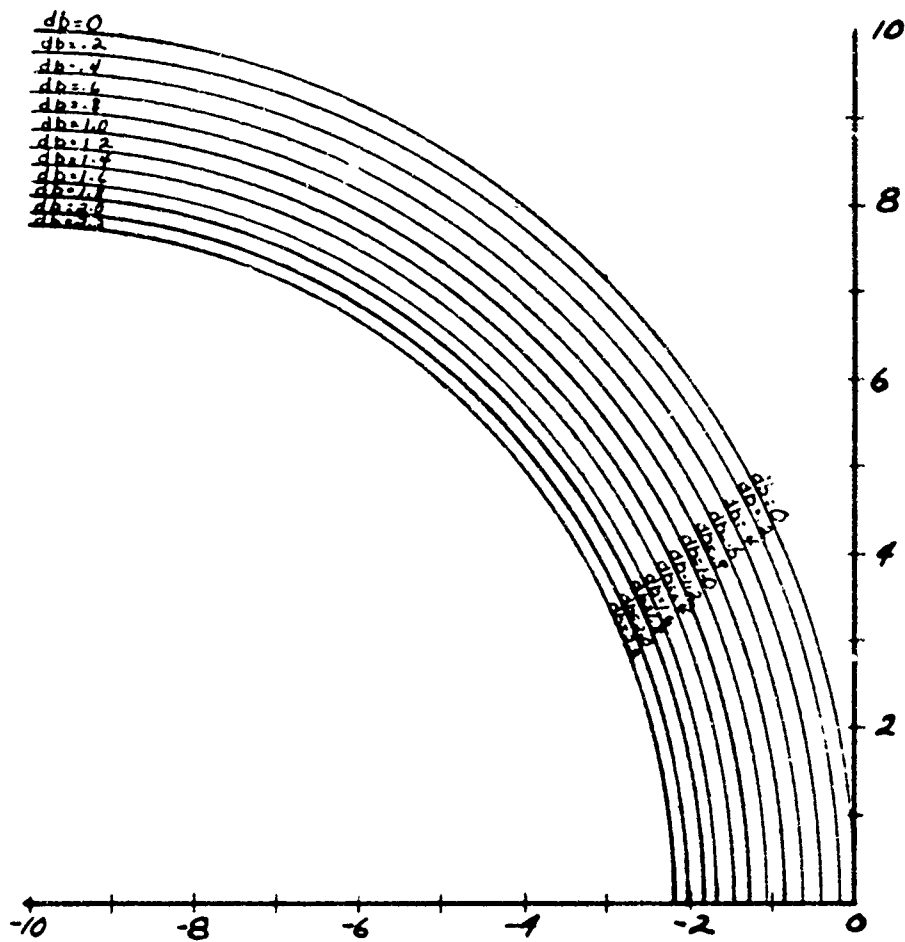


FIGURE 6

$\rho = .1$

with decreasing  $f$ . Figures 7-10 show the loss of a particular radome versus frequency for various average incidence angles  $\theta$ .  $\theta = 0$  corresponds to a flat radome. Typically  $\theta$  is 10 to 20° for spherical radomes. Each figure is for different element widths and depths as indicated. A similar plot was shown in Figure 10 of [1] for still a different element including comparison with measured values. Figure 11 is a photograph of measurements of insertion loss of a partial radome. Figure 12 shows measured and theoretical loss of two such radomes, which were designed for optimum electrical and structural performance as described in Part II, p. 100.

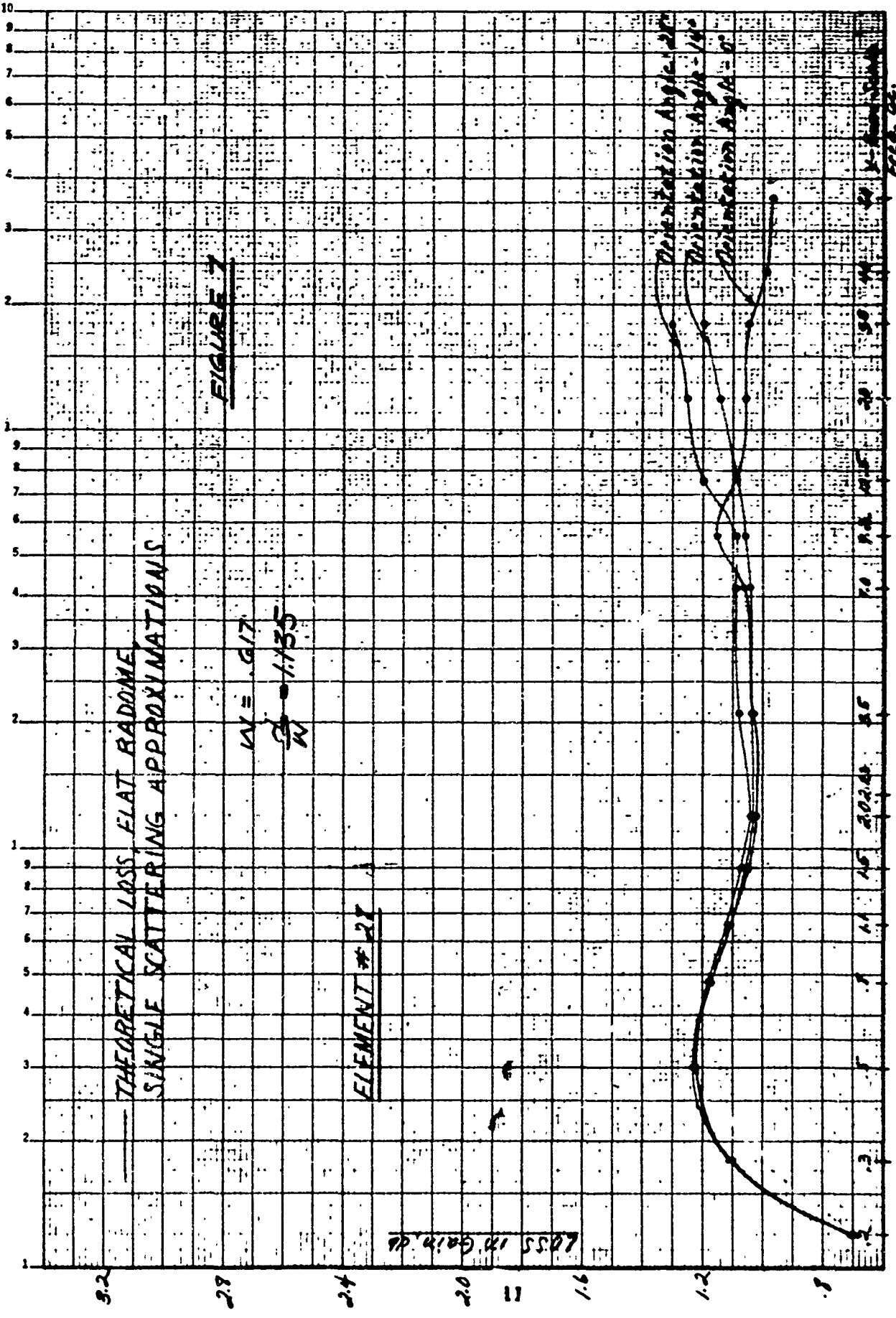
An empirical formula for  $G$  has been obtained by observation of the general behavior in Figures 1 to 3 and other similar data, as follows:

$$(4) \quad 10 \log_{10} G = \frac{1}{L} \left\{ 39.5W + 3.5d + .147 \frac{d\lambda}{W} + \frac{cW(d-W)}{\lambda} \right\}$$

where  $c$  is a parameter depending only on the curvature of the radome over the projected area of the antenna, or approximately on the average incidence angle  $\theta$ . If  $\theta = 12^\circ$ ,  $c = 4.46$ . If  $\theta = 25^\circ$ ,  $c = 11.8$ . Equation(4) is reasonably valid provided

$$W < 2\lambda, \quad W \leq d \leq 10W, \quad |10 \log_{10} G| < 3 \text{ db.}$$

This validity is shown in Figures 13-29 where equation(4) is compared



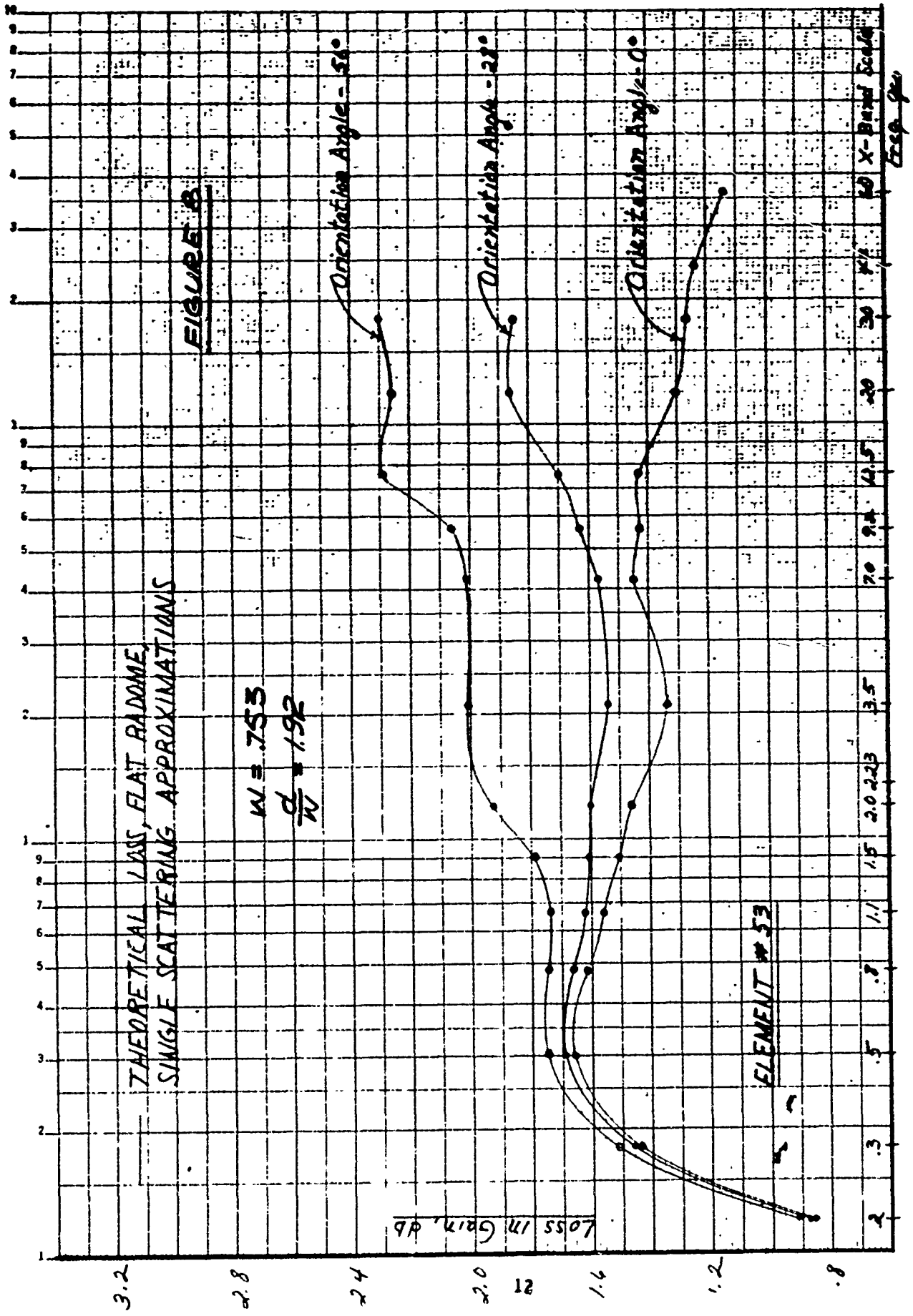
THEORETICAL LOSS, FLAT RADOME,  
SINGLE SCATTERING APPROXIMATIONS

$$W = 7.53$$

$$\frac{d}{N} = 1.92$$

ELEMENT # 53

FIGURE B



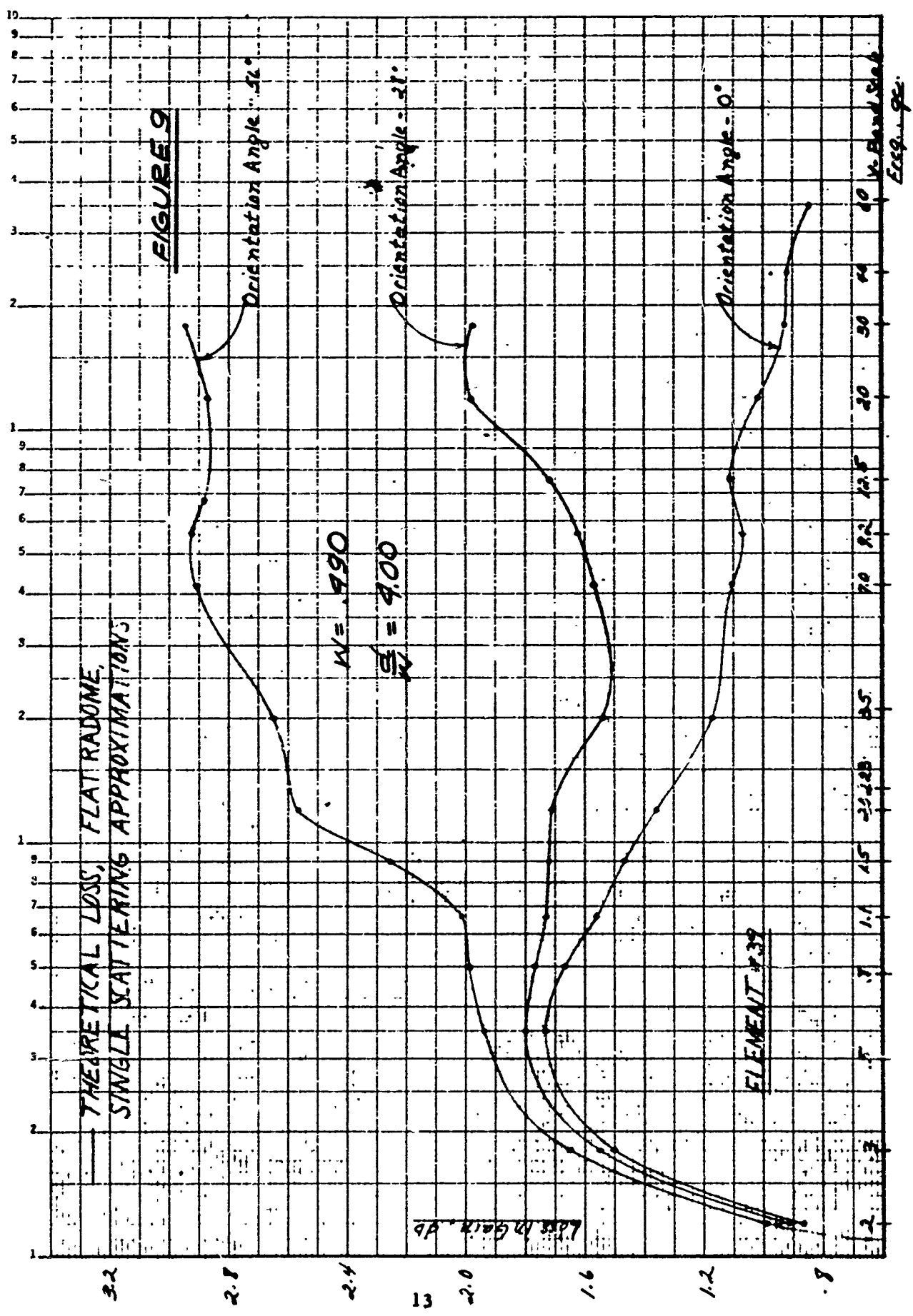
Orientation Angle - 56°

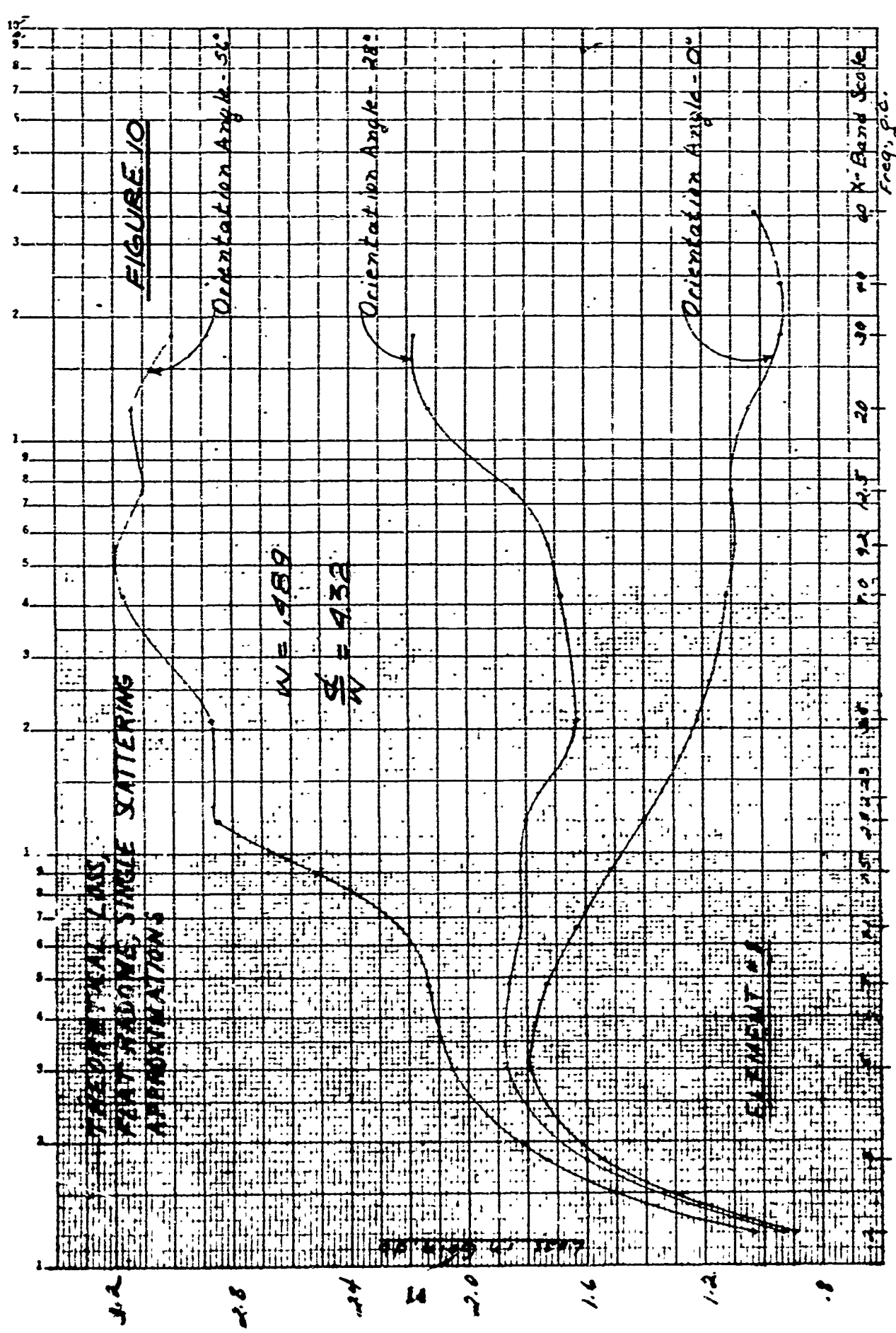
Orientation Angle - 28°

Orientation Angle - 0°

Loss in Gain, dB

X-Beam Scale  
ESP. 9/20





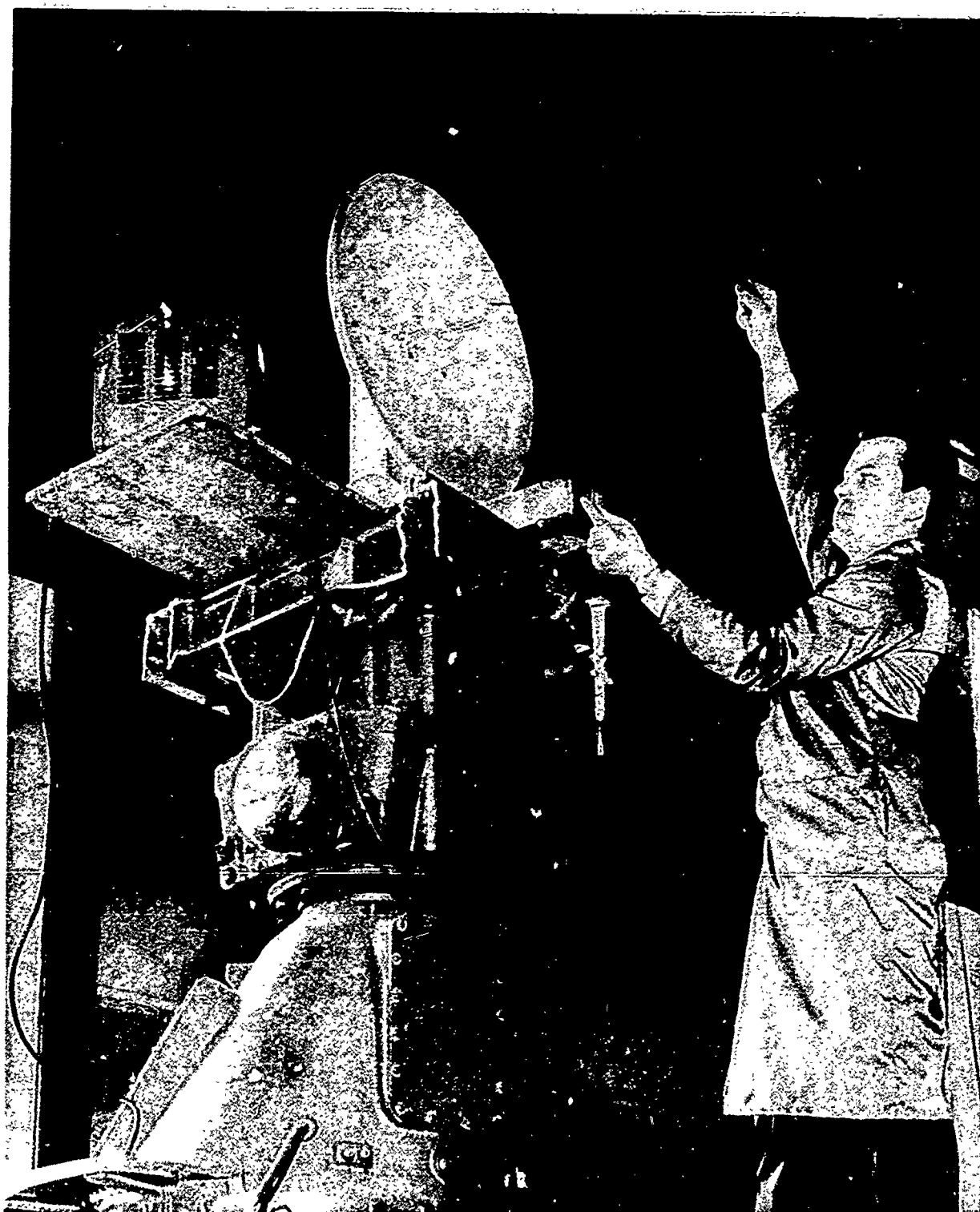


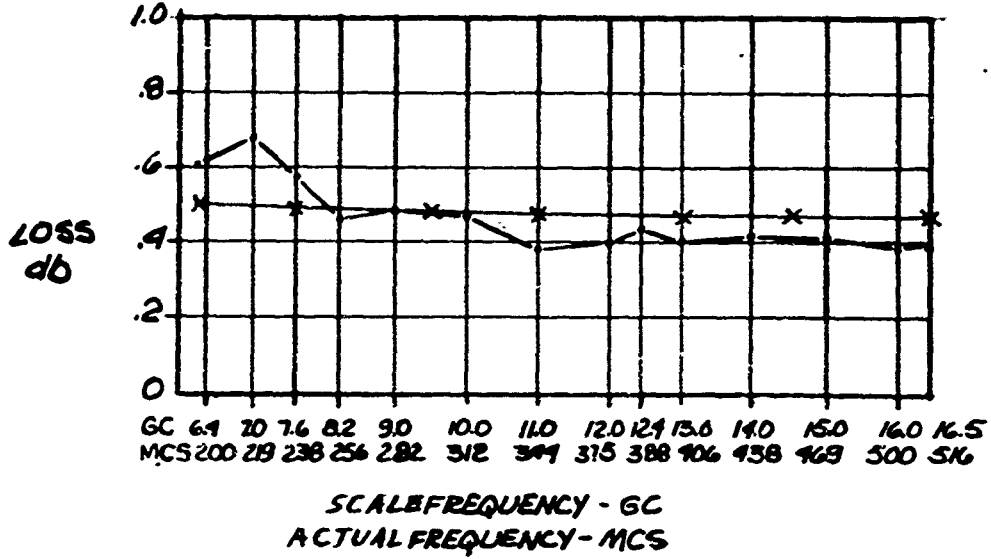
FIGURE 11

SPACE FRAME INSERTION LOSS

SCALE	FULL SCALE
W = .062	1.49"
d = .066	1.59"
L = 6"	144"

**FIGURE 12**

SCALE = 82:1

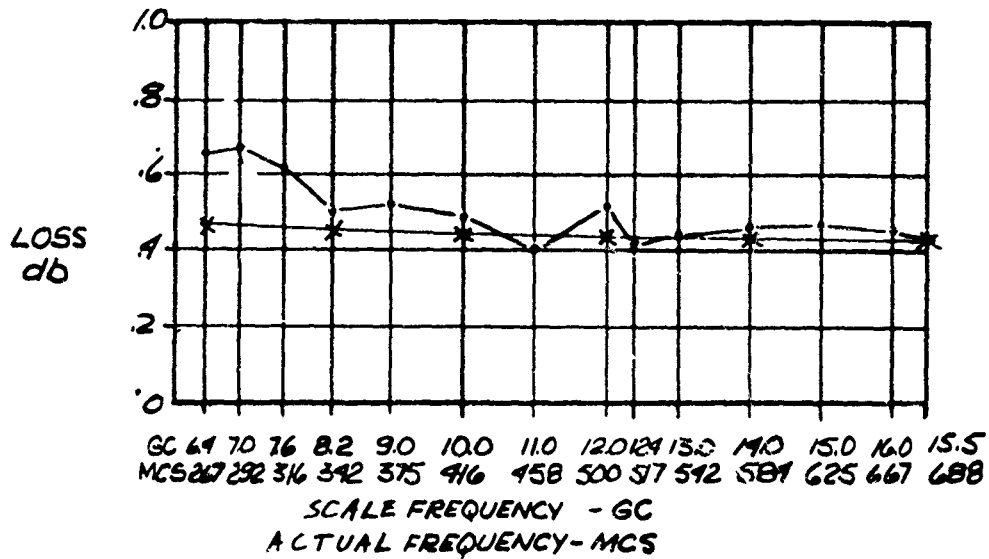


— EXPERIMENTAL  
 x-x-x THEORETICAL EQ. NO. 4

SPACE FRAME INSERTION LOSS

SCALE	FULL SCALE
W = .062"	1.49
d = .161"	3.87
L = 8"	192"

SCALE = 29:1



— SCALE FREQUENCY - GC  
 — ACTUAL FREQUENCY - MCS

with equation(1). From eq(4) we observe that depth  $d$  appearing in the second term, is about one-tenth the importance in producing loss of the width  $w$  appearing in the first term. The third term expresses the frequency dependence and shows that the loss of a given radome tends to increase with increasing  $\lambda$  at a rate proportional to  $d/w$ . The last term expresses the effect of curvature of the radome. The latter effect becomes negligible as the element becomes square ( $d \rightarrow w$ ) or at sufficiently low frequencies or low average incidence angles. In any case the first term usually dominates this expression. In Figures 13-29, the approximation (4) to the more exact formula (1) is probably more accurate for the cases where the two disagree considerably, since this disagreement occurs when mutual coupling is important and the loss indicated by (1) is too small.

#### LOSS DUE TO HUBS

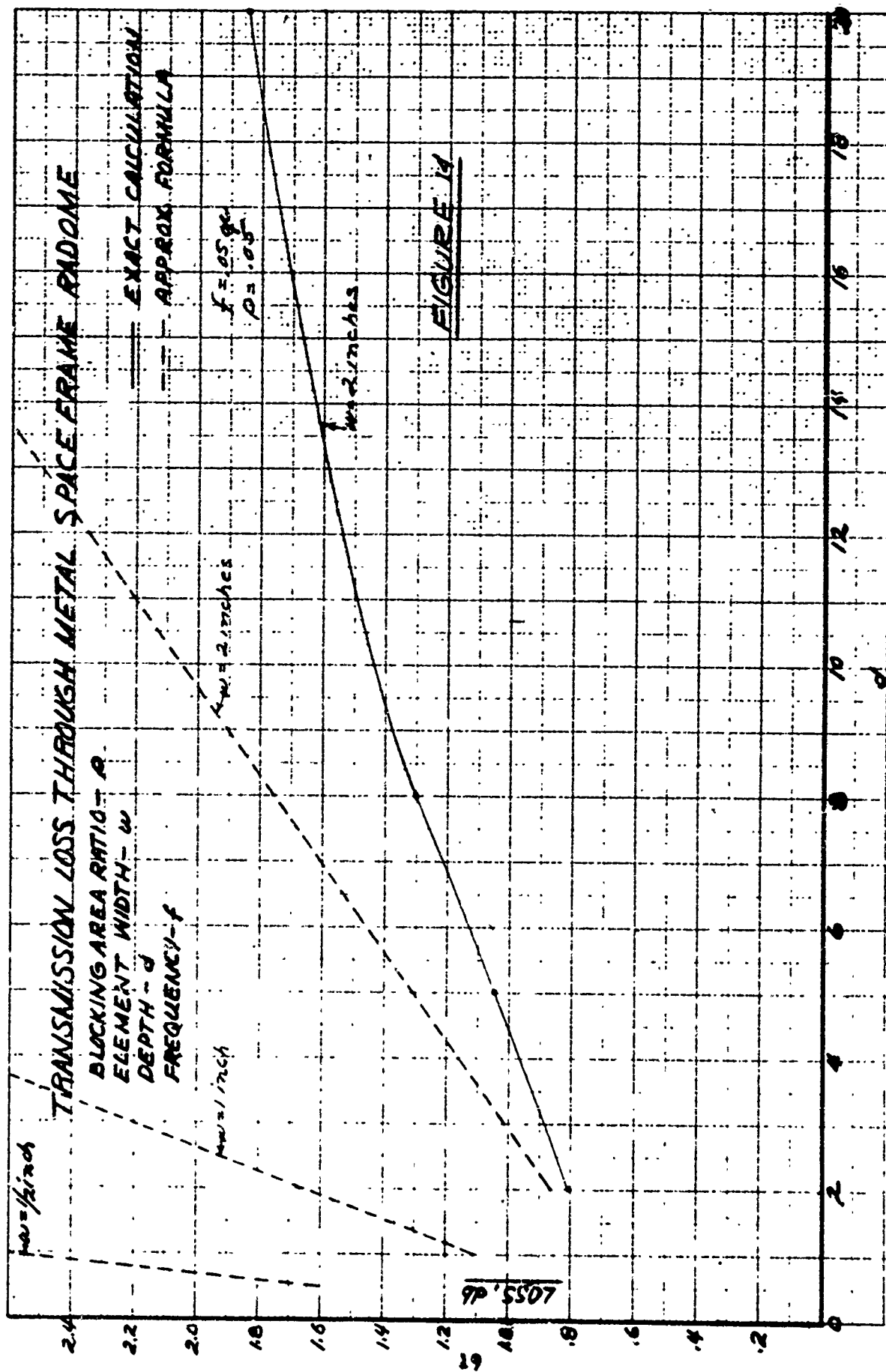
Let  $D$  be the hub diameter and  $L$  the average element length from hub center to hub center. The analogous formula to (1) including the effect of hubs is

$$(5) \quad G = \left| 1 + \left( \frac{L-D}{L} \right) \rho_{g_{av}} - \rho_1 \right|^2$$

where  $\rho_1$  is the blocking area ratio of the hubs, assuming optical blocking of the hubs. In a triangular or quadrilateral geometry  $\rho_1$  is approximately

$$(6) \quad \rho_1 = \frac{\pi D^2 \rho}{12WL} \approx .9 \left( \frac{D}{L} \right)^2$$





9P'5507

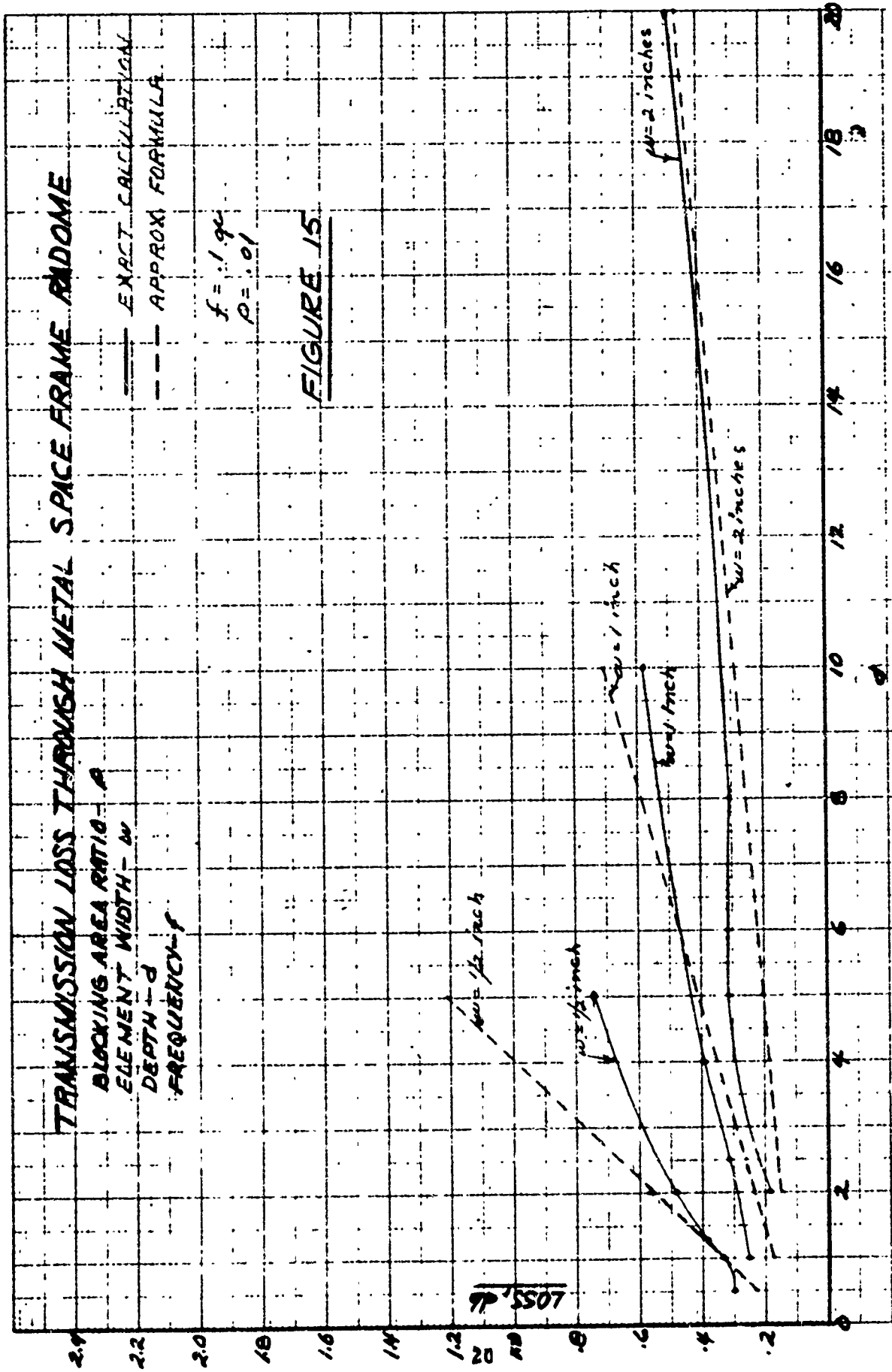
# TRANSMISSION LOSS THROUGH METAL SPACE FRAME RADOME

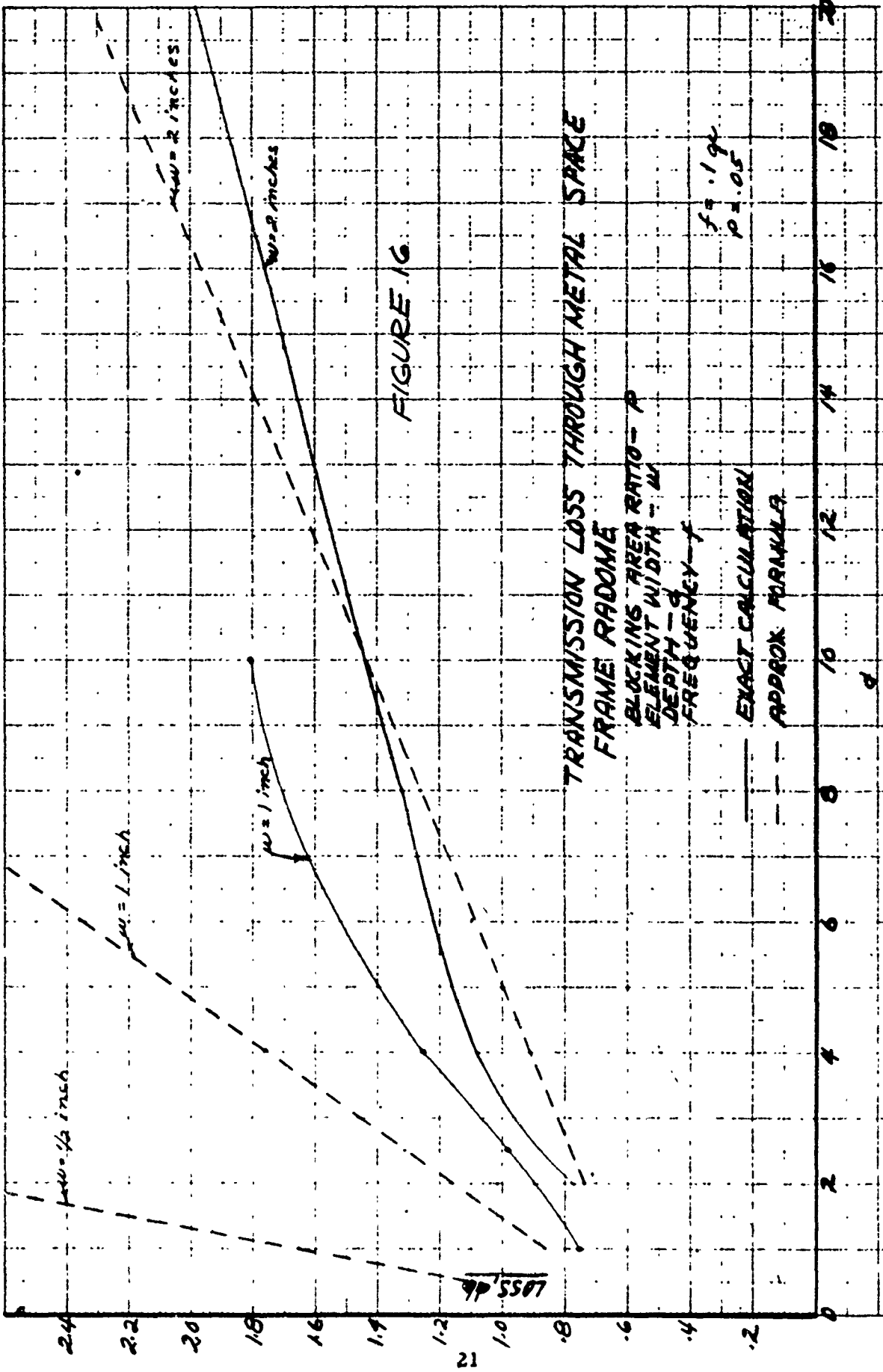
BLOCKING AREA RATIO - A  
 ELEMENT WIDTH - w  
 DEPTH - d  
 FREQUENCY - f

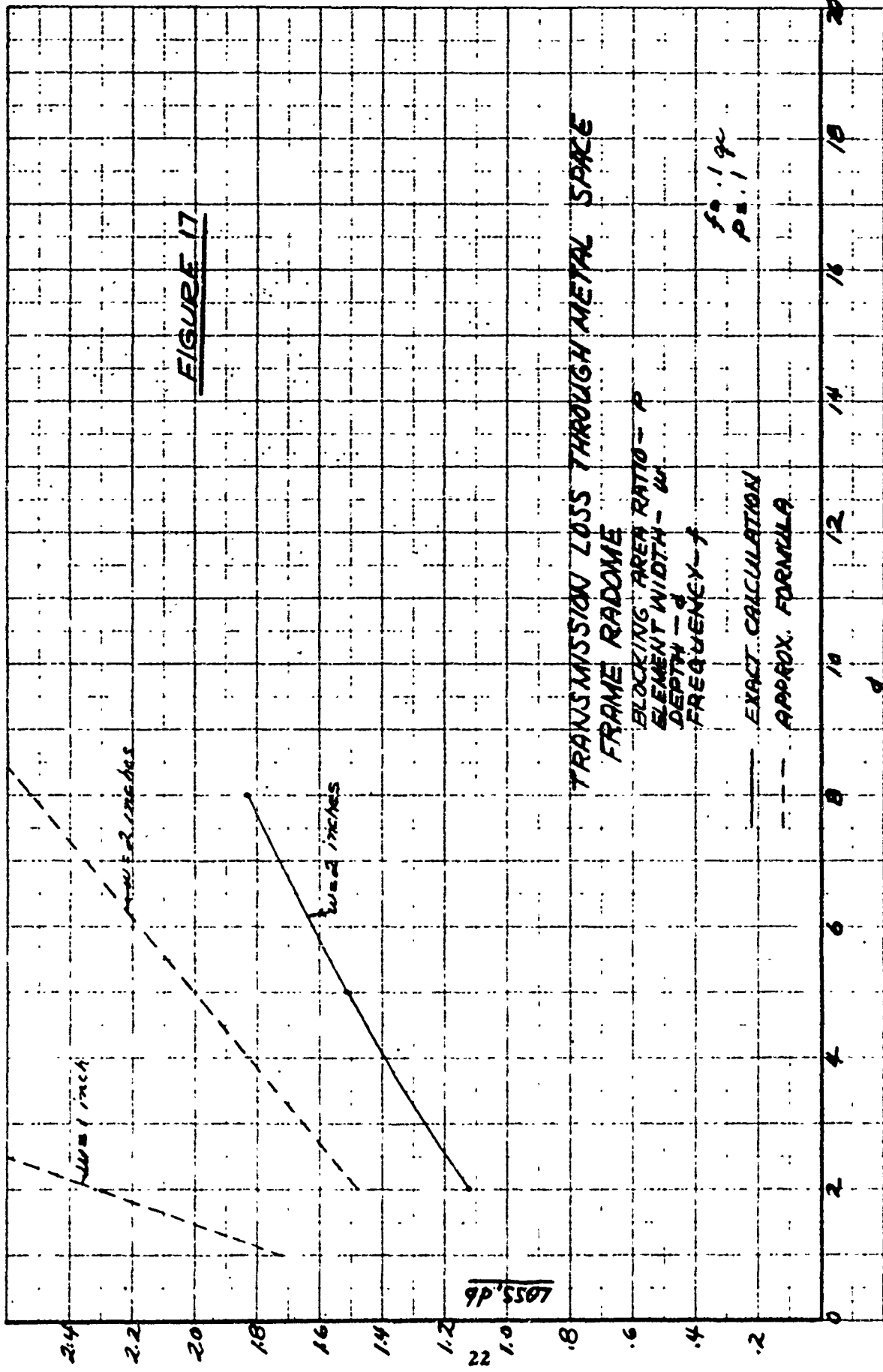
— EXACT CALCULATION  
 - - - APPROX FORMULA

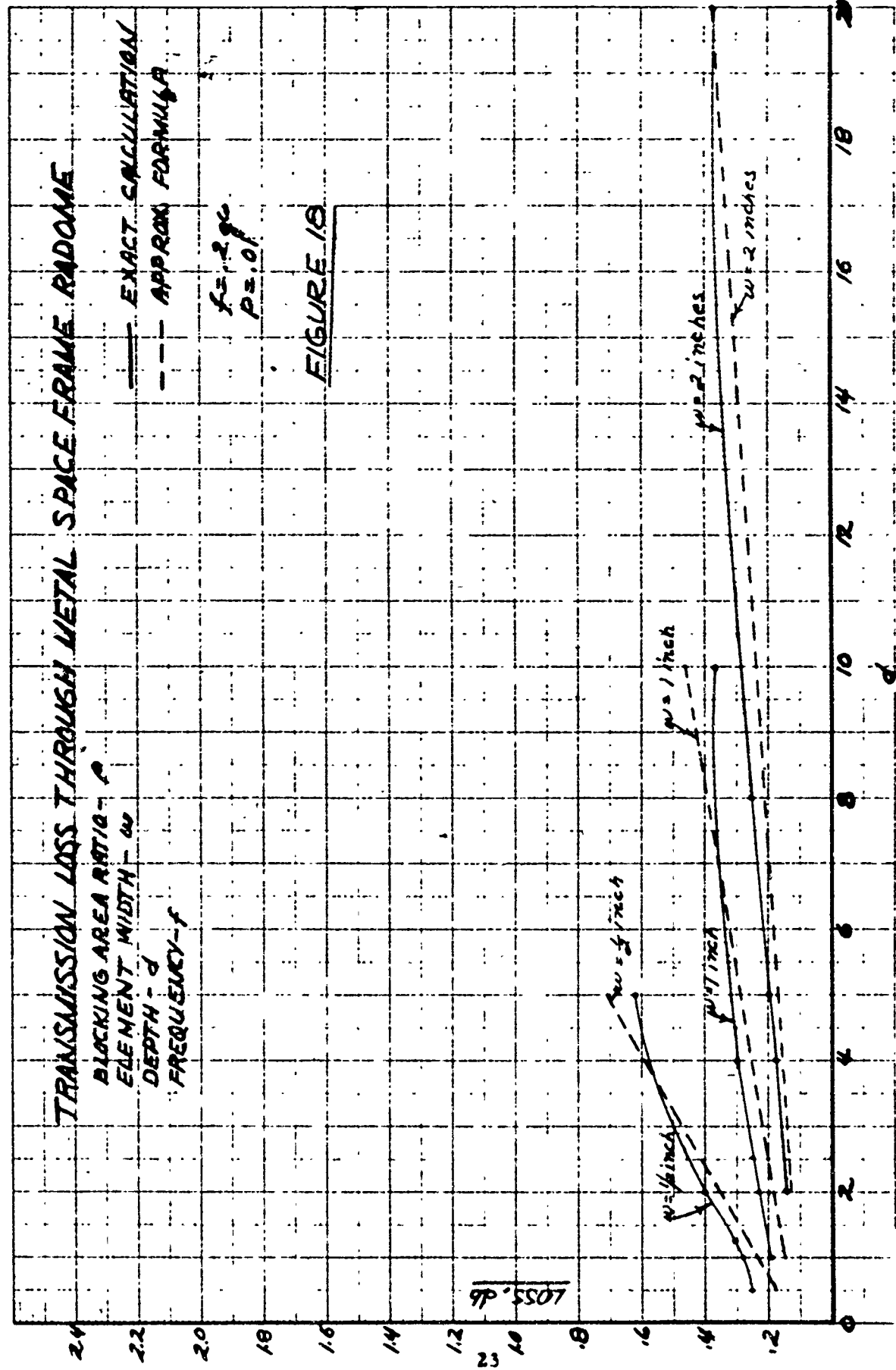
f = 1.9c  
 p = .01

FIGURE 15

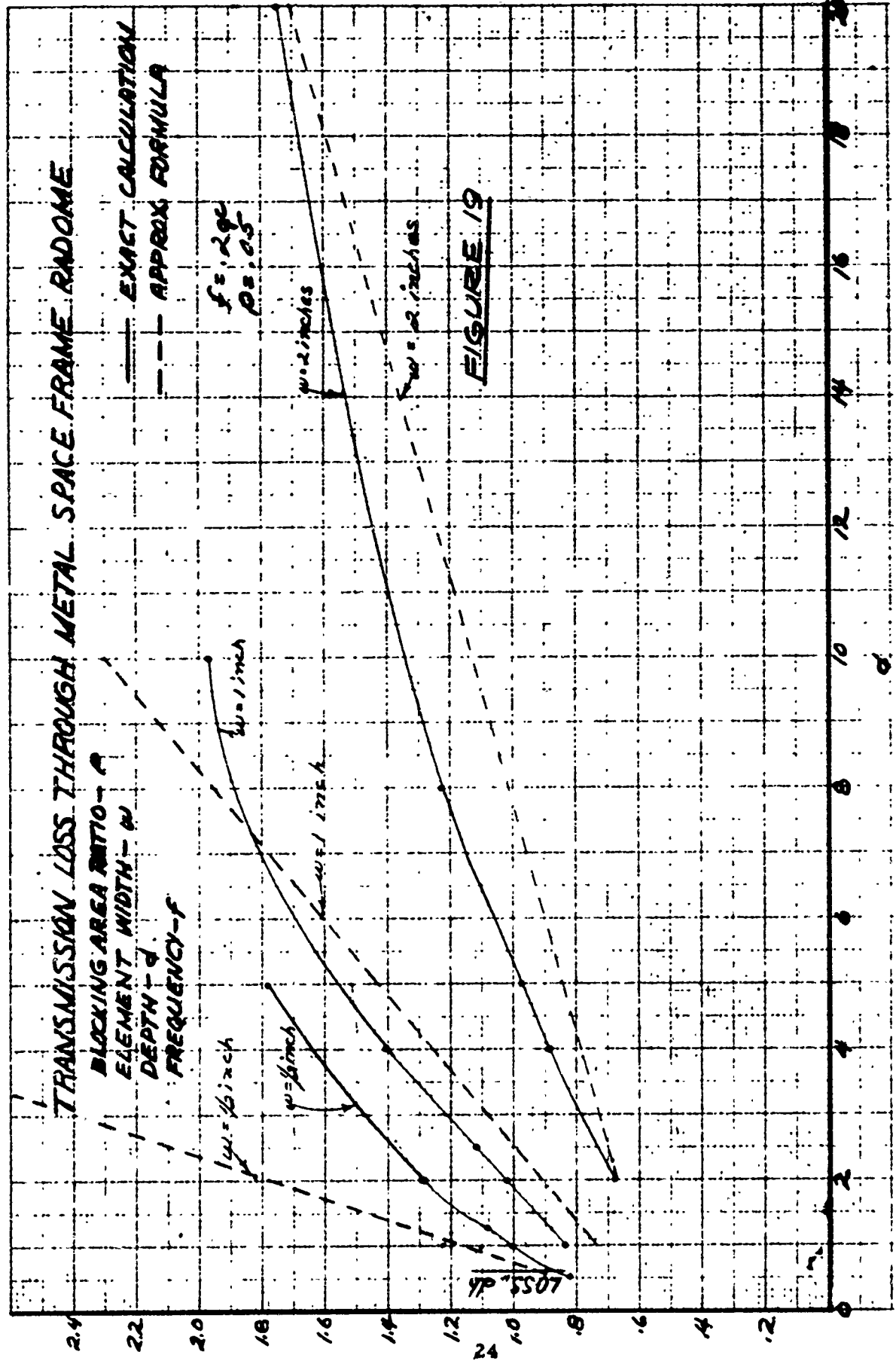


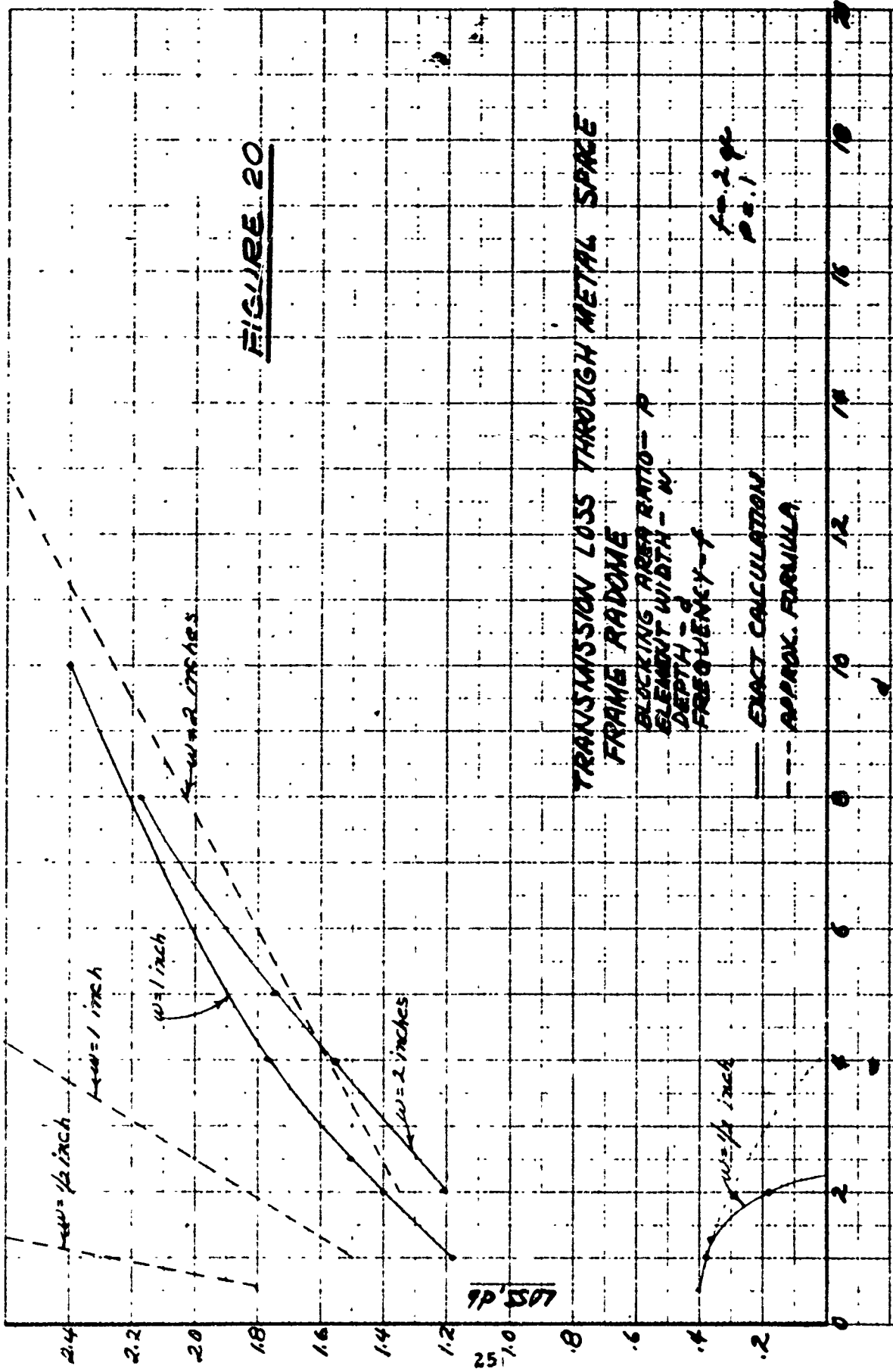






TRANSMISSION LOSS THROUGH METAL SPACE FRAME RADOME





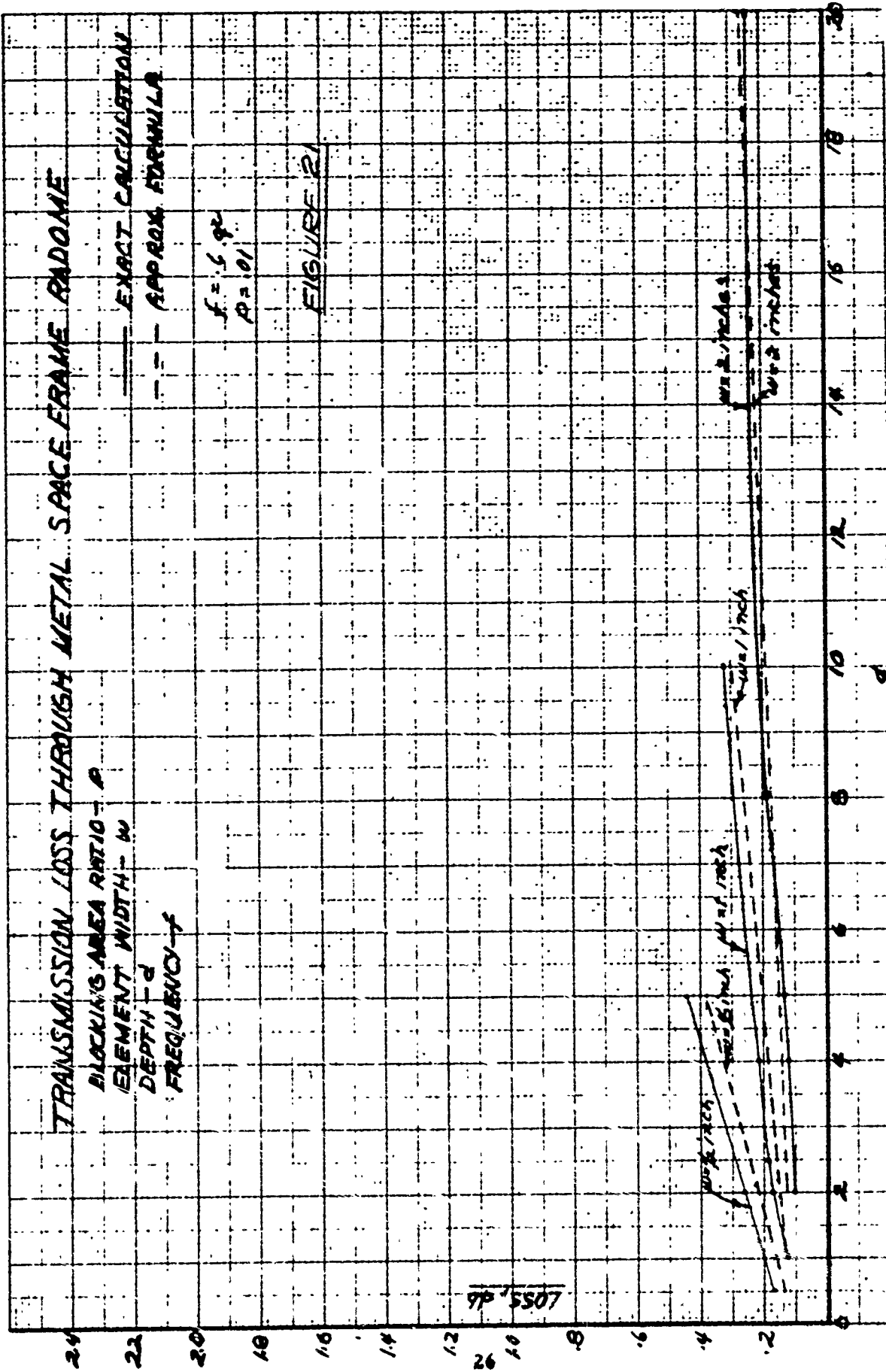
TRANSMISSION LOSS THROUGH METAL SPACE FRAME RADOME

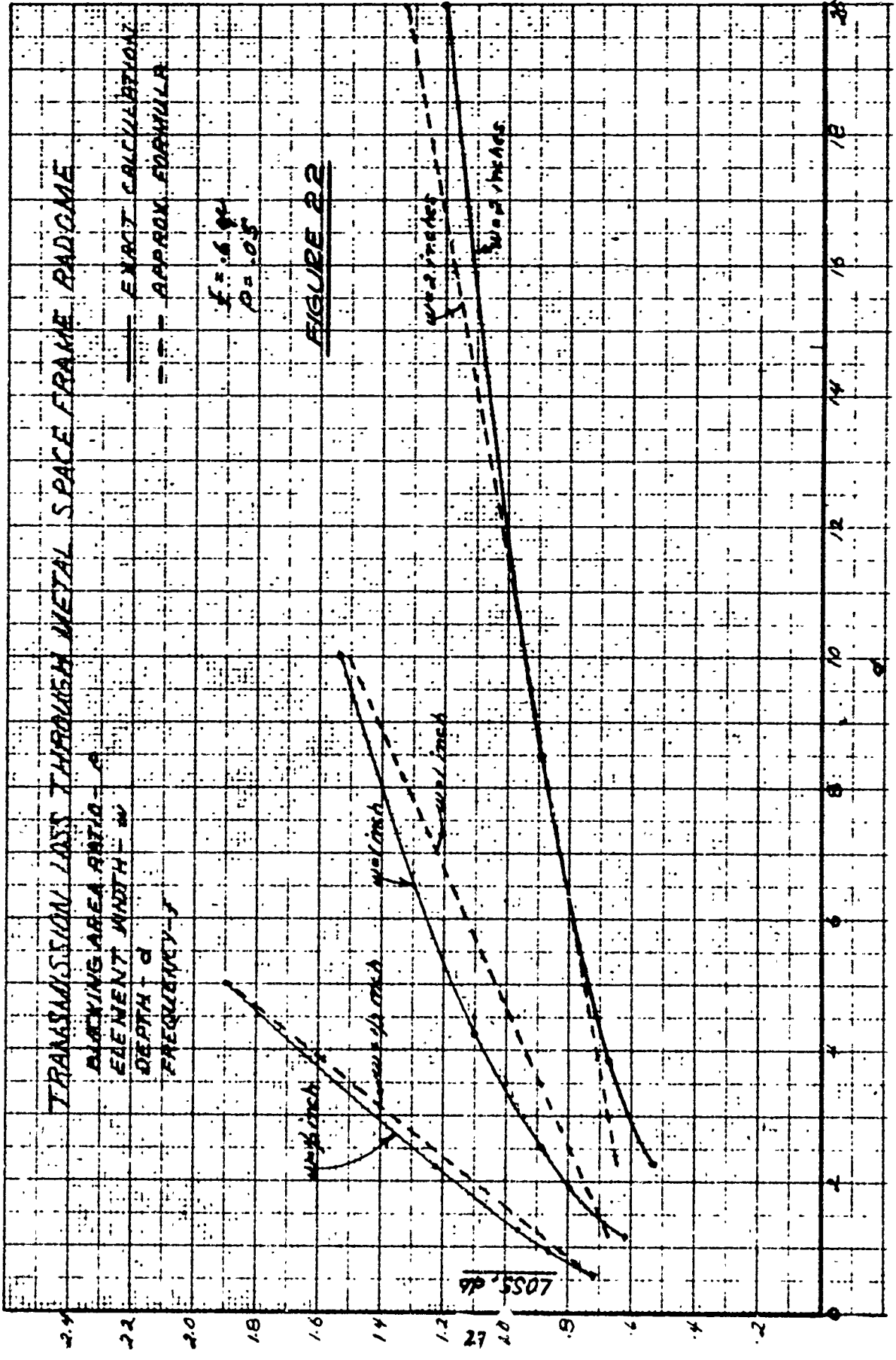
BLOCKING AREA RATIO -  $P$   
 ELEMENT WIDTH -  $w$   
 DEPTH -  $d$   
 FREQUENCY -  $f$

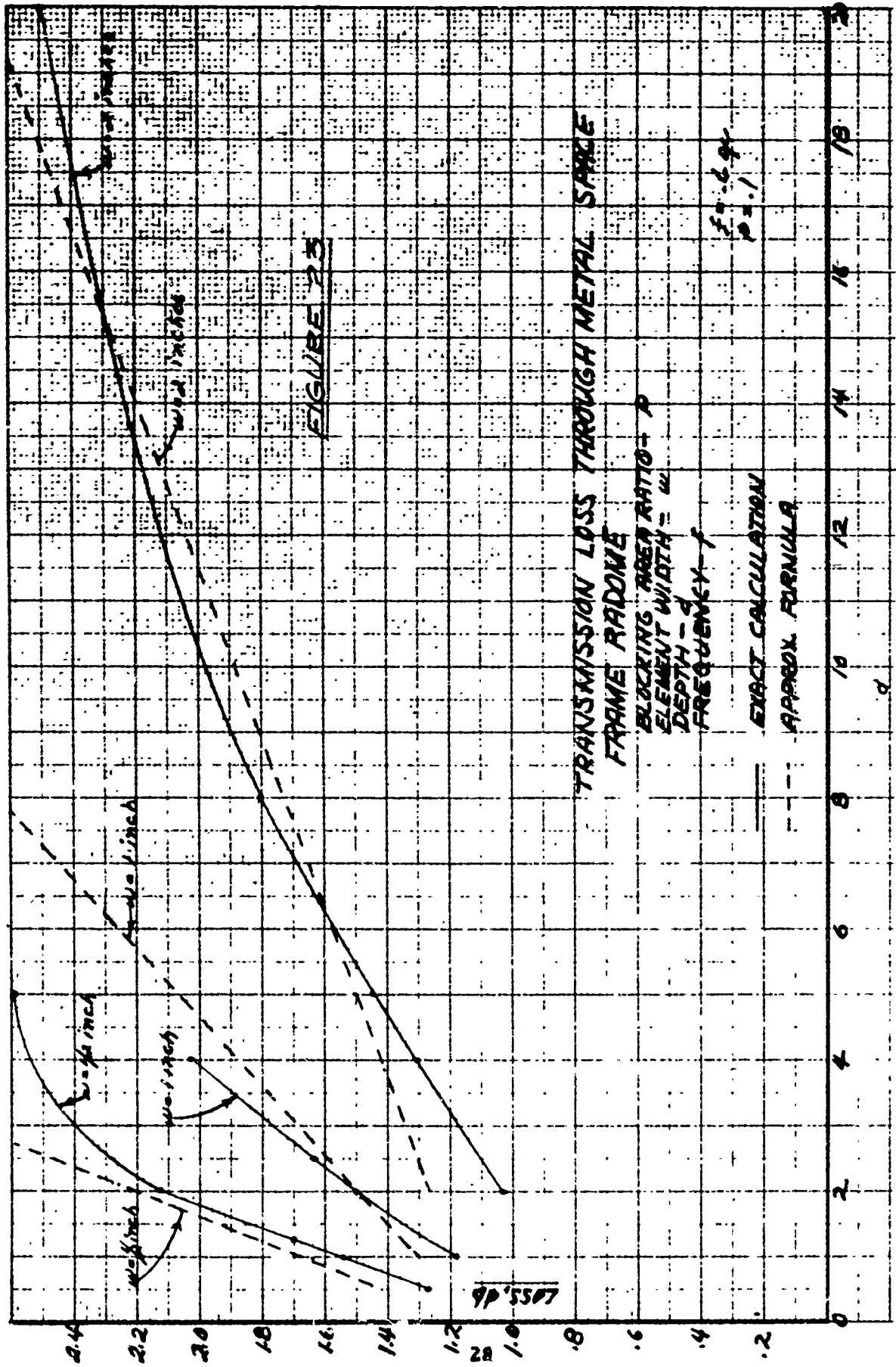
— EXACT CALCULATION  
 - - - APPROX. FORMULA

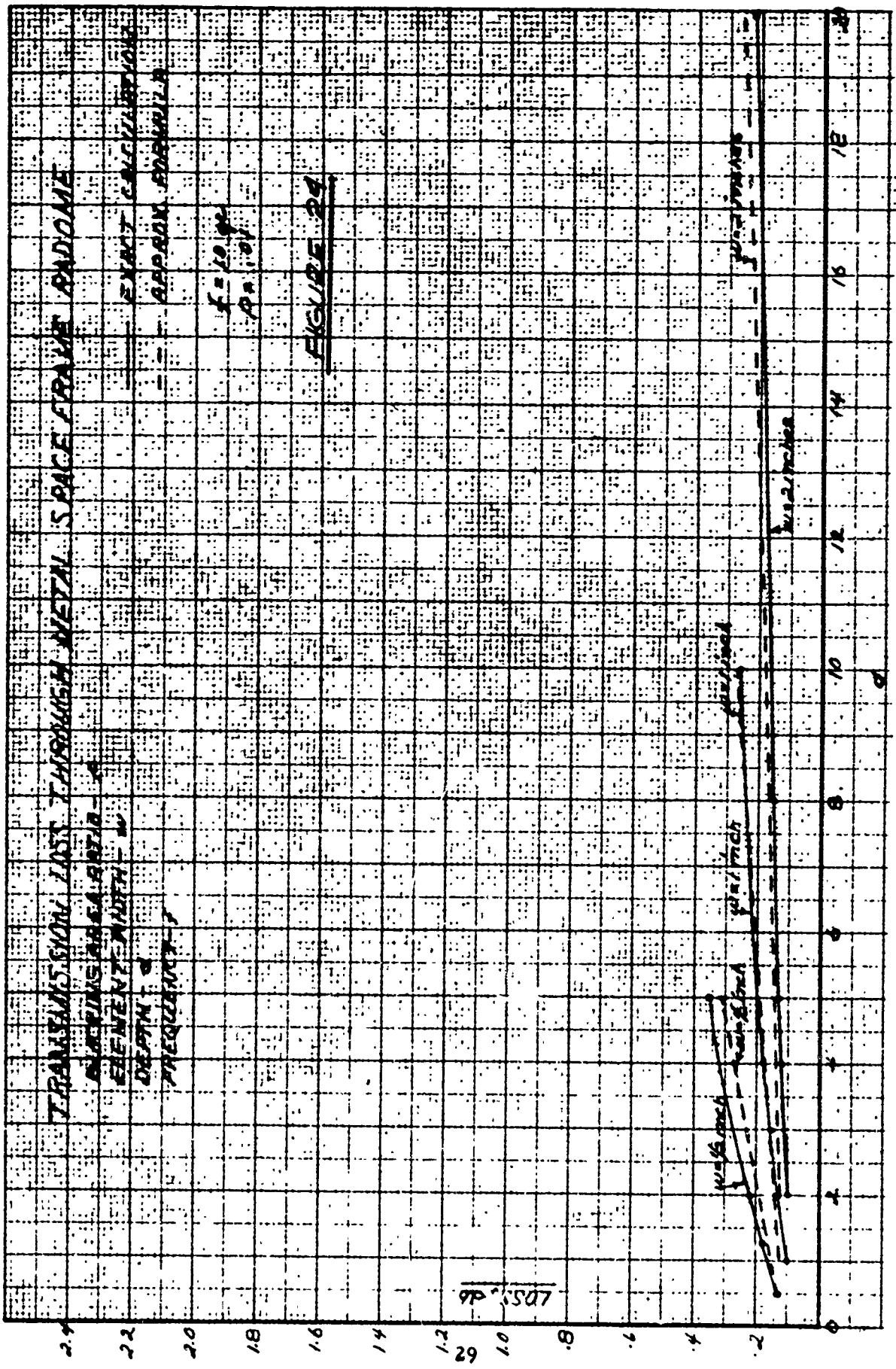
$f = 1.92$   
 $P = 0.1$

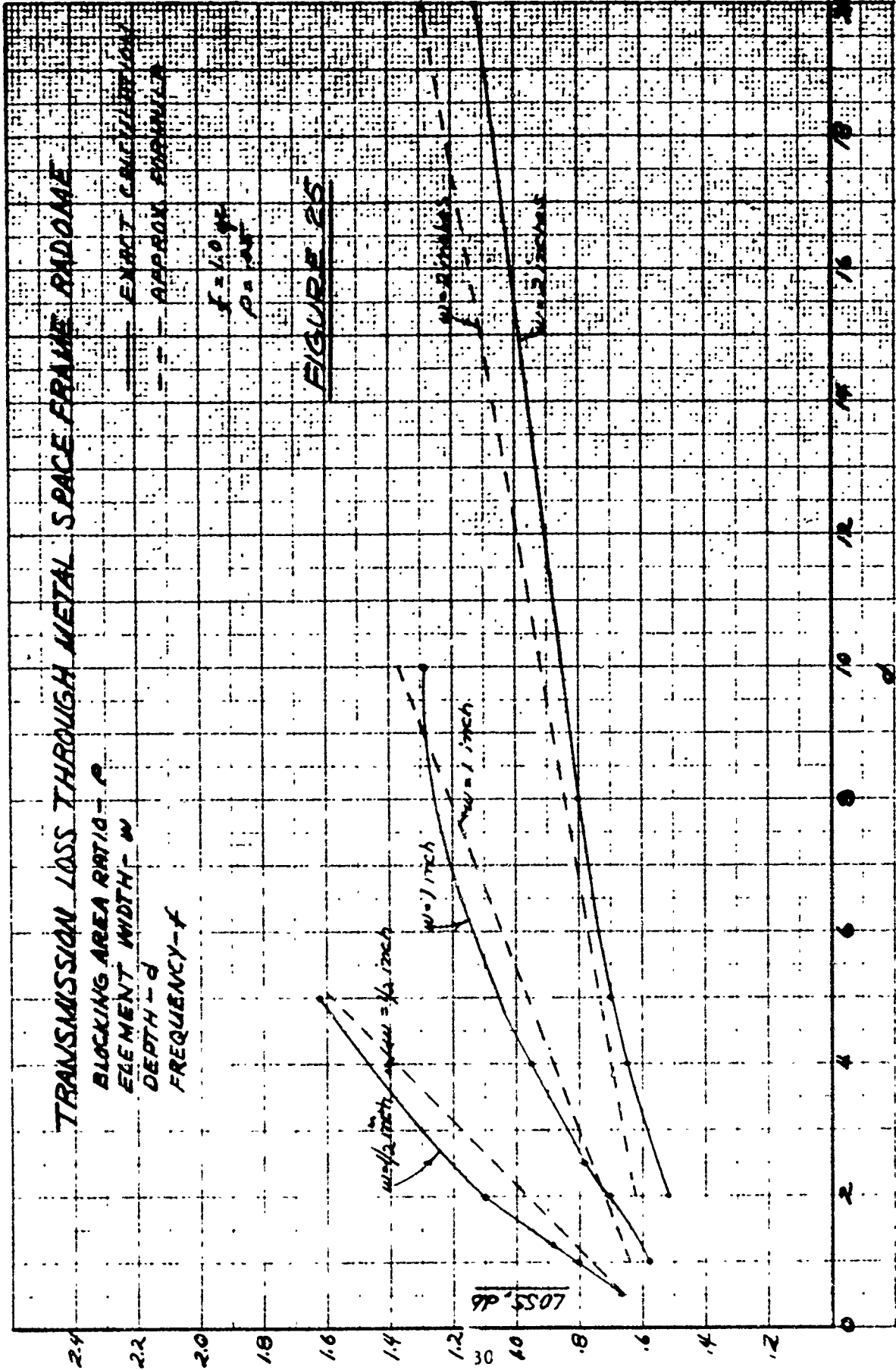
FIGURE 21

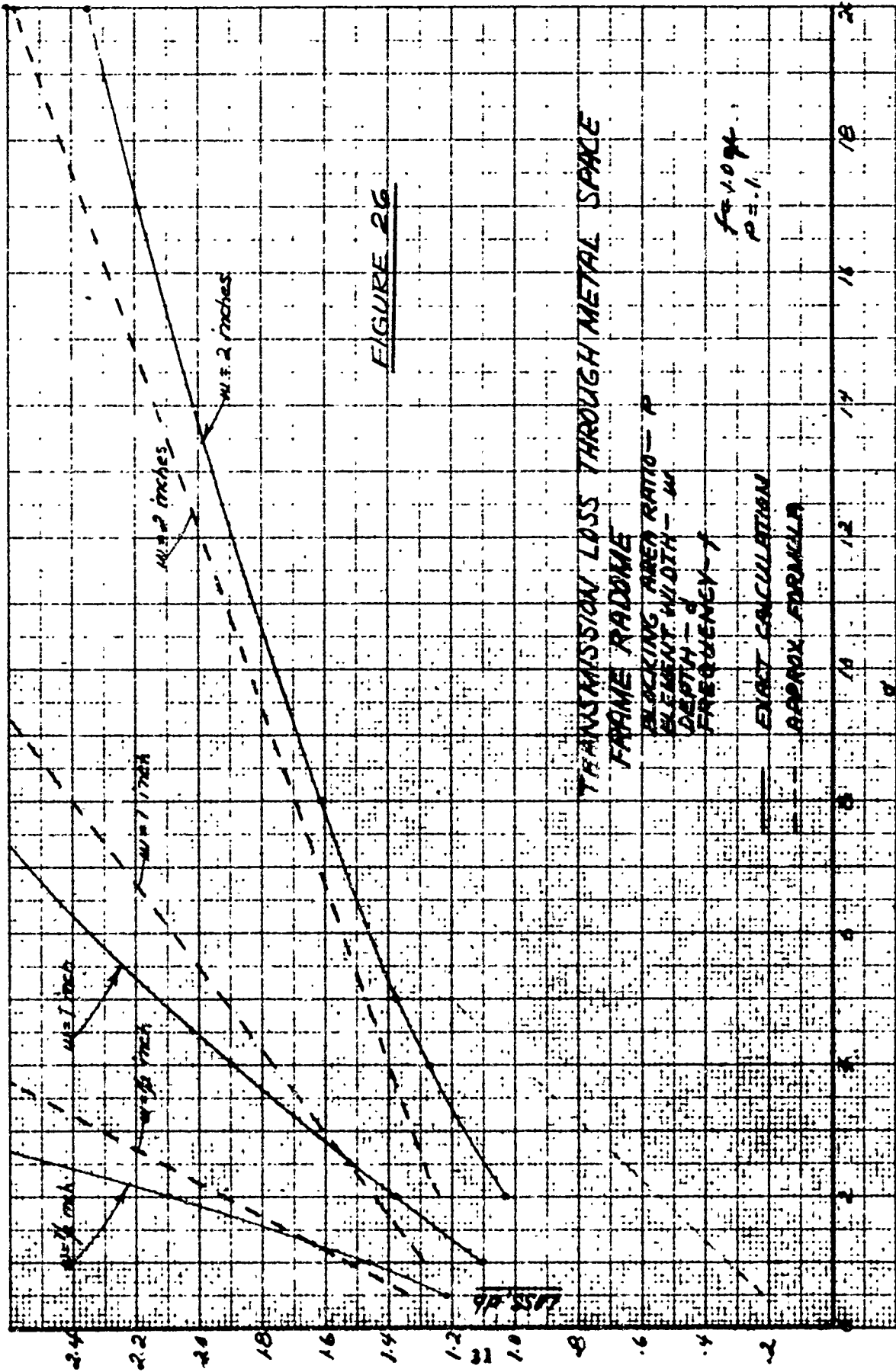


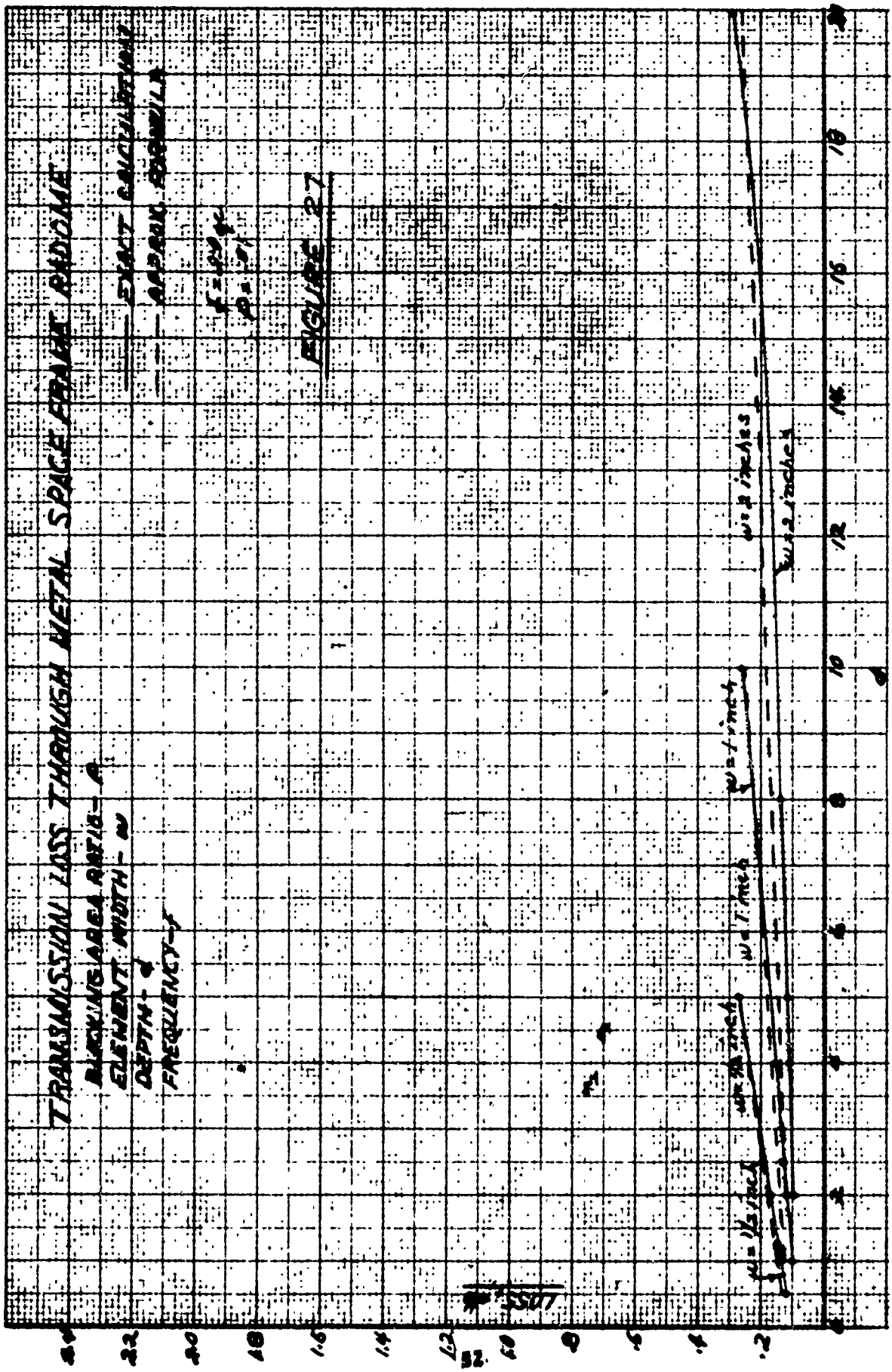


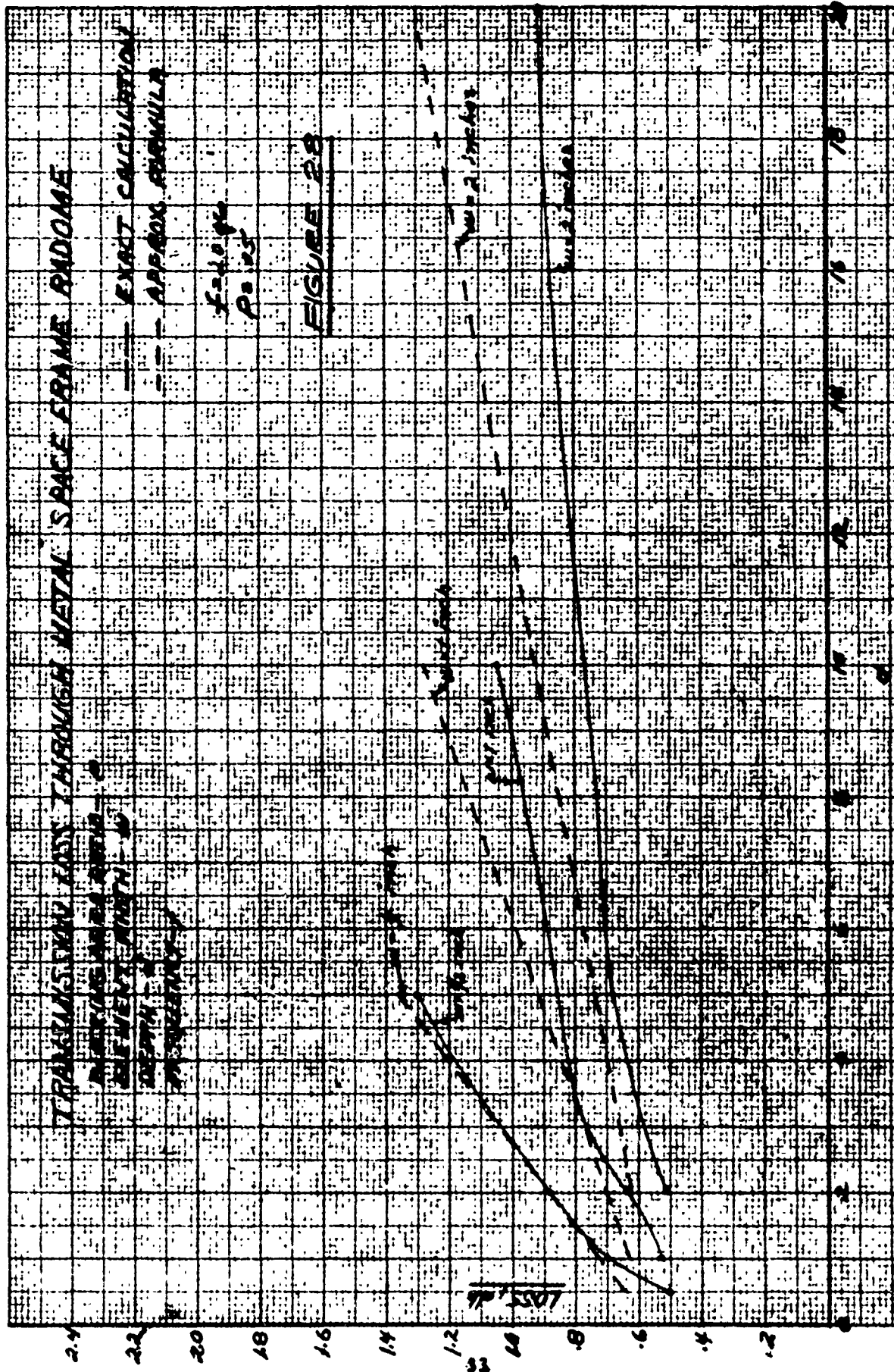


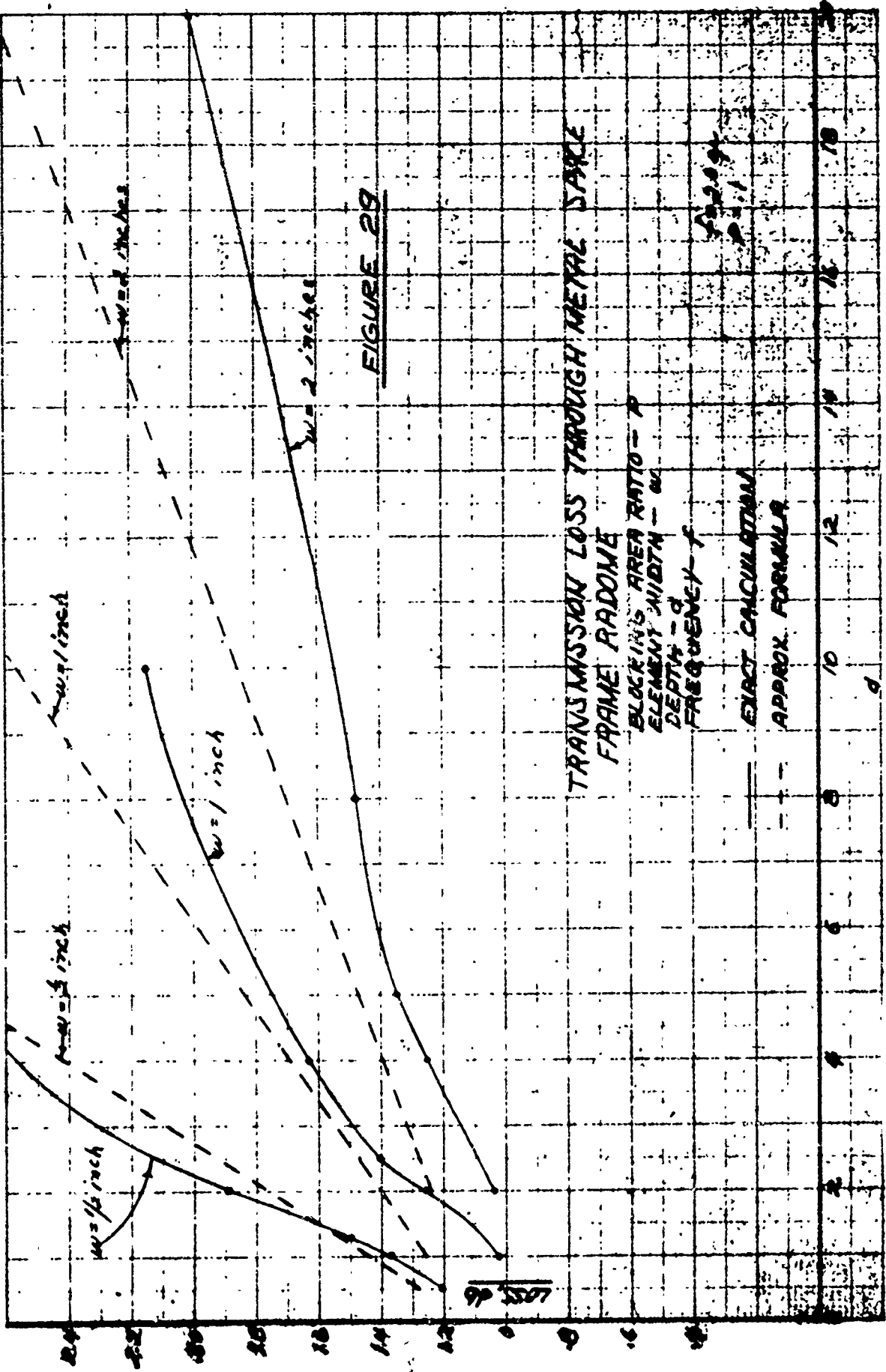












Hence (5) can be written as

$$(7) \quad G = \left| 1 + \frac{3.5Wg}{L+D} - .9\left(\frac{D}{L}\right)^2 \right|^2, \quad D \ll L.$$

With reasonable structural design the effect of the hubs is usually a small correction to the effect of the elements.

#### LOSS DUE TO DIELECTRIC SKINS

In a space frame radome, at least up to 10gc, the skins will be thin compared to a wavelength and the loss will be entirely due to reflection for practical purposes if low loss dielectric windows are used. The reflection loss in db is

$$(8) \quad 10 \log_{10} \left( 1 + \frac{(1-\epsilon)^2 \sin^2 \left( \frac{2\pi\delta\sqrt{\epsilon}}{\lambda} \right)}{4\epsilon} \right)$$

where  $\delta$  is the skin thickness and  $\epsilon$  is the dielectric constant. Equation(8) applies to normal incidence but is a good approximation for spherical radomes. For thin radomes a sufficient approximation is

$$(9) \quad 10 \log_{10} \left( 1 + (\epsilon-1)^2 \left( \frac{\pi\delta}{\lambda} \right)^2 \right).$$

For radomes below 2gc the loss expressed by (9) is usually entirely negligible. Above 2gc it rises rapidly. Sufficiently thin skinned radomes can

only be realized above 10gc with considerable care in structural design.

### BORESIGHT ERROR

Equation (26) of [1] is a fundamental approximate formula for boresight error due to a space frame radome or, if properly interpreted, for any source of aperture phase errors. This equation is as follows:

$$(10) \quad \theta' = \frac{\lambda \int_0^a r f(r) \int_0^{2\pi} \psi(r, \eta) \cos \eta d\eta dr}{2\pi^2 \int_0^a r^2 f(r) dr}$$

Here  $\theta'$  is the boresight shift in radians in the plane  $\eta=0$  where  $f(r)\cos\eta$  is an approximation to a monopulse difference pattern,  $(r, \eta)$  are polar coordinates in the aperture of radius  $a$ , and  $\lambda$  is the wavelength.  $\psi(r, \eta)$  is the phase error at  $(r, \eta)$ . In this section we shall use this equation to determine the boresight error due to many commonly occurring factors. Equation (10) and the results of this section apply to monopulse systems. However, they are reasonably accurate for conical scan or peak shift determinations if  $f(r)$  is considered as the aperture illumination of a sum or even symmetry mode.

The types of errors considered are indicated schematically in Figures 30-36 as variations from the small boresight shift of a basic radome or from no boresight shift at all.

The following notation is used:

$\lambda$  = wavelength

$a$  = radius of antenna aperture =  $D/2$

$f(r)$ ,  $0 < r < a$  = illumination of aperture (circularly symmetric)

$W$ ,  $L$ ,  $d$  = nominal element width, average length, and depth respectively

$\Delta W$ ,  $\Delta L$ ,  $\Delta d$  = tolerance or design variation in  $W$ ,  $L$ , or  $d$ , respectively,

for elements specified

$\rho$  = blocking area ratio  $\approx 3.5 W/L$  for triangular or quadrilateral division of sphere

$\mathcal{I}_i(g)$  = imaginary part of the induced field ratio, IFR. If polarization is random or averages to  $45^\circ$  over particular elements causing boresight shift, then

$$g = \frac{g_l + g_t}{2} = g_{av}$$

is the algebraic average of the longitudinal and transverse polarization IFR's.

If not, applicable  $g_l$  or  $g_t$  or weighted average must be used.

$\Delta \mathcal{I}_i(g)$  = tolerance or design variation in  $\mathcal{I}_i(g)$  of elements specified.

$A$  = total area of radome where tolerance or design variation may occur.

$\left\{ \begin{matrix} \mu \\ n \end{matrix} \right\} = \left\{ \begin{matrix} \text{fraction} \\ \text{number} \end{matrix} \right\}$  of elements, hubs, or windows having a specified

tolerance or design variation;  $0 \leq \mu \leq 1$ .

$\epsilon, \delta$  = nominal dielectric constant and skin thickness of windows

$\Delta \epsilon, \Delta \delta$  = variation in  $\epsilon$  or  $\delta$

All boresight errors are in radians.

Note that

$$\Delta(W \mathcal{I}_i(g) L) \approx W \mathcal{I}_i(g) \Delta L + W L \Delta \mathcal{I}_i(g) + L \mathcal{I}_i(g) \Delta W .$$

We now consider six different sources of boresight error:

1) A small number  $n$ ,  $n = 1, 2, \dots$  of extra elements are located in one local region of the radome, small compared to the antenna diameter  $D$ . The worst error occurs when the extra elements are at the peak of the difference pattern, when the beam shifts away from this location by an angle

$$(11) \quad \theta' = \lambda n L W \mathcal{J}_n'(g) c_0$$

where  $g$  is the IFR value of the extra elements and  $c_0$  depends only on the illumination taper

$$(12) \quad c_0 = \frac{\max_{0 < r < a} \{f(r)\}}{2\pi \int_0^a r^2 f(r) dr} \approx \begin{cases} .27/a^3, & 10\text{db taper} \\ .37/a^3, & 20\text{db taper} \end{cases} \quad (\text{see Fig. 30})$$

2) Certain elements of the space frame which are randomly distributed in the space frame and constitute a fraction  $\mu$  of the total number of elements, have a different width  $W_1 = W_0 + \Delta W$  and/or depth  $d_1 = d_0 + \Delta d$  from the remaining elements which are assumed to be such that if  $\Delta W = \Delta d = 0$  then there is no boresight error. RMS boresight shift is then

$$(13) \quad \theta'_{\text{rms}} = \lambda^2 \Delta \left( \frac{W \mathcal{J}_n'(g)}{\lambda} \right) \sqrt{\mu} c_1 \quad \left\{ \begin{array}{l} \text{triangulated} \\ \text{radome} \end{array} \right.$$

where

$$(14) \quad c_1 = \frac{\int_0^a 3.5\pi r f^2(r) dr}{2\pi \int_0^a r^2 f(r) dr} \approx \begin{cases} .42/a^2, & 10\text{db taper} \\ .50/a^2, & 20\text{db taper} \end{cases}$$

If the radome is not triangulated by the space frame, but has some other arrangement of elements, (12) applies with  $\mu$  replaced by

$$(15) \quad \frac{\mu L \rho}{3.5W} \quad (\text{see Fig.31}).$$

3) Given tolerances  $\Delta W$  and  $\Delta d$  in dimensions of all elements

a) Largest possible boresight error occurs when  $+\Delta W$ ,  $+\Delta d$  occurs on one side of dish;  $-\Delta W$ ,  $-\Delta d$  occurs on other (Figure 32a). Beam shifts towards the least metal area by an amount

$$(16) \quad \theta = \frac{\lambda \Delta(W \rho(g)) c_2}{L}$$

where

$$(17) \quad c_2 = \frac{\int_0^a 7 r f(r) dr}{\pi \int_0^a r^2 f(r) dr} = \begin{cases} 1.19/a, & 10\text{db taper} \\ 1.30/a, & 20\text{db taper} \end{cases}$$

b) Variation of  $\Delta W$ ,  $\Delta d$  is limited to an area A whose maximum diameter is small compared to D. Boresight shift is

$$(18) \quad \theta = \frac{\lambda \Delta (W \Delta(g)) c_3}{L}$$

where

$$(19) \quad c_3 = \frac{3.5 \max_{0 < r < a} \{ f(r) \}}{2\pi \int_0^a r^2 f(r) dr} = \begin{cases} .94/a^3, & 10\text{db taper} \\ 1.30/a^3, & 20\text{db taper} \end{cases} \quad (\text{see Fig. 32b}).$$

c) Variations in dimensions of elements of a space frame are random with  $\Delta W$  and  $\Delta d$  being rms values of the variations in  $W$  and  $d$ . Then rms value of boresight error is

$$(20) \quad \theta_{\text{rms}} = \lambda \Delta (W \Delta(g)) c_1 \quad (\text{see Fig. 32c})$$

4) Rms boresight error for a random space frame geometry (most probable boresight error if a number of elements are randomly distributed over sphere) is

$$(21a) \quad \theta_{\text{rms}} = \lambda W \Delta(g) L \sqrt{n} c_1'$$

$$c_1' = \frac{\sqrt{\int_0^a f^2(r) r dr}}{2\pi \int_0^a r^2 f(r) dr} \approx \begin{cases} .13/a^3, & 10\text{db taper} \\ .15/a^3, & 20\text{db taper} \end{cases}$$

where  $n = \pi a^2 \rho / WL$  is the number of elements seen by the antenna. For a triangular or quadrilateral geometry

$$\rho = \frac{3.5W}{L}$$

and then

$$(21b) \quad \theta_{\text{rms}} = \lambda W \int_0^g c_1 \quad (\text{see Fig. 33}).$$

Mutual coupling between elements is neglected in (21a).

5) A small number  $n$ ,  $n = 1, 2, \dots$  of dielectric windows (each of average area:  $4L^2$ ) with variations  $\Delta\epsilon$  and  $\Delta\delta$  in dielectric constant and wall thickness are all located in an area of the radome whose maximum diameter is small compared to  $a$ . The maximum boresight error occurs when these windows are at a difference pattern peak, and is given by

$$(22) \quad \theta = nL^2 c_4 \left[ (\sqrt{\epsilon} - 1) \Delta\delta + \frac{\int \Delta\epsilon}{\sqrt{\epsilon}} \right]$$

$$(23) \quad c_4 = \frac{.4 \max\{f(r)\}}{\pi \int_0^a r^2 f(r) dr} \approx \begin{cases} .68/a^3, & 10\text{db taper} \\ .94/a^3, & 20\text{db taper} \end{cases} \quad (\text{see Fig. 34}).$$

6) A certain fraction  $\mu$  of windows which are randomly distributed over the

aperture have a different dielectric constant  $\epsilon = \epsilon_0 + \Delta\epsilon$  and/or thickness

$\delta = \delta_0 + \Delta\delta$  from the remaining elements, which are assumed to be such that

if  $\Delta\epsilon = \Delta\delta = 0$ , then there is no boresight error.

$$(24) \quad \theta_{\text{rms}} = \left[ (\sqrt{\epsilon} - 1)\Delta\delta + \frac{\delta\Delta\epsilon}{\sqrt{\epsilon}} \right] \sqrt{\mu} Lc_5$$

$$c_5 = \frac{\sqrt{\frac{.4}{\pi} \int_0^a r f^2(r) dr}}{\int_0^a r^2 f(r) dr} = \begin{cases} .89/a^2, & 10\text{db taper} \\ 1.06/a^2, & 20\text{db taper} \end{cases} \quad (\text{see Fig.35})$$

Given tolerances  $\Delta\epsilon$  and  $\Delta\delta$  in all windows

a) Largest possible boresight error occurs when  $+\Delta\epsilon$  and  $+\Delta\delta$  occurs on one side of dish;  $-\Delta\epsilon$ ,  $-\Delta\delta$  occurs on the other side. Beam shifts towards the most dielectric area by an amount

$$(25) \quad \theta = \left[ (\sqrt{\epsilon} - 1)\Delta\delta + \frac{\delta\Delta\epsilon}{\sqrt{\epsilon}} \right] c_6$$

$$(26) \quad c_6 = \frac{4}{\pi} \frac{\int_0^a r f(r) dr}{\int_0^a r^2 f(r) dr} = \begin{cases} 2.14/a, & 10\text{db taper} \\ 2.34/a, & 20\text{db taper} \end{cases} \quad (\text{see Fig.36a})$$

b) Variation is random and windows are distributed uniformly over

surface of radome with  $\Delta\epsilon$  and  $\Delta\delta$  being rms values of the variation in  $\epsilon$  and  $\delta$ . Then rms value of boresight error is

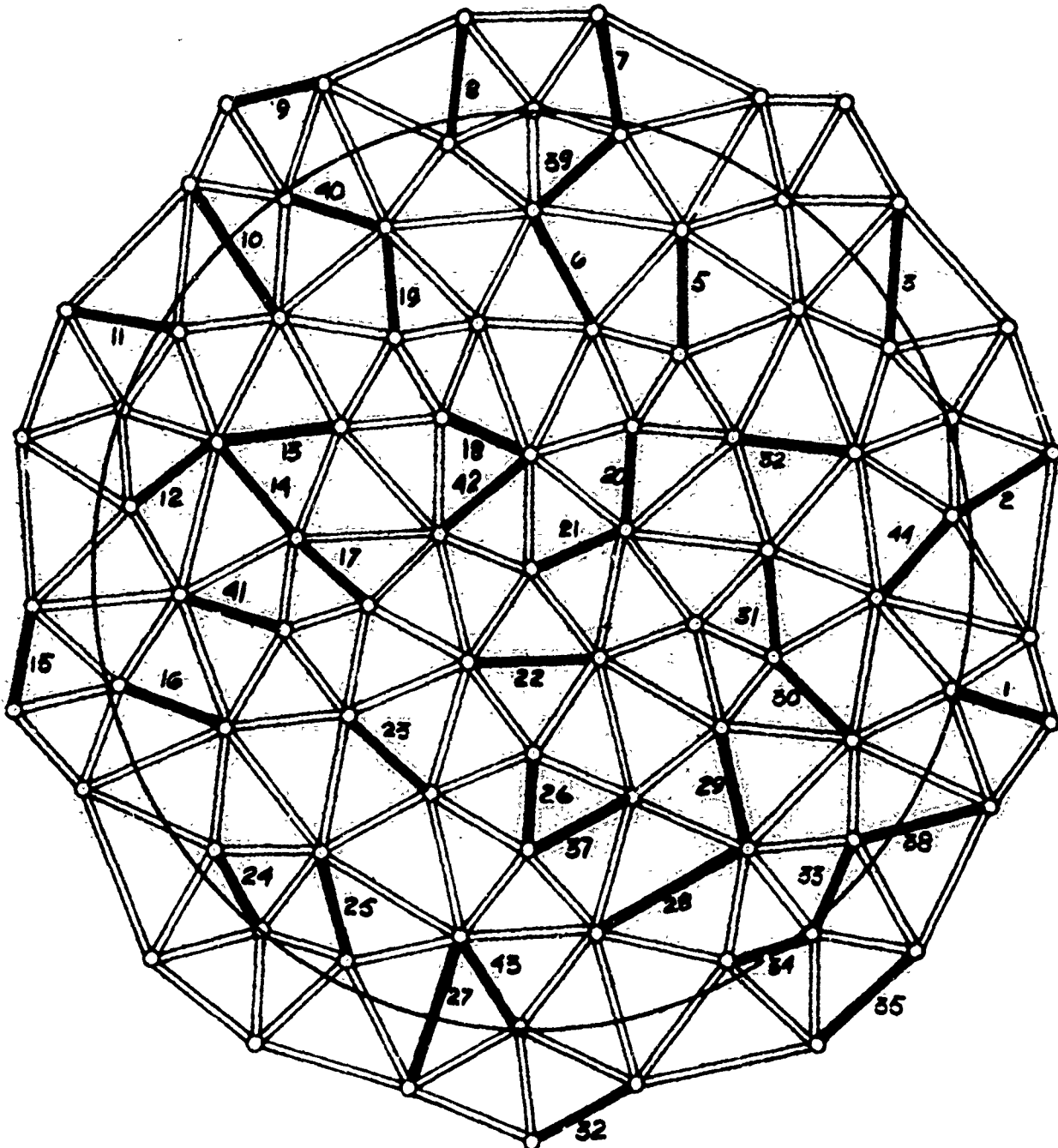
$$(27) \quad \theta_{\text{rms}} = \left[ (\sqrt{\epsilon}-1)\Delta\delta + \frac{\delta\Delta\epsilon}{\sqrt{\epsilon}} \right] Lc_5 \quad (\text{see Fig 36b}).$$

Figure 37 is a plot of  $\frac{W}{\lambda} |g_{av}|$  for various  $d/\lambda$  and  $W/\lambda$ . From this graph the preceding formulas may be evaluated explicitly. As an example, we consider two cases - the first a gross geometry with loose tolerances, the second a finer geometry with tighter tolerances.

	Case 1	Case 2
L	30'	10'
W	1"	.5"
d	10"	3"
$\Delta W$	.1"	.005"
$\Delta d$	1"	.025"
n	4	4
$\lambda$	1'	1'
a	60'	60'
taper	10db	10db
$\mu$	.2	.2
A	.05( $\pi a^2$ )	.05( $\pi a^2$ )
$\epsilon$	4	4
$\Delta\epsilon$	.5	.1
$\delta$	.100"	.050"
$\Delta\delta$	.025"	.005"
$ g_{av} ^2$	14.44	18.84



FIGURE 31

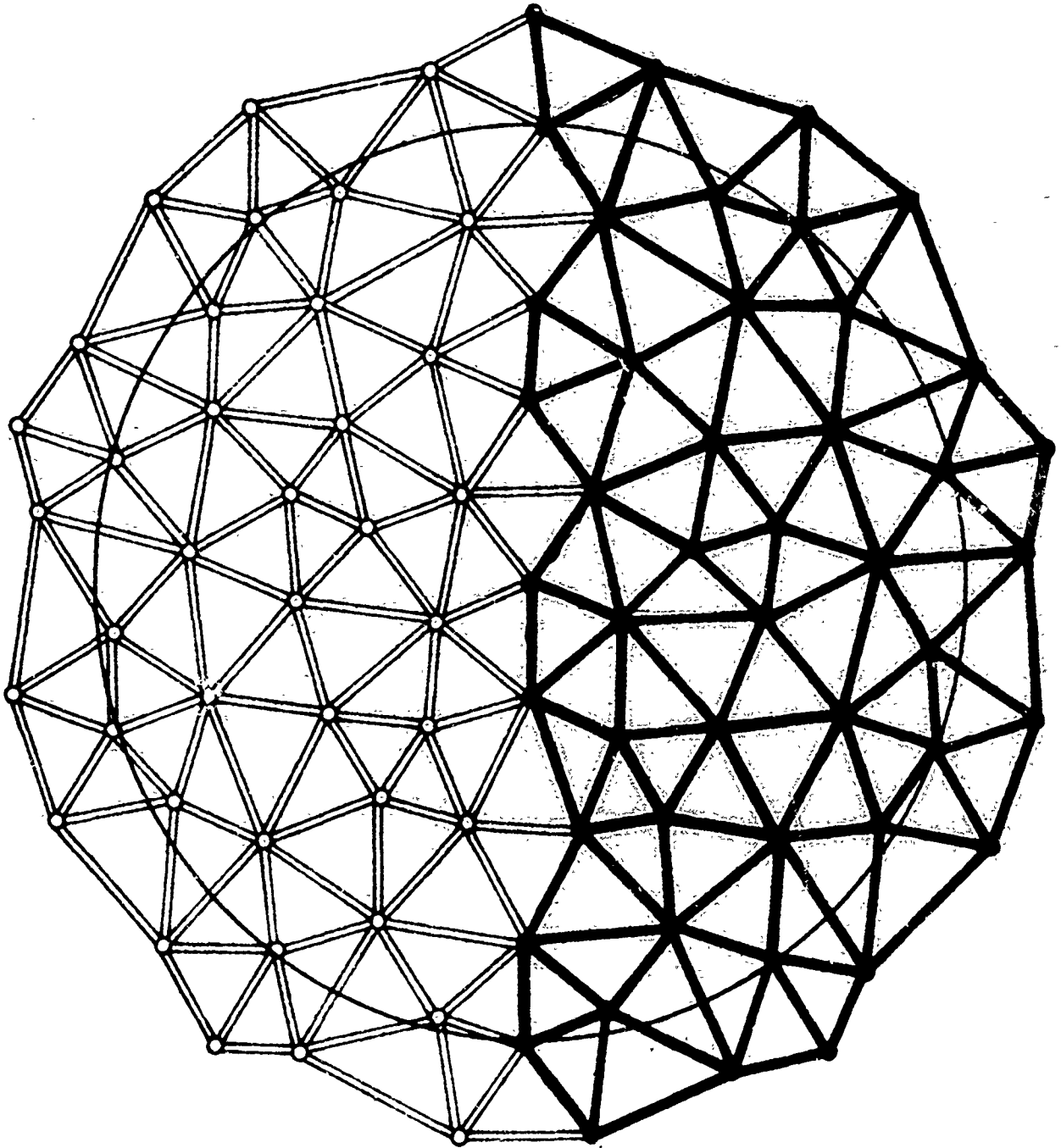


A FRACTION OF ELEMENTS RANDOMLY PLACED  
WITH EXTREME TOLERANCES

CASE 1 : .0021  $m_r$

CASE 2 : .00013  $m_r$

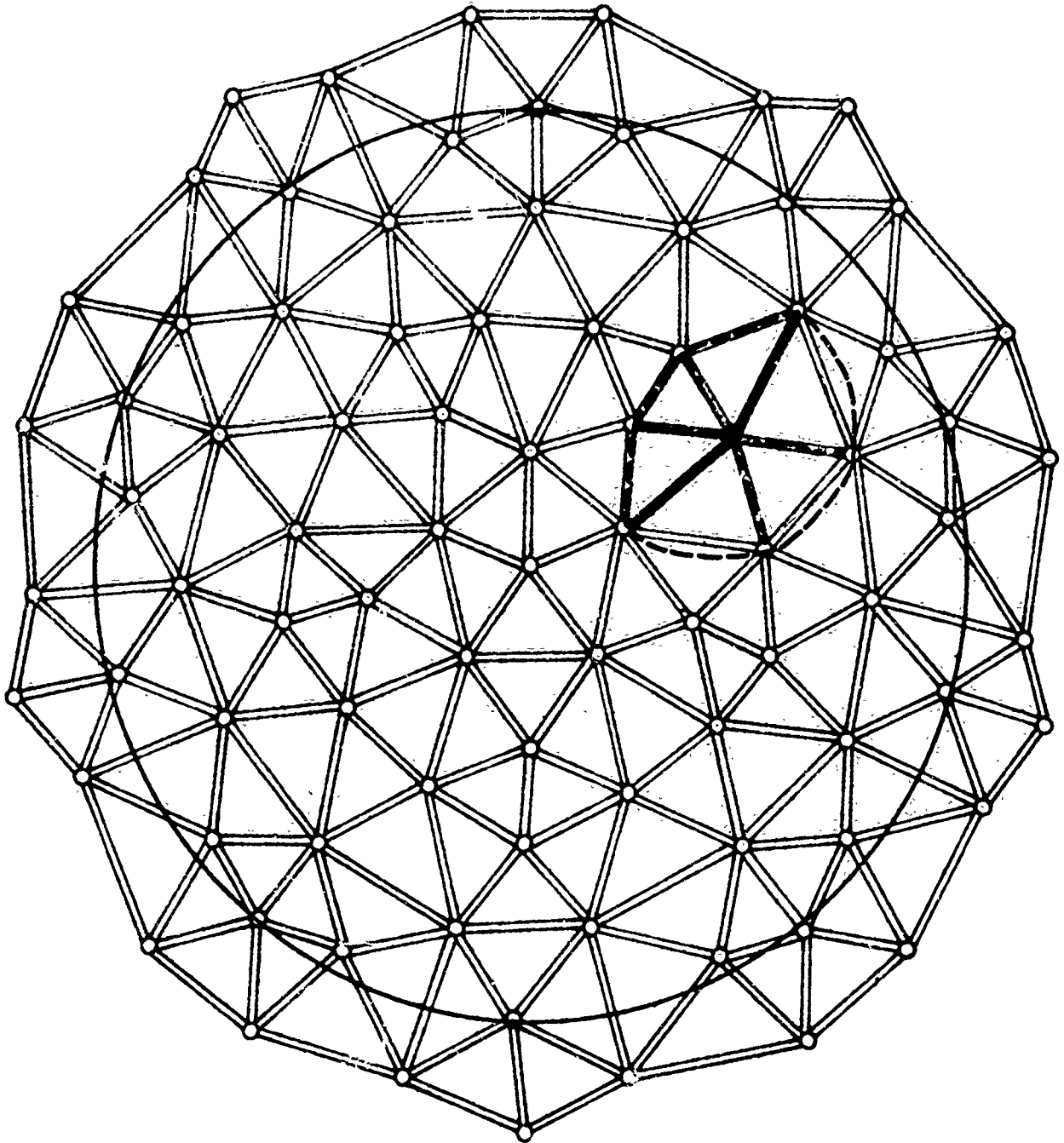
FIGURE 32a.



*MOST BORESIGHT SHIFT FOR GIVEN ELEMENT  
TOLERANCE*

*CASE 1 : .027 mr*  
*CASE 2 : .005 mr*

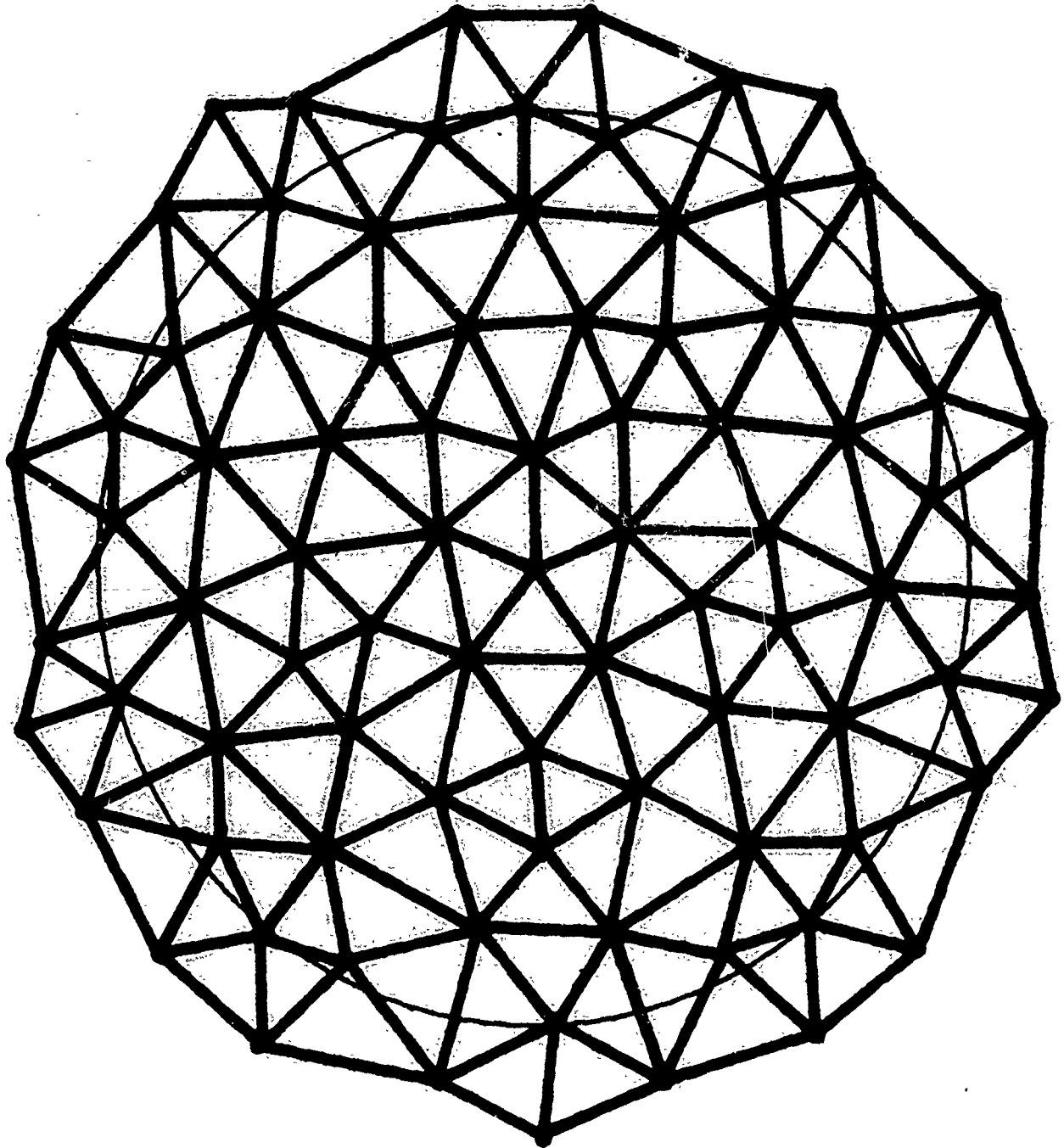
FIGURE 32 b



**ELEMENT TOLERANCES IN A LOCALIZED AREA**  
 **$A = 2.4 L^2$**

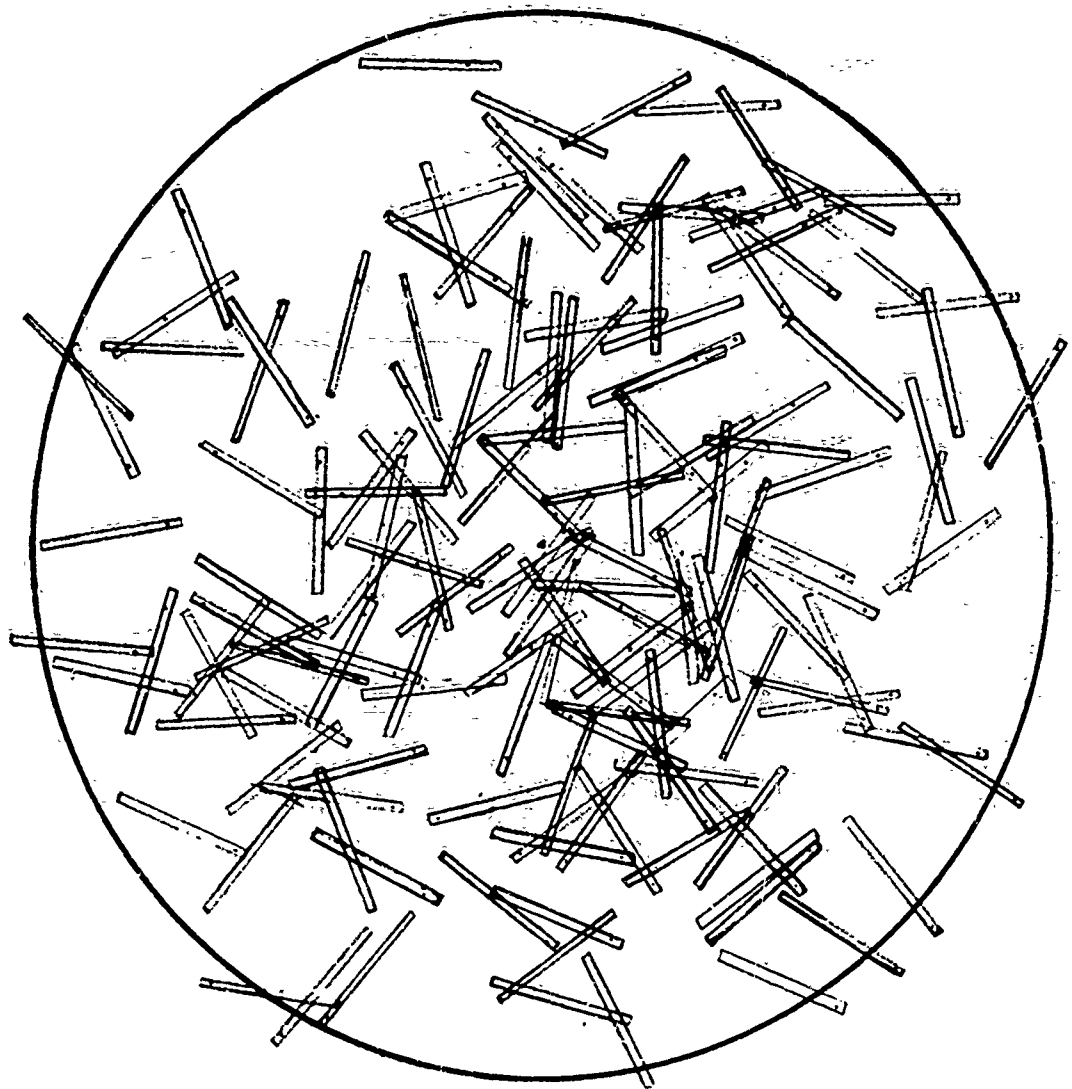
**CASE 1: .0039**  
**CASE 2: .00062**

FIGURE 32.3



*RANDOM TOLERANCES ALL ELEMENTS*

FIGURE 33

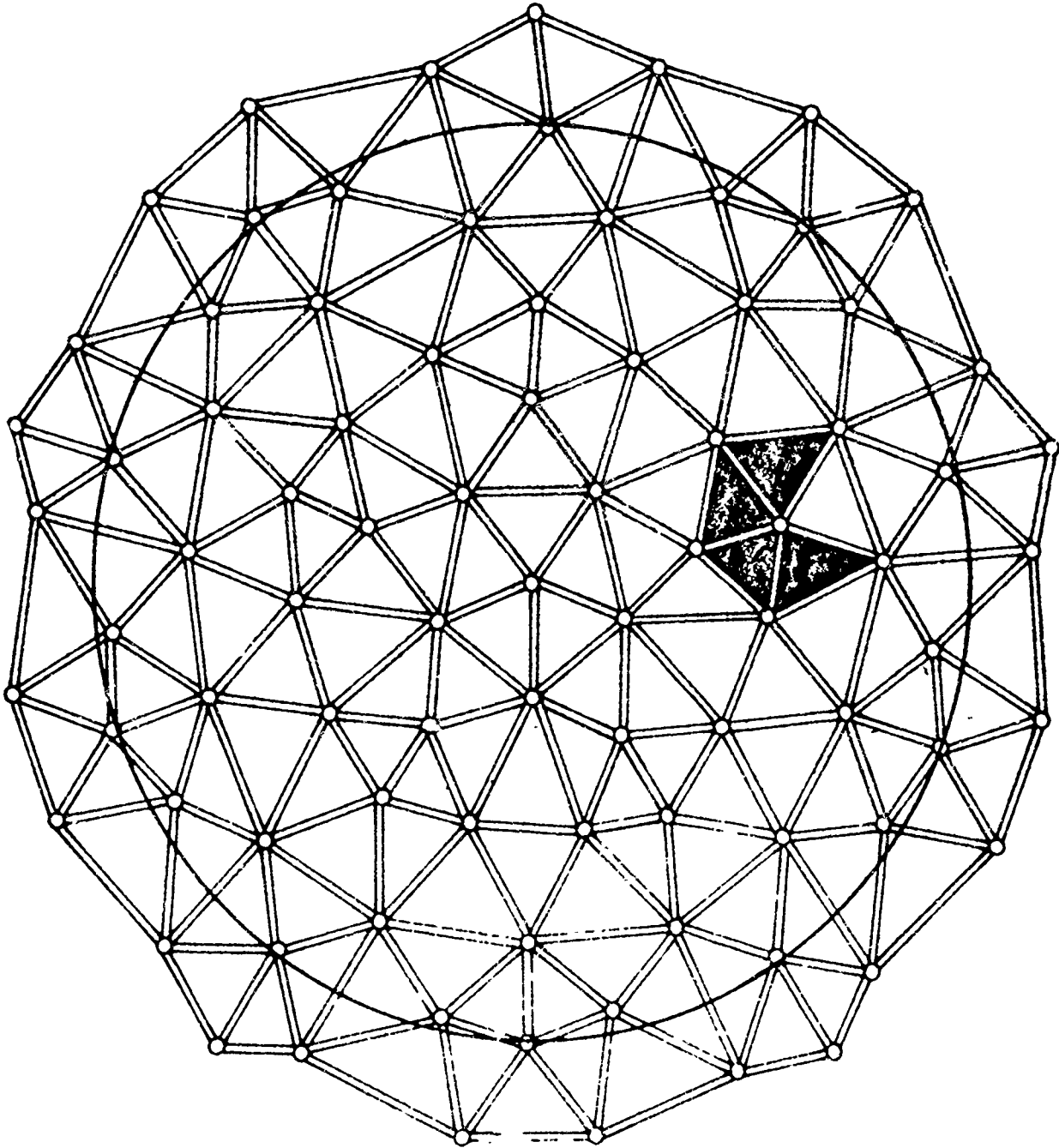


ALL ELEMENTS RANDOM

CASE 1 : .0256 *mr*

CASE 2 : .01485 *mr*

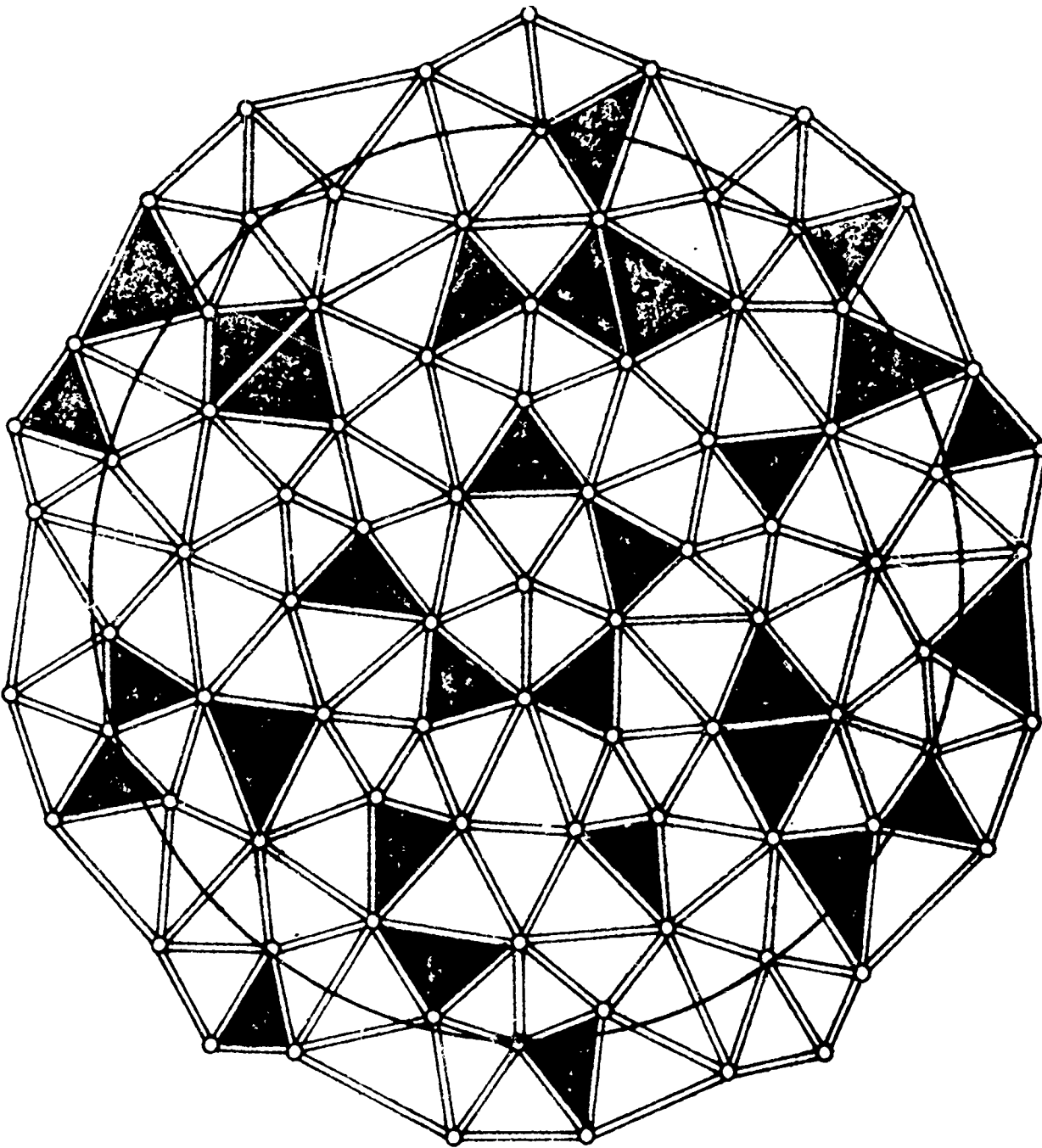
FIGURE 34



ADJACENT WINDOWS WITH EXTREME  
TOLERANCES

CASE 1 : .013 mr  
CASE 2 : .0079 mr  
N = 9

FIGURE 35

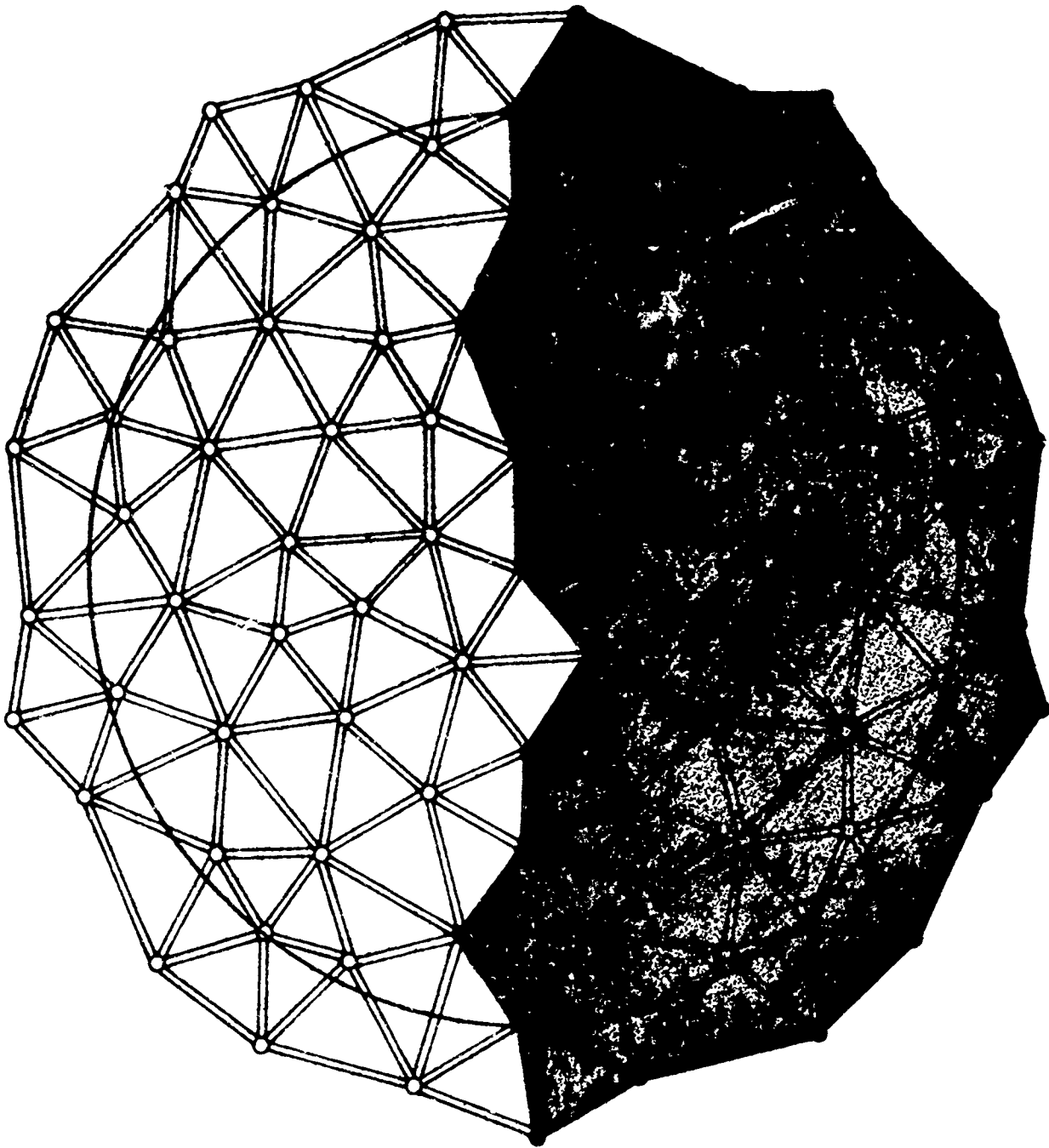


*SOME RANDOMLY PLACED WINDOWS AT  
EXTREME TOLERANCES*

*CASE 1: .0095 TYP*

*CASE 2: .00053 TYP*

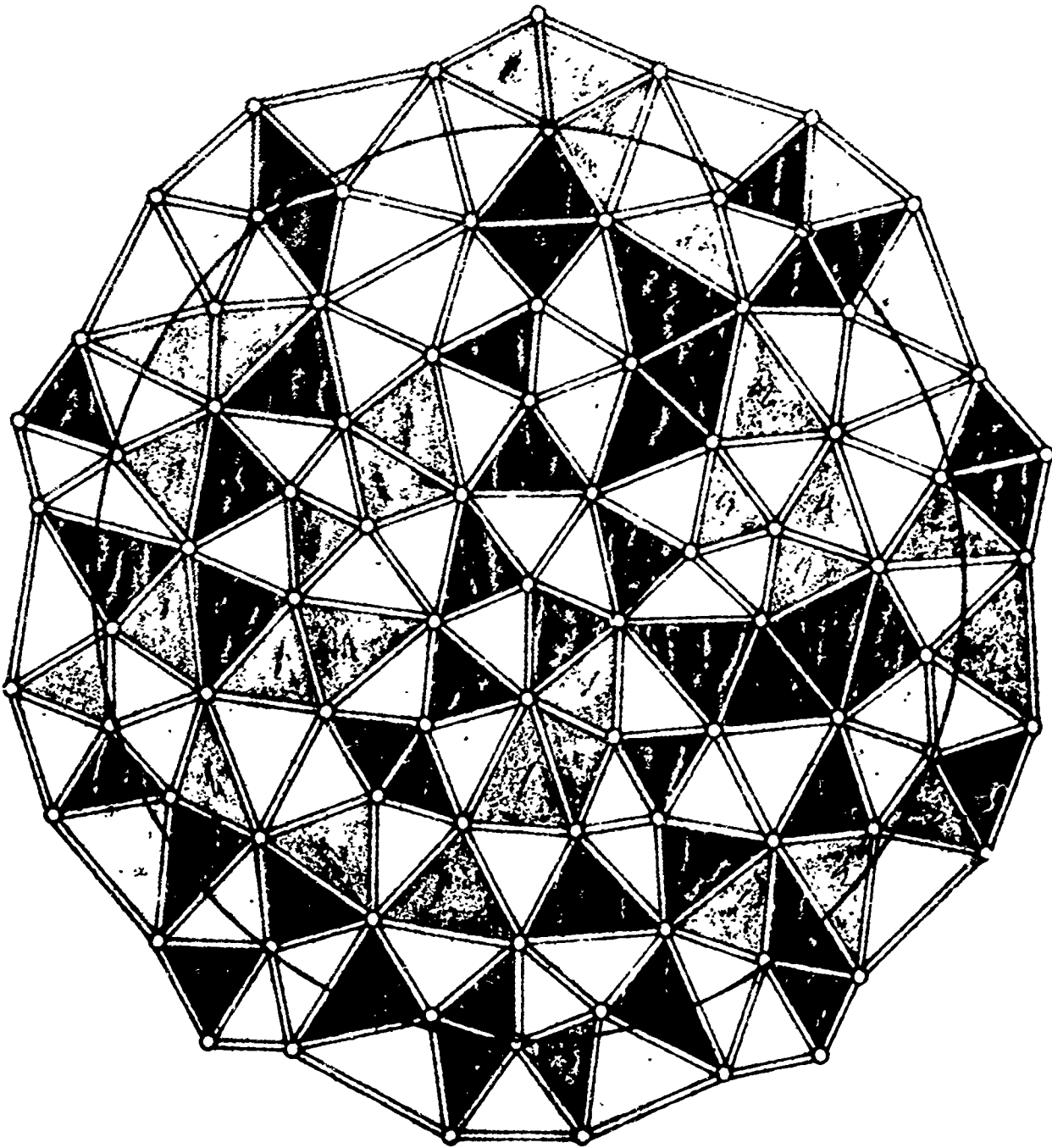
FIGURE 36a



MAXIMUM ERROR DUE TO WINDOW  
TOLERANCES

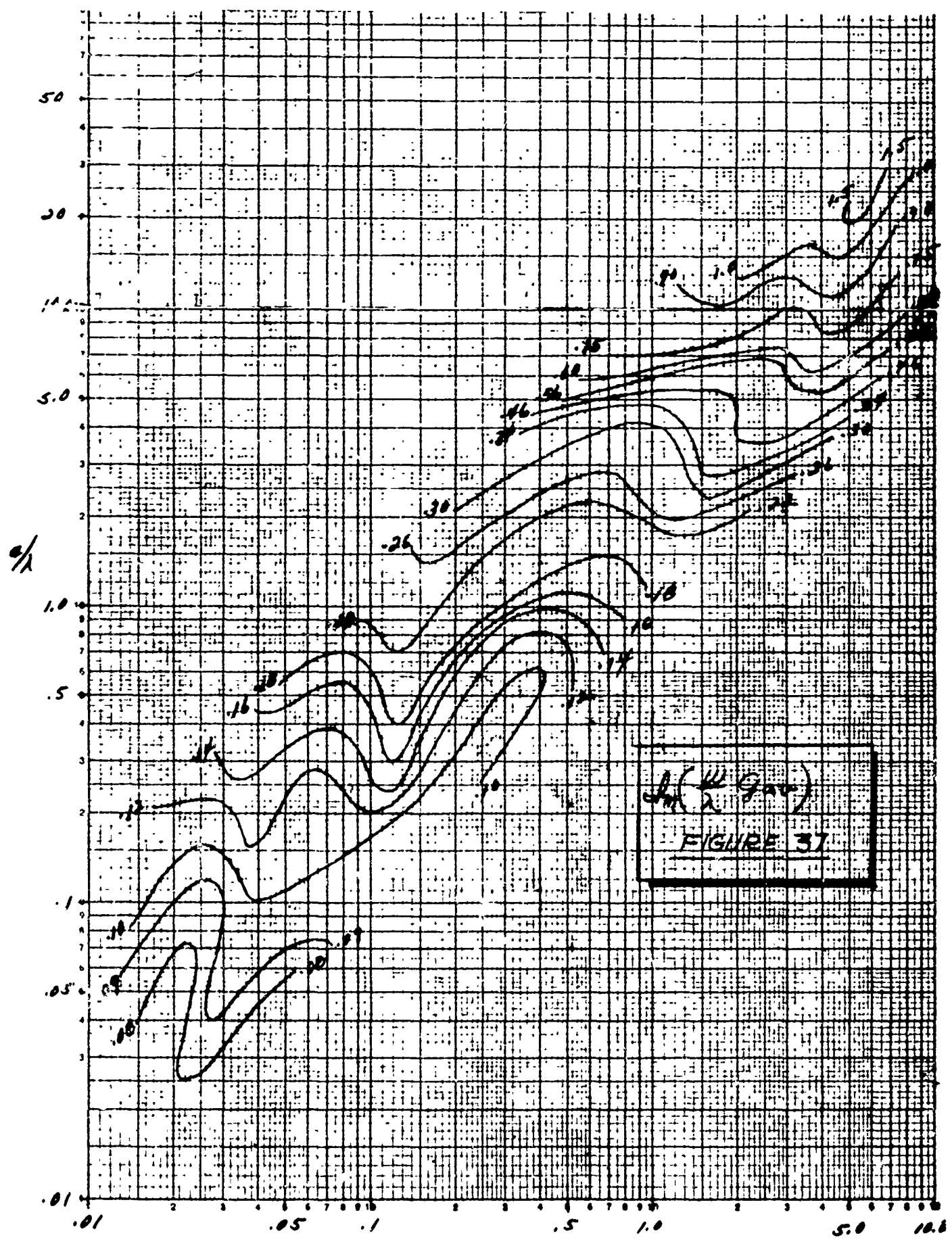
CASE 1: .134 mm  
CASE 2: .022 mm

FIGURE 36b



*Rms ERROR WITH Rms WINDOW  
TOLERANCE*

*CASE 1: .021  $\mu$ r*  
*CASE 2: .0012  $\mu$ r*



The resulting values of boresight shift computed from eqs(14) to (27) are shown directly on the figures, 30 thru 36 as cases 1 and 2.

#### EXPECTED SIDELobe LEVELS DUE TO THE SPACE FRAME

As pointed out in pp. 14-15 of [1] the expected close-in sidelobe level due to the presence of the radome increases even though the expected average field values are unchanged by the radome. A rough formula for the expected increase in close-in relative sidelobe level relative to the peak of the pattern is

$$(28) \quad \frac{27W^3 |g_{av}|^2}{a^2 L},$$

which is derived in the Appendix.

Values of average sidelobe level increases computed by (28) are usually small compared to peak sidelobe increases which may even be an order of magnitude larger. However (28) is useful in showing how the various parameters effect expected sidelobe increase.

Another sidelobe phenomenon often occurs with space frame radomes, namely at some angle(s) far from the main lobe, sidelobe(s) may arise as high or higher than the close-in sidelobes. There are called the diffraction sidelobes, in analogy with diffraction grating effect. Since to the extent that the elements are parallel, equi-spaced and coplanar, i. e. a diffraction grating, these lobes will be higher and more noticeable. At angles out to  $0 \leq \theta \leq \lambda/2L$ ,

the expected field values with the radome are proportional to those without, the proportionality constant being independent of  $\theta$ . Except for the small effect considered above (or, in detail, in the Appendix), the relative sidelobe level with and without the radome in the range  $0 \leq \theta < \lambda/2L$  is the same. If the scattering patterns of the individual elements were isotropic outside of this range and if the scattered fields were randomly, or even better, uniformly, distributed in phase, the energy scattered by the space frame would be scattered essentially isotropically, i. e. uniformly distributed in all space and the far-out sidelobe levels would be well below the isotropic level of the total radiation and hence usually not observable except on an average basis, by sensitive radiometric measurements. However, this is not generally the case and diffraction lobes do arise.

\*

The IBM 7090 program will predict these lobes accurately. However, in order to obtain an approximate formula for rapid calculation of their levels and to see how and to what extent they will occur, we derive here an approximate formula for them.

Suppose  $L$  is the average length of an element, and suppose the direction of propagation is along the  $z$ -axis. Suppose an element is at a distance  $t$  from the axis. The phase  $\Delta$  as observed in direction  $\theta$  of the field incident on the element is

$$(29) \quad \Delta = k(\overline{OB} - \overline{AC}) = kR \sqrt{1 - \left(\frac{t}{R}\right)^2} - kR \cos(\theta - \sin^{-1}\left(\frac{t}{R}\right))$$

\* described in [1]

where  $k = 2\pi/\lambda$ .

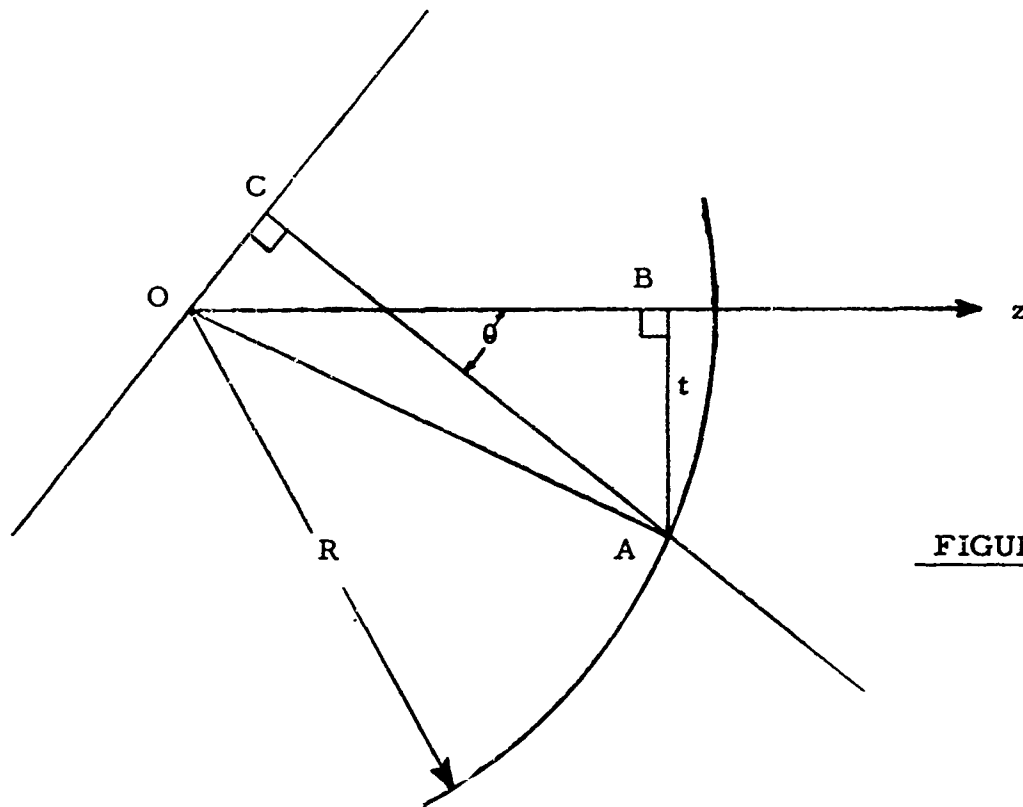


FIGURE 38

Referenced to the axial point  $t = 0$ , this becomes

$$(30) \quad \Delta - \Delta_0 = kR \left( \sqrt{1 - \left(\frac{t}{R}\right)^2} - 1 + \cos \theta - \cos\left(\theta - \sin^{-1}\left(\frac{t}{R}\right)\right) \right).$$

If  $t \ll R$ , this is approximately

$$(31) \quad \Delta - \Delta_0 \approx kR \left( \frac{t}{R} \sin \theta - \frac{t^2}{2R^2} \right) = kt \sin \theta - \frac{kt^2}{2R}.$$

Now if the radome were flat, the last term in (31) would be zero and, it turns

out, (31) would be exact

$$(32) \quad \Delta - \Delta_0 = kt \sin \theta \quad (R = \infty).$$

Hence the last term in (31) is the first order correction term for phase variation of the fields scattered by the elements due to the curvature of the radome.

If  $L$  is the average element length, the average element center to center spacing is about  $L/2$  for a triangulated space frame (see Figure 39).

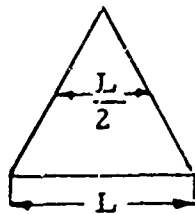


Figure indicates distance between phase centers averages about  $L/2$ .

FIGURE 39

To a first approximation, in the case of a flat radome, from eq(32) a diffraction grating lobe would occur at an angle  $\theta_g$  where

$$(33) \quad \frac{kL}{2} \sin \theta_g = \pi.$$

The curvature correction term in (31) implies that only a certain number of elements near the axis contribute coherently to the grating lobe, those elements, in fact for which  $t$  is less than  $t_0$  where

$$(34) \quad \frac{kt_0^2}{2R} = \pi.$$

Other elements for which  $t$  exceeds the limit set by (34) are essentially incoherent or have random phase. From another point of view, elements with  $t < t_0$  are in the first Fresnel zone for in-phase contribution to the scattered field in direction  $\theta = \theta_g$ .

The gain  $G_s(\theta_g)$  of the scattered field in direction  $\theta = \theta_g$ , equals  $1/\pi$  times the gain of a uniformly illuminated disc of radius  $t_0$  multiplied by the fraction  $\rho |g_{av}|^2$  of the relative effective blocking area of the space frame, multiplied by 2, and finally multiplied by the periodicity factor  $P$

$$(35) \quad G_s(\theta_g) = 8\rho |g_{av}|^2 P \pi \frac{t_0^2}{\lambda^2} \quad (\text{if } t_0 \ll R).$$

The factor 2 is an approximation to the fact that the elements near the center of the aperture are more heavily illuminated than an average element in the aperture because of the antenna illumination taper. The factor  $1/\pi$  is due to the phase error in the first Fresnel zone (which has a max of  $\pi$ , by definition). The validity of the use of this factor is proved in ref[5], p. 15, case  $N = 1$ . The periodicity factor  $P$  is a measure of the parallelness and periodicity of the elements.  $P$  may be defined as follows: Consider the Fresnel zones in the projected dish aperture as observed from the angle  $\theta_g$ . These are parallel strips of width equal to the average periodicity  $\alpha$  of the space frame (approx  $L/2$ ). Let the total element area in the even and odd zones, respectively, be

$$(36) \quad A_e \simeq N_e LW \quad \text{and} \quad A_o \simeq N_o LW$$

where  $N_e$  and  $N_o$  are the numbers of elements in the even and odd zones respectively. Then

$$(37) \quad P = \left| \frac{A_e - A_o}{A_e + A_o} \right|$$

If all of the elements are parallel (diffraction grating) then  $P = 1$  (Figure 40).

If the elements are in a regular rectangular array then  $P = 1/2$  (Figure 41).

If the elements are in a regular triangular array then  $P = 1/3$  (Figure 42).

For a regular hexagonal array in the orientation shown in Figure 43  $P \approx .6$ .

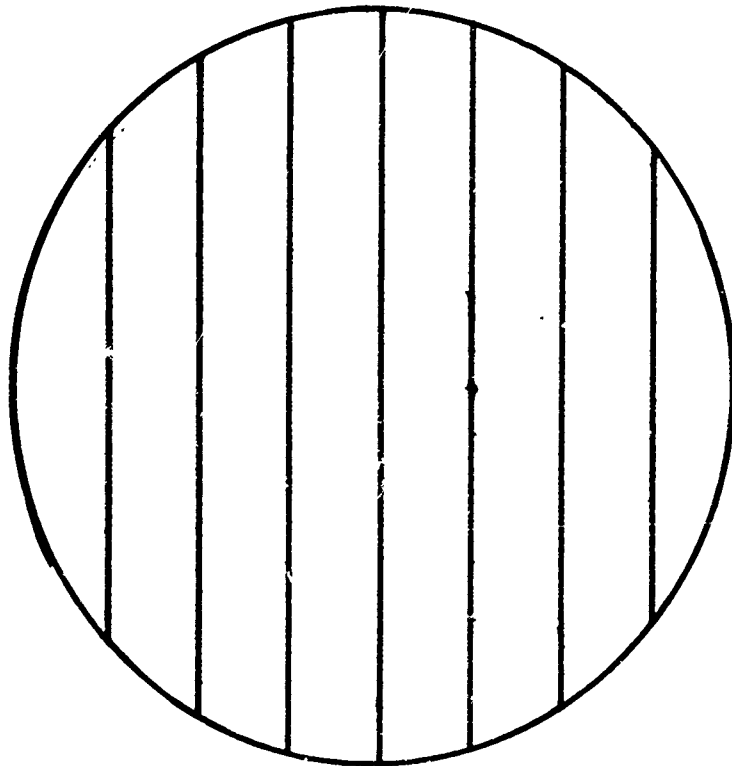
The preceding considerations must be modified if the elements in either the even or odd Fresnel zones have a strongly preferred direction which is not at  $45^\circ$  to the polarization, and if  $|g_\rho|$  is substantially larger than  $|g_t|$ .

For example, in the case of the hexagonal arrays or rectangular arrays, if  $|g_\rho| \gg |g_t|$  and the polarization is parallel to the Fresnel zone boundaries, then  $P$  might be close to unity.

Assuming a 50% aperture efficiency with the radome in place, the gain of the antenna is

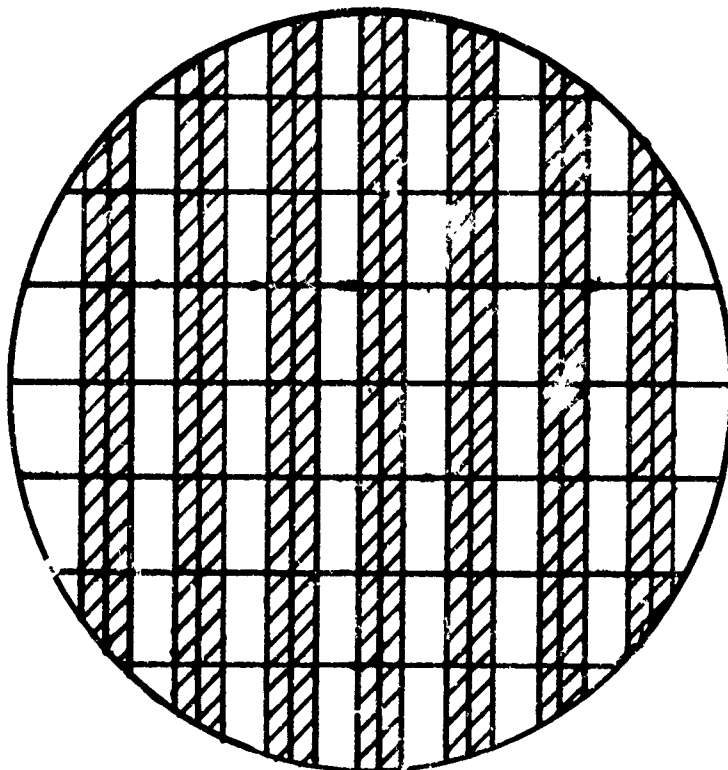
$$(38) \quad G_0 = \frac{1}{2} \left( \frac{t_0}{\lambda} \right)^2 .$$

Combining (34), (35) and (38) gives  $G_s(\theta_g)$  relative to the maximum gain of the antenna.



**Planar  
Diffraction  
Grating**

FIGURE 40



**Rectangular  
Diffraction Grating  
with Fresnel Zones  
Shaded for Diffraction  
Grating Lobe**

FIGURE 41



$$(39) \quad \frac{G_s(\theta_g)}{G_0} = \begin{cases} \frac{16\lambda R}{\pi D^2} P \rho |g_{av}|^2, & \lambda R < D^2 \\ P \rho |g_{av}|^2, & R = \infty \end{cases}$$

We may make a table of maximum grating sidelobe level as observed in the IBM7090 calculations and those predicted by (39) for various cases where the quantity

$$(40) \quad \frac{16\lambda R}{\pi D^2} = .045 = 13.5 \text{ db}$$

Geometry	Element No. Table 1 of [1]	IBM7090 Calc. Max. Diff Lobe (db)	Equation (39)		
			P	$10 \log_{10} \{ \rho  g_{av} ^2 \}$	Max. Diff. Lobe (db)
1) Regular Snub-dodecahedron	52	25.4	.33	7.7	26.0
2) Regular Snub-dodecahedron	6	22.6	.33	5.7	24.0
3) Regular Snub-dodecahedron	53	22.2	.33	5.4	23.7
4) Random Icosahedral	52	34.2	.0058	8.3	34.2

In the regular geometry case, the value of  $P = .33$  was chosen because this geometry is close to a regular triangular case. The agreement in the above table shows that this value of  $P$  is reasonable. The dependence on element shape checks out fairly well. In the random case the value of  $P$  was chosen to make

the two calculations of diffraction lobe level agree. This result shows that the random geometry elements are about five times more uniformly distributed in angle than the elements of the regular geometry

#### COMPARISON OF DIELECTRIC AND METAL STIFFENING RIBS

In the design of a space frame radome, there is always a compromise between structural strength and transmission loss. The question arises as to whether one does better in this tradeoff using a dielectric or metal space frame. In each case we would normally use the highest strength materials available - steel for the metallic space frame and Fiberglas laminate for the dielectric frame. If the transverse dimensions of the elements are comparable to a wavelength, data exists [2] which indicates that the scattering cross section or IFR of metallic and dielectric elements are roughly the same. Since the metal enjoys a considerable strength advantage, there seems little question that in this case the metal is superior. Let us consider the case where the maximum diameter is small compared to a wavelength. In this case, there is no advantage in shaping the metal element, so that we may as well consider it rectangular of width  $W_m$  and depth  $d_m$ . There is even less dependence on shape for scattering by the dielectric element so that we may consider it also a rectangle of width  $W_d$  and depth  $d_d$ . There are two rough criteria for equivalent structural strength of the metal and dielectric elements: equal axial stiffness and equal radial bending stiffness, either of which may apparently govern under different circumstances. These imply respectively.

$$(41) \quad E_m W_m d_m = E_d W_d d_d$$

$$(42) \quad E_m W_m d_m^2 = E_d W_d d_d^2$$

where  $E_m/E_d$  is the ratio of metal to dielectric Young's modulus, which in our case is about 15. Let us use (41). We have then equivalent elements satisfying

$$(43) \quad W_d d_d = 15 W_m d_m = A_d$$

where  $A_d$  is the section area of the dielectric. If (42) were used instead, very little difference would be found in the general results which follow.

We may use the results of Mei and Van Bladel<sup>[3]</sup> to compare the two structurally equivalent elements electrically. At transverse polarization, from Figures 5 and 6 and eq(7) of [3], we observe that for both metal and dielectric the narrow dimension should be transverse to the direction of propagation for best results, i. e.  $W \leq d$ , so that Figure 6 is appropriate. It can be observed that typically  $\alpha_2$  is about twice as large for metal as for dielectric with the Fiberglass dielectric constant ( $\approx 4$ ) and that the term  $2S^2$  in eq(7) is about equal to or smaller than the term  $a^2/\epsilon_0^2$  for metal. Accordingly the scattering cross section ratio  $\sigma_m/\sigma_d$  for elements with the same dimensions is about 4 or 5. But both  $\sigma_{rn}$

and  $\tilde{\sigma}_d$  are proportional to the square of the section area in wavelengths, and hence for structurally equivalent elements satisfying (43) the ratio is

$$(44) \quad \frac{\tilde{\sigma}_m}{\tilde{\sigma}_d} \simeq \frac{4 \text{ or } 5}{15^2}.$$

Thus the metal is superior electrically by about 50 to 1.

In the case of parallel polarization the situation is different. The asymptotic formula (10) of [3] can not be used since it becomes inaccurate in the range of interest (indeed, blows up when the perimeter of the metal rectangle is  $\lambda/2\pi$ ). However, from [4] eqs(15) and (16), we may relate the IFR at longitudinal polarization,  $g_\ell$ , to  $\sigma_m$  as

$$(45) \quad \sigma_m = k |g_\ell W_m|^2, \quad k = \frac{2\pi}{\lambda}.$$

From eq(11) of [3], with a dielectric constant of  $\epsilon$  in this case,

$$(46) \quad \sigma_d = \frac{(\epsilon-1)^2 k^3 A_d^2}{4}$$

and from (43), (45) and (46)  $\sigma_m \leq \sigma_d$  if

$$(47) \quad k |g_\ell W_m|^2 \leq \frac{(\epsilon-1)^2 k^3 225 W_m^2 d_m^2}{4}$$

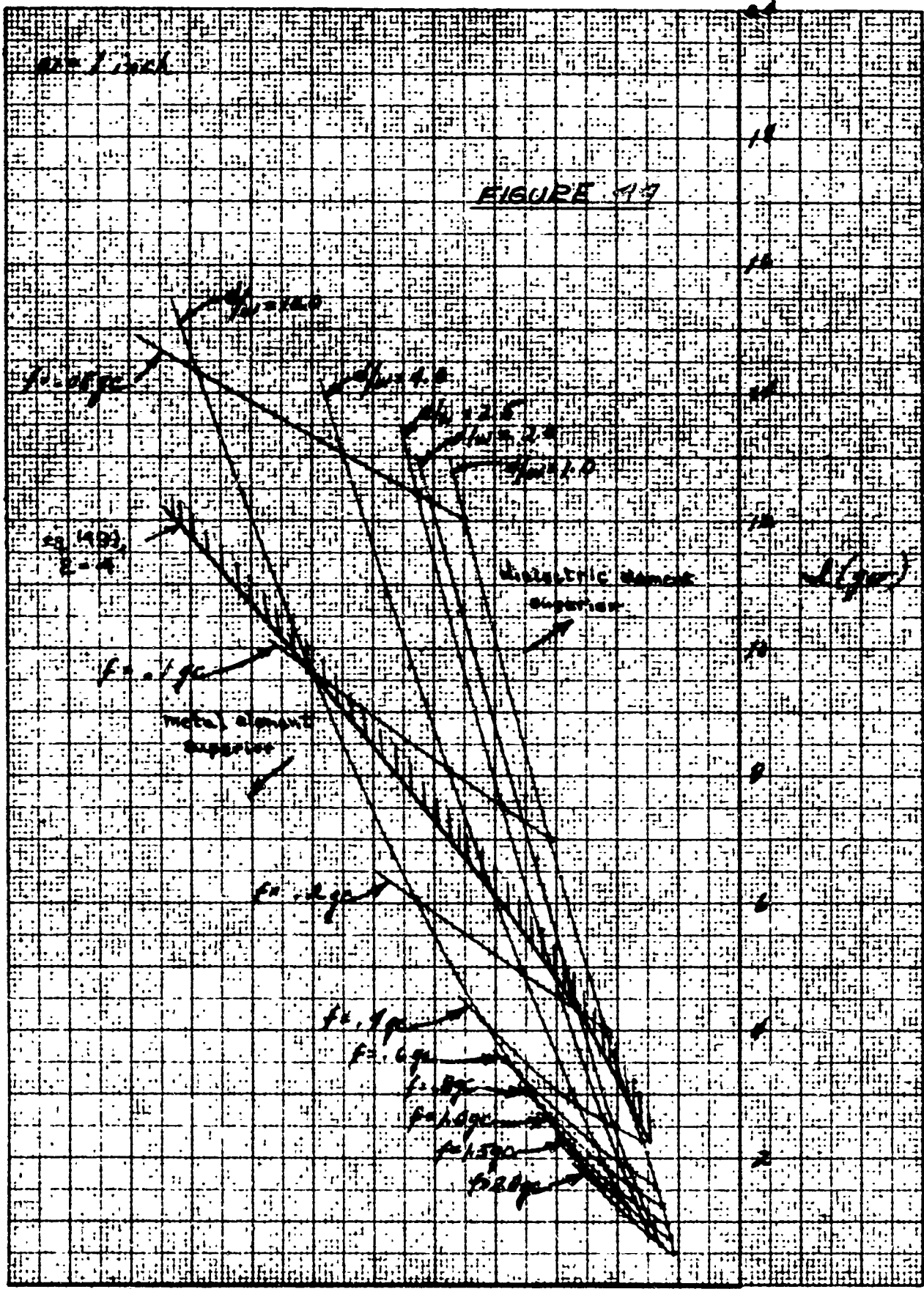
or

$$(48) \quad |g_{\ell}| \leq \frac{15(\epsilon-1)kd_m}{2}$$

In Figure 44  $g_{av}$  is plotted for various  $W_m$ ,  $d_m$  and frequencies. Where equality holds in (48)  $|g_t|$  is much smaller than  $|g_{\ell}|$  and hence

$$(49) \quad |g_{av}| \simeq \frac{1}{2}|g_{\ell}| \leq \frac{15(\epsilon-1)kd_m}{4} .$$

We have plotted where equality in (49) holds in Figure 44 for the case  $\epsilon = 4$ .



-10    -8    -6    -4    -2    0  
 R(gaw) 60

## PART II - STRUCTURAL DESIGN AND OPTIMUM ELECTRICAL- STRUCTURAL DESIGN

### SUMMARY

The object of this project was the construction of a systematic procedure, amenable to simple calculation, for the optimization of large space frame radome design. Consideration of three design aspects (electrical, structural, and mechanical) formed the basis of the optimization procedure. Specific attention was directed to radomes of 140-160 feet in diameter used with RF systems radiating within a 200-500 mc band.

The project study involved three phases: (1) the application of an electrical performance evaluation technique to predict radome transmission loss, (2) a survey of the radome literature for structural analysis and mechanical design concepts, and (3) the consolidation of pertinent design considerations into a design procedure for an optimum radome within practical limitations.

The evaluation of the electrical performance of a space frame radome involved the prediction of the transmission loss due to scattering effects caused by induced currents on the elements of the blocking structure. The theory relates the gain of the radome to the cross sectional shape and length of the space frame elements. A specification of the maximum allowable reduction in gain fixes a holonomic relationship between the width, depth and length of the elements. This relationship was defined as the electrical constraint on the radome element design.

The accumulation and survey of the pertinent literature (see Bibliography) was a prerequisite to the formulation of a suitable structural constraint on the

element design. In the literature is provided a complete structural design guide [6] for the sizing of the radome elements which lacks the inclusion of any electrical constraint. Therefore, it is not possible to quantitatively discriminate the degree of compromise inherent in a particular design between electrical performance and structural integrity. This is not a satisfactory design condition if optimization is the objective. It was concluded that the simultaneous imposition of an electrical and structural constraint on the analysis of the elements would constitute the design approach.

In addition to the literature survey, consultation with several radome developers and manufacturers was conducted. The consultations included personnel of Lincoln Laboratory, Bell Telephone Laboratory, Goodyear Aircraft, North American Aviation, and M. I. T.

Other efforts in space frame radome development are being directed toward hardening against nuclear blast induced dynamic loads. This concept is not considered in the subject study which directs attention to static load conditions consistent with normal environments. The significance of the hardened radome development to this study exists in the fact that substantiation of the general shell analogy concept of analysis has continuously precipitated. If advances in fundamental design procedures exist, they are apparently numerical in nature. The STRESS(MIT) and STAIR (LL) routines are examples of digital computer programs for analyzing space frame structures of high order. The matrix theory of structural analysis provides a powerful computational tool but is limited by computer capacity and as yet programs have not been composed

which display general design capability. Since the project specifications require a design procedure propitious to hand or simple machine calculation, the equivalent shell analysis was adopted for the optimization procedure rather than alternatively pursuing advanced computer program development.

The formulation of a structural constraint consisted of comparing the criteria of strength and stability of the space frame which assures the integrity of the structure. The criterion which imposes the most severe design conditions was selected as the structural constraint.

The concept of optimum radome design requires the definition of a criterion by which comparison of selected designs can be made. There are many criteria relative to which good design principles can be directed. Two such examples are: (1) the minimization of transmission loss subject to a structural constraint, and (2) reduction of structural weight in conjunction with an electrical and structural constraint. Examples of these two approaches are developed later in this report. The problem of producing the best radome design within practical limitations cannot be solved by a single direct analytic approach. It is first necessary to select the element size subject to an optimization criterion and second to generate sound mechanical design. This study is predominantly concerned with the optimum sizing of elements and includes some recommendations and goals for the ensuing mechanical design effort.

#### ELECTRICAL CONSTRAINT ON THE ELEMENT

For the purpose of optimum design of a radome over the 200-500 mc band, we may write eq(4) of Part I as

$$10 \log_{10} G = \frac{1}{L} \left\{ 39.5W + 3.5d + \frac{.147d\lambda}{W} \right\} , \quad \text{db}$$

if we neglect the curvature term which is usually small at lower frequencies. This is tantamount to observing that at the low frequency end, the curves of Figures 7 to 10 are almost independent of  $\theta$ . With this approximation it is clear that the loss is greatest at the lowest frequency in the band. Setting  $\lambda = 61''$  (194 mc) and  $10 \log_{10} G = .5$  we may write an electrical constraint, such that for any radome satisfying

$$L \geq 79W + 7d + \frac{18d}{W}$$

with all dimensions in inches, the loss will be less than .5db.

## STRUCTURAL ANALYSIS OF SPACE FRAME

### A. External Loads

It is recognized that the most significant load modalities on a spherical radome are those associated with kinetic energy of the incident wind and the structural weight. Ice and snow loads are of minor magnitude and experience indicates that snow and ice build-up seldom occurs on large radomes.

The analytic representation of the wind pressure distribution adopted for the structural analysis was that based on the potential flow theory. A polynomial representation of the pressure distribution [9] ascertained from wind tunnel data is more realistic than the distribution of the potential flow theory,

but, since little deviation between the two formulations exists on the windward side of the radome and significant difference exists in the case of application to the shell equations the potential flow representation was accepted. The fact that buckling stability is critical only on the compressive or windward side of the radome where the two representations agree (see Figure 1) helps justify the choice. Figure 1 illustrates the variation in magnitude of the two formulations for typical wind tunnel data. [7]

### B. Structural Analysis

The equations which establish the conditions for stability and strength of the radome were developed by applying classical theory of elasticity to a spherical isotropic shell of structural equivalence to the radome space frame. This technique is well defined in the literature [6] and was closely followed in the development of a structural design constraint.

The conversion of the radome to an equivalent shell requires two independent equivalences, elastic and stress. The elastic equivalence is stated by equating the extensional and flexural stiffness of the radome to that of the shell. This is represented as:

$$(1) \quad E_R I_R = E_S I_S$$

$$(2) \quad E_R A_R = E_S A_S$$

The stress equivalence is required due to the inherent difference in elastic behavior of a space frame compared to a shell. The stress equivalence

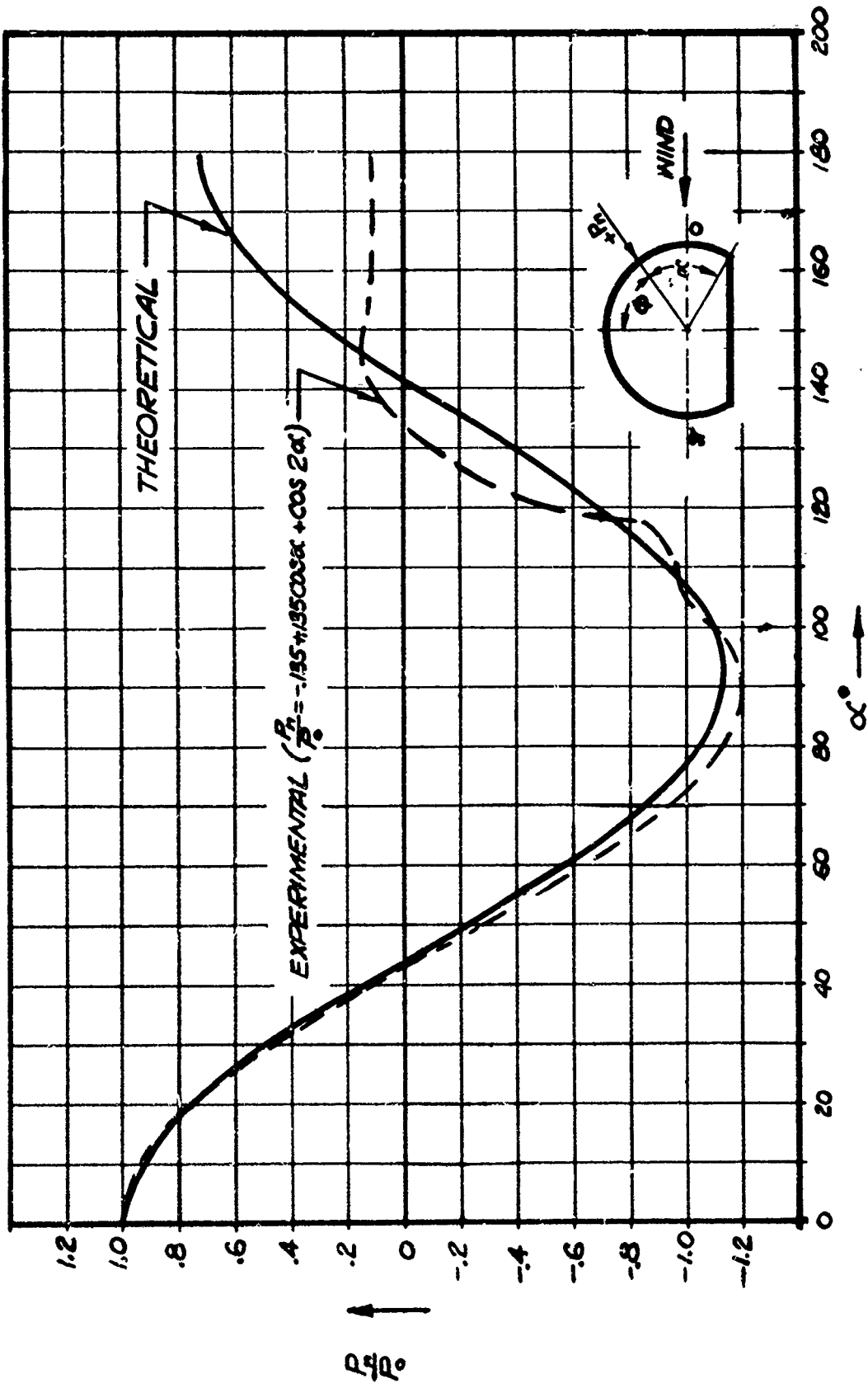


**Fig. 1**  
**EXPERIMENTAL AND THEORETICAL WIND LOAD DISTRIBUTION**  
**ALONG ANY MERIDIAN [REF FIG. 7]**

relationship equates the cross sectional area of an element to a comparative cross sectional area of shell. If a large number of elements make up the radome structure the equivalence condition is satisfied when the volume of the shell is one-half the volume of the space frame, [7] or for elements of rectangular cross section.

$$(3) \quad 4\pi R^2 t_S = \frac{1}{2} w d \sum_i^N L_i .$$

Then, since the element resists the same stress as some equivalent section of shell

$$(4) \quad w d = S t_S .$$

The equations expressing the equivalent shell thickness and modulus of elasticity are

$$(5) \quad t_S = \sqrt{\mu} d$$

$$(6) \quad E_S = \frac{E_R w}{\sqrt{\mu} S} .$$

In order to apply these equations the effective spacing must be derived

in terms of the radome parameters. This was done by letting M equal the number of panels making up the surface of the radome and N equal to the total number of elements. If the space frame is considered to be a triangulated structure typical of radomes with random or regular geometries then  $3M = 2N^*$  and the area of an individual panel equals

$$(7) \quad A_p = \frac{6\pi R^2 k}{N}$$

where k is a constant accounting for the truncation of the sphere. The value of k is expressed as the ratio of areas of a truncated to complete sphere and is:

$$(8) \quad k = \frac{1 - \cos \phi_0}{2}$$

where  $\phi_0$  is the meridional angle to the radome base. The average panel area was also expressed in terms of the average element length and is

$$(9) \quad A_p \leq \frac{\sqrt{3}}{4} L^2$$

depending on the radome geometry. Since the larger  $A_p$  is the more conservative the design must be. Equation(9) was taken as an equality. Equating equations (7) and (9) and solving for the total length of elements gives

---

\* This is exact only for a non-truncated radome. For small truncated radomes it is an approximation.

**MERIDIONAL ANGLE  $\phi$  AND CIRCUMFERENTIAL ANGLE  $\theta$  RELATIVE TO RECTILINEAR COORDINATES**

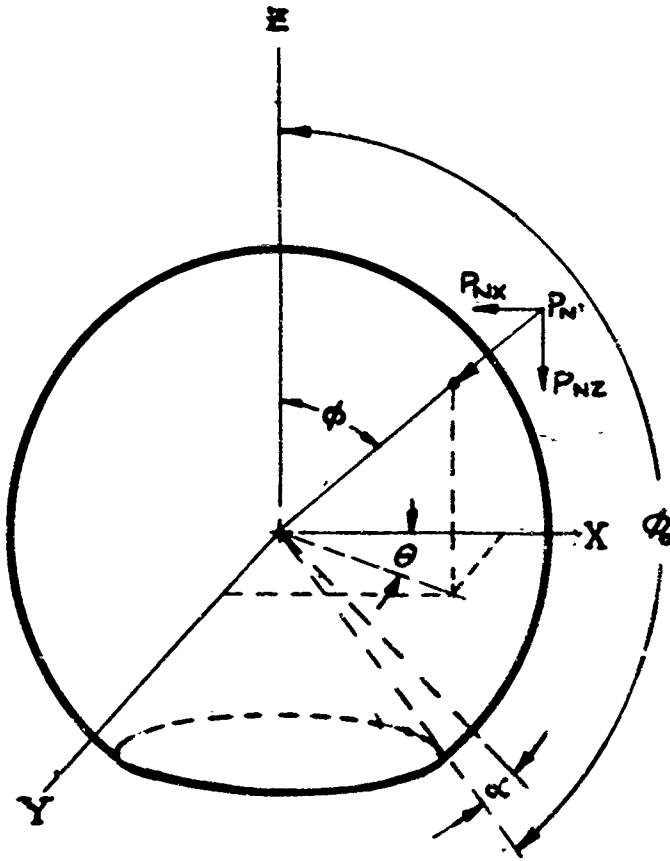


**FIG. 2**

$$(10) \quad NL = \frac{24\pi R^2 k}{\sqrt{3}L} .$$

The effective spacing,  $S$ , was expressed by combining the equivalent stress equations (3) and (4) such that

$$(11) \quad S = \frac{wd}{t_S} = \frac{8\pi R^2}{N \sum_i L_i} \quad \text{and substituting}$$

for the total length of elements gives

$$(12) \quad S = \frac{8\pi R^2}{(N-1)L} = \frac{2\sqrt{3} L}{3(1-\cos \phi_0)} .$$

The elastic equivalence relations were then written as

$$(13) \quad t_S = \sqrt{\mu} d$$

$$(14) \quad E_S = \frac{3E_R (1-\cos \phi_0) w}{2\sqrt{3\mu} L} .$$

The general buckling stability of the radome was evaluated by applying the Tsien-VonKarman equation [2] to the equivalent spherical shell. Substitution of the equivalence relations into the buckling equation defines a critical

buckling pressure in terms of the element dimensions which is

$$(15) \quad P_{cr} = \frac{3KE_R \mu (1 - \cos \phi_0) w d^2}{2\sqrt{3\mu} R^2 L}$$

The axial stress developed in the space frame elements was evaluated by applying the general membrane theory of shells. The partial differential equations of equilibrium for the equivalent shell subjected to a wind pressure distribution are

$$(16) \quad R \frac{\partial}{\partial \phi} (\sin \phi N_{\phi}) + R \frac{\partial}{\partial \theta} (N_{\phi\theta}) - RN_{\theta} \cos \phi = 0$$

$$(17) \quad R \frac{\partial}{\partial \phi} (\sin \phi N_{\phi\theta}) + R \frac{\partial}{\partial \theta} (N_{\phi}) + RN_{\phi\theta} \cos \phi = 0$$

$$(18) \quad N_{\phi} + N_{\theta} = -P_0 R \sin \phi \cos \theta$$

where the angles  $\phi$  and  $\theta$  are defined in Figure 2. These equations have the general solutions [3]

$$(19) \quad N_{\phi} = \frac{\cos \theta}{\sin^3 \phi} \left[ \frac{C_1 + C_2}{2} + \frac{C_1 - C_2}{2} \cos \phi + P_0 R (\cos^2 \phi - \frac{1}{3} \cos^4 \phi) \right]$$

$$(20) \quad N_{\phi\theta} = \frac{\sin \theta}{\sin^3 \phi} \left[ \frac{C_1 - C_2}{2} + \frac{C_1 + C_2}{2} \cos \phi + P_0 R (\cos \phi - \frac{1}{3} \cos^3 \phi) \right]$$

$$(21) \quad N_\theta = - \left[ N_\phi + P_0 R \sin \phi \cos \theta \right].$$

In order to obtain unique solutions for the stress resultants ( $N_\phi$ ,  $N_\theta$ ,  $N_{\phi\theta}$ ) equations (19) and (20) were made to satisfy two boundary conditions and the integration constants  $C_1$  and  $C_2$  were determined.

The first boundary condition was that the external moment about an axis in the plane of the radome base and normal to the wind vector must be equal to the moment due to the internal reaction forces of the shell about the same axis. Since the axis is in the plane of the base the only stress resultant contributing to the reaction moment is  $N_\phi$ .

The external moment is caused by the  $x$  component of the normal wind pressure (see Figure 2) and is equal to

$$(22) \quad M_e = \int_0^{2\pi} \int_0^{\phi_0} P_0 R^3 \cos \phi_0 \sin^3 \phi \cos^2 \theta \, d\phi \, d\theta.$$

The reaction moment due to the meridian stress resultant at the base ( $N_{\phi_b}$ ) equals

$$(23) \quad M_i = \int_0^{2\pi} R^2 \sin^3 \phi_b N_{\phi_b} \cos \theta \, d\theta$$

where  $N_{\phi_b}$  indicates the stress resultant evaluated at the radome base. Integrating and equating the two expressions gives the following equation which satisfies the first boundary condition

$$(24) \quad \frac{N_{\phi_b}}{\cos \theta} = \frac{1}{3} P_0 R \cos \phi_b [2 - \cos \phi_b (\sin^2 \phi_b + 2)] .$$

The second boundary condition was that the total horizontal external force be equal to the total horizontal reaction at the radome base. Two stress resultants contribute to the horizontal reaction,  $N_{\phi}$  and  $N_{\phi_0}$ . The total horizontal external force equals

$$(25) \quad F_{xe} = \int_0^{2\pi} \int_0^{\phi_b} R_0 R^2 \sin^2 \phi \cos^2 \theta \, d\phi \, d\theta .$$

The total horizontal reaction at the base equals

$$(26) \quad F_{xi} = R \sin \phi_b \int_0^{2\pi} N_{\phi_b} \sin \theta \, d\theta + R \sin \phi_b \cos \phi_0 \int_0^{2\pi} N_{\phi_b} \cos \theta \, d\theta$$

where the stress resultants  $N_{\phi_0}$  and  $N_{\phi}$  are evaluated at the radome base.

Integrating and equating the two expressions gives the following equation which satisfies the second boundary condition.

$$(27) \quad \left[ \frac{N_{\phi_b}}{\cos \theta} \cos \phi_b + \frac{N_{\phi_b \theta}}{\sin \theta} \right] \sin \phi_b = \frac{1}{3} P_0 R [2 - \cos \phi_b (\sin^2 \phi_b + 2)] .$$

The simultaneous solution of equations (24) and (27) provide the solution for the integration constants as a function of the meridian base angle  $\phi_b$ . One-half the sum and difference of the integration constants are plotted in Figure 3.

A secondary axial stress is developed in the equivalent shell due to the weight of the structure. The equilibrium equations for a spherical shell subject to a uniform gravity load are

$$(28) \quad R \frac{\partial}{\partial \phi} (\sin \phi N_{\phi}) + R \frac{\partial}{\partial \theta} (N_{\phi\theta}) - RN_{\theta} \cos \theta = t_S \cos \phi$$

$$(29) \quad R \frac{\partial}{\partial \phi} (\sin \phi N_{\phi\theta}) + R \frac{\partial}{\partial \theta} (N_{\phi}) + RN_{\phi\theta} \cos \theta = 0$$

$$(30) \quad N_{\phi} + N_{\theta} = \rho t \sin^2 \phi \cos \theta .$$

The solution of these equations for the stress resultants are given as [4]

$$(31) \quad N_{\phi} = - \frac{\rho R t_S}{1 + \cos \phi}$$

$$(32) \quad N_{\phi\theta} = 0$$

**SUM AND DIFFERENCE OF THE INTEGRATION  
CONSTANTS FOR THE SOLUTIONS OF THE EQUILIBRIUM  
EQUATIONS OF A MEMBRANE SHELL SUBJECT TO  
WIND PRESSURE**

$$\underline{P_n = P_0 S \ln \phi \cos \Theta}$$

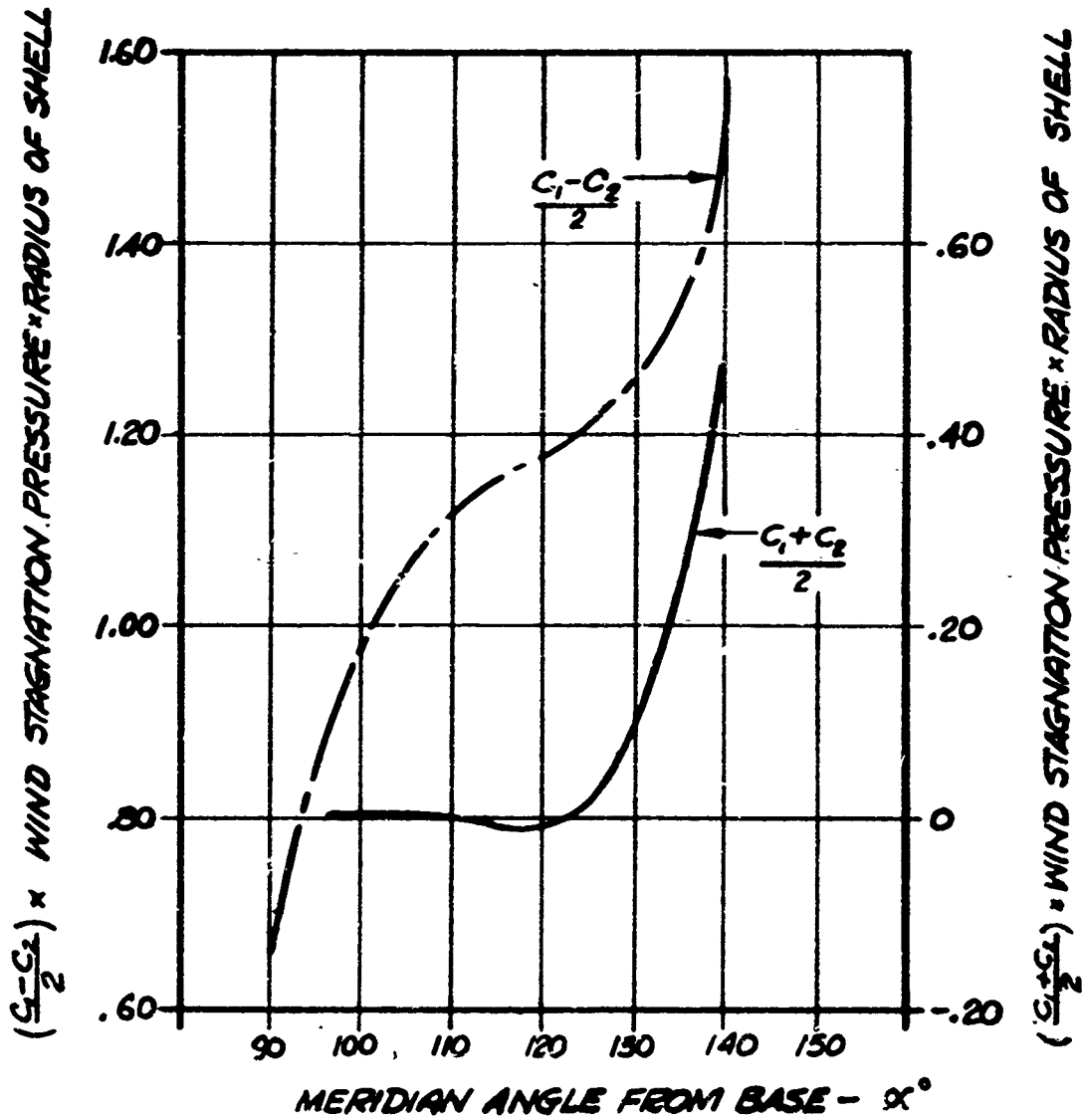


**FIG. 3**

$$(33) \quad N_{\theta} = \rho R t_S \left[ \frac{1}{1 + \cos \phi} - \cos \phi \right]$$

The total axial stress resultants are equal to the combination of each component due to the external loads of wind pressure and structural weight.

The axial stress that the space frame elements must sustain is related to the stress resultants produced in the equivalent shell. The maximum element stress consists of the product of the effective spacing of the elements and the maximum compressive stress resultant divided by the cross sectional area of the element, or

$$(34) \quad \sigma_{\max} = \frac{2\sqrt{3}(N_{\max})L}{3(1 - \cos \phi_b)wd}$$

The maximum compressive stress resultant exists at the wind stagnation point where  $\theta = 0$  and  $\phi = \pi/2$ . The general stress resultant equations simplify to

$$(35) \quad N_{\phi_{\max}} = \frac{1}{2}(C_1 + C_2) - \rho R t_S$$

$$(36) \quad N_{\theta_{\max}} = -\frac{1}{2}(C_1 + C_2) - P_0 R + \rho R t_S$$

$$(37) \quad N_{\phi_0} = 0$$

at the stagnation point and become the principle axial stress resultants.

The wind pressure distribution on the surface of the radome transmits a transverse force to the individual elements. This force distribution on the elements causes flexure stress to be developed in addition to the axial stress expressed in equation(34). In analyzing the flexure stress, the transverse force distribution was assumed triangular with a maximum unit force located at mid-span. A distribution was assumed in order to eliminate contention with the elasticity of the dielectric panels and the consideration of elastic foundation theory.

The magnitude of the transverse force distribution was defined such that the total maximum force resisted by the element equalled two-thirds of the total external force applied to the entire panel. The distribution varies from zero at the ends of the element to a maximum at mid-span and was expressed as

$$(38) \quad q = \begin{cases} \sqrt{3}P_0x, & 0 < x < \frac{L}{2} \\ \frac{\sqrt{3}}{2}P_0L - \sqrt{3}P_0(x - \frac{L}{2}), & \frac{L}{2} < x < L. \end{cases}$$

The maximum flexure stress developed from simple beam theory for a condition element end fixity equals:

$$(39) \quad \sigma_{f \max} = \frac{6M_{\max}}{wd^2} = \frac{\sqrt{3}}{16} P_0 \frac{L^3}{wd^2} .$$

The design criterion adopted which governs the selection of element dimensions when combination of column (axial compression) and beam (flexure) loading occurs, was such that the sum of the ratios of actual to allowable axial and flexure stress be equal to or less than unity. [10] The allowable flexure stress at the outer fiber of the element was chosen to be the material yield stress and the allowable axial stress was defined as the critical Eulu buckling stress. The design criterion was expressed as

$$(40) \quad \frac{\sigma_{f \max}}{\sigma_{yp}} + \frac{\sigma_{\max}}{\sigma_{cr}} \leq 1$$

which upon the substitution of the maximum flexure stress equation (39) and Eulu's critical stress equation (40) becomes

$$(41) \quad \frac{\sqrt{3}P_0L^3}{16\sigma_{yp}wd^2} + \frac{2\sqrt{3}(N_{\max})L^3}{R^2E_R(1-\cos \phi_b)wd^3} \leq 1 .$$

The development of equations (15), (39), and (41) completes the derivation of the structural design constraints. The constraint equations were developed within the framework of simple beam theory and the shell membrane theory. It is shown in ref [3] that the ratio of membrane stress to bending stress is small. Therefore, the assumption that the radome equivalent shell

behaves like a membrane is valid, provided that the base edge of the radome is free to expand. However the base of the radome is fixed by a restraining ring causing a discrepancy in the boundary conditions. This situation is rectified by superimposing a distributed moment around the edge of the shell of such a magnitude that the membrane displacements are made to vanish. The addition of a reaction moment to the base results in an increase of stress in the neighborhood of the base and element reinforcement design is required to accommodate this condition.

The calculation of the reaction moments at the radome base requires consideration of the general theory of bending in shells. A formulation and solution of this problem is available in ref [3], section 130, which gives two particular equations

$$(42) \quad \delta_{\phi_b} = \frac{2Z^2 \sin \phi_b}{E_S t_S} M_{\phi_b} - \frac{2RZ \sin^2 \phi_b}{E_S t_S} H$$

$$(43) \quad \psi_{\phi_b} = - \frac{4Z^3}{RE_S t_S} M_{\phi_b} + \frac{2Z^2 \sin \phi_b}{E_S t_S} H$$

where  $\delta_{\phi_0}$  and  $\psi_{\phi_0}$  are the displacement and rotation of the radome edge and  $M_{\phi_0}$  and  $H$  are the reaction moment and force at the radome edge.

$$(44) \quad Z^4 = 3(1-\mu^2) \left( \frac{R}{t_S} \right)^2 .$$

In order to utilize these equations for the solution of the reactive moment at the base the displacement at the base must be evaluated.

The computation for the displacement is greatly simplified if the external loading is assumed symmetrical. Therefore a modified external load is imposed on the radome to facilitate the calculation of the reaction moment. The loading is assumed to be a combination of a uniform normal pressure equal in magnitude to the wind stagnation pressure and a uniform structural weight.

The displacement is shown in the ref[3] to be equal to

$$(45) \quad \delta_{\phi_b} = \frac{R \sin \phi_b}{E_S t_S} (N_{\theta} - \mu N_{\phi}) \phi_b$$

where

$$(46) \quad N_{\phi} = -\left(\frac{P_0 R}{2} + \frac{QR}{1 + \cos \phi_b}\right)$$

$$(47) \quad N_{\theta} = -\left[\frac{P_0 R}{2} + QR\left(\cos \phi - \frac{1}{1 + \cos \phi}\right)\right].$$

By substitution of equations(46) and (47) into equation (45) the displacement becomes

$$(48) \quad \delta_{\phi_0} = -\frac{R \sin \phi_b}{E_S t_S} \left[ \left(\frac{P_0 R}{2} + \frac{QR}{1 + \cos \phi_b}\right)(1 - \mu) + QR \cos \phi_b \right].$$

The boundary conditions of radome base consist of requiring the rotation to equal zero and the displacement to be equal and opposite of  $\delta_{\phi_b}$ . Therefore by setting  $\psi_{\phi_0}$  equal to zero and substituting equation (48) into equation (42) the reaction at the radome base was evaluated directly and equals

$$(49) \quad M_{\phi_b} = - \frac{Rt_S}{2\sqrt{3(1-\mu^2)}} \left[ \left( \frac{P_0}{2} - \frac{Q}{1 - \cos \phi_b} \right) (1-\mu) + Q \cos \phi_b \right].$$

The optimum elements which satisfy the structural constraint expressed by equation(41) must be reinforced to accommodate the reaction moments distributed around the base. The degree of reinforcement was determined by requiring that the maximum stress in the modified elements be no greater than the maximum stress in the optimum element.

The reinforcement design is completed by specifying the number of elements to be modified. It was necessary, then, to investigate the nature of the bending solutions in the neighborhood of the base. It has been shown<sup>[4]</sup> that the bending moment equations can be expressed in the form

$$(50) \quad M_{\phi} = \frac{R}{2\beta} e^{-\beta a} [(A_1 + A_2) \cos \beta a - (A_1 - A_2) \sin \beta a]$$

$$(51) \quad M_{\theta} = \mu M_{\phi}$$

where

$$(52) \quad \beta^4 = 3(1 - \mu^2) \frac{R^2}{t_S} .$$

The exponential term in the moment equation causes the rapid decay of the moment at the radome base as the angle  $\alpha$  (see Figure 2) increases, and by evaluating the rate of decay the number of panel tiers requiring reinforced elements was determined.

This completes the description of the structural analysis which provides the equations and techniques to evaluate, (1) a structural constraint for the majority of elements distal to the radome base, (2) a procedure to calculate the reinforcement required by the elements proximal to the radome base, and (3) the member of elements requiring reinforcement.

#### OPTIMUM DESIGN CRITERION

The concept of optimum design implies a methodological assignment of system parameters such that the system performance is maximized relative to a defined criterion. There are several possible criteria which could be applied to radome design. Two criteria were selected for consideration in this study and are (1) minimization of the radome transmission loss subject to a holonomic structural constraint, and (2) the reduction of the total element weight subject to an electrical constraint which fixes a minimum transmission loss and a structural constraint insuring radome stability and strength.

A description of the optimization procedures initially requires a definition of a single structural constraint based on the equations developed in the

structural analysis. The structural constraint utilized was the most severe design condition imposed on the element sizing by either the general or local buckling equations expressed by equations (15) and (41). A comparison of the two design equations was made by graphing the maximum allowable wind velocity permitted by each equation (see Figures 4, 5, and 6). The equation which permits the least wind velocity for a particular set structural and environmental conditions becomes the constraint and is written in the form

$$(53) \quad F(L, w, d) = 0 .$$

The equation for the transmission loss is also a function of the element dimensions and is written as

$$(54) \quad G = G(L, w, d).$$

The procedure for obtaining the element dimensions which will result in an extremum for the transmission loss (G) subject to the constraint (F) involves the application of the method of Lagrangian Multipliers [11] and is outlined below.

The total differential of the transmission loss is written and set equal to zero:

$$(55) \quad dG = \frac{\partial G}{\partial L} dL + \frac{\partial G}{\partial w} dw + \frac{\partial G}{\partial d} dd = 0 .$$

LOCAL BUCKLING DESIGN CONSTRAINT  
ON ALUMINUM ELEMENTS OF  
150 FT. DIA. RADOME

$$(1.316 + 0.0832d) L^3 \times 10^{-5} = wd^3$$

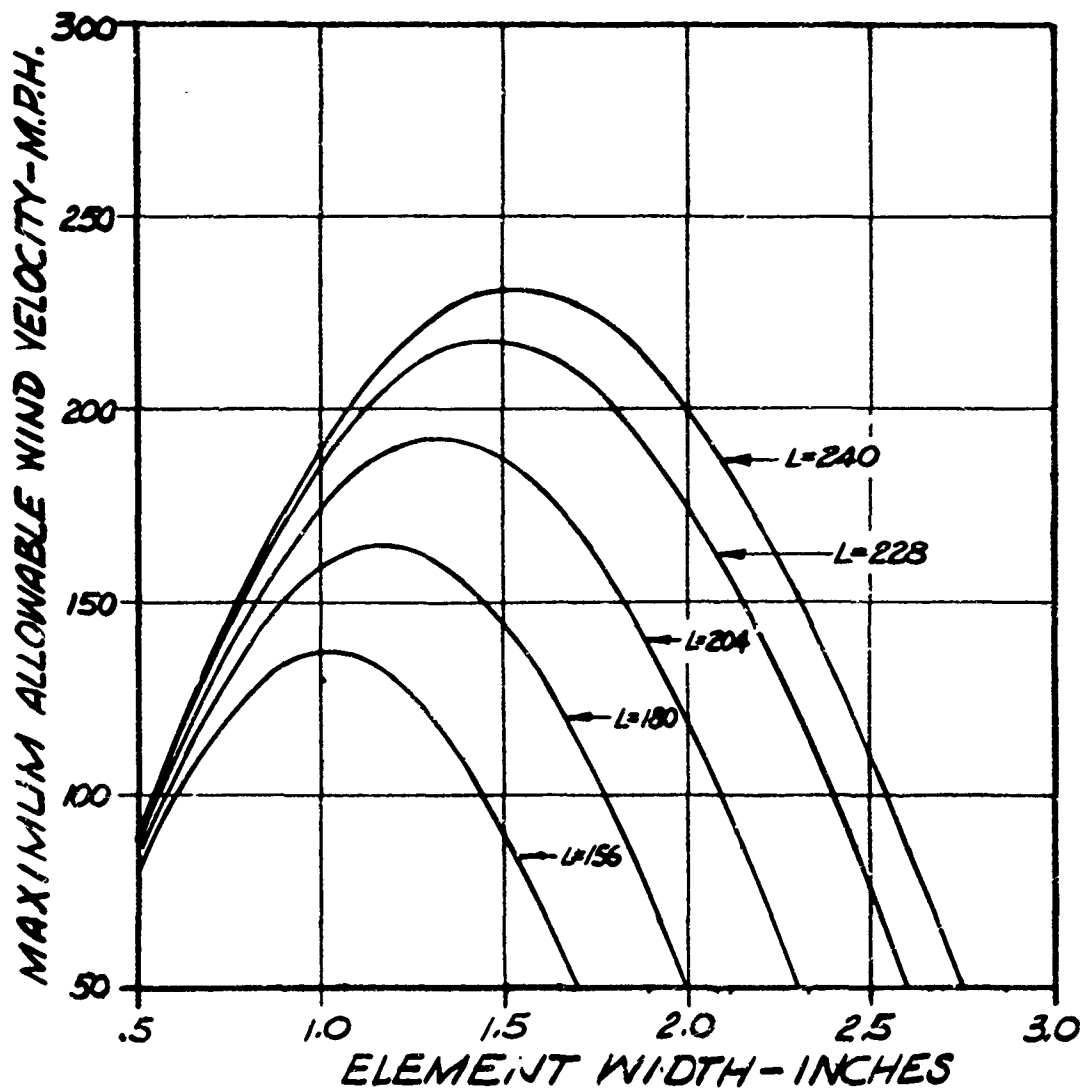


FIG. 4

GENERAL BUCKLING DESIGN CONSTRAINT  
ON ALUMINUM ELEMENTS OF  
150 FT. DIA. RADOME

$$P_{cr} = 4.64 \frac{wd^2}{L}$$

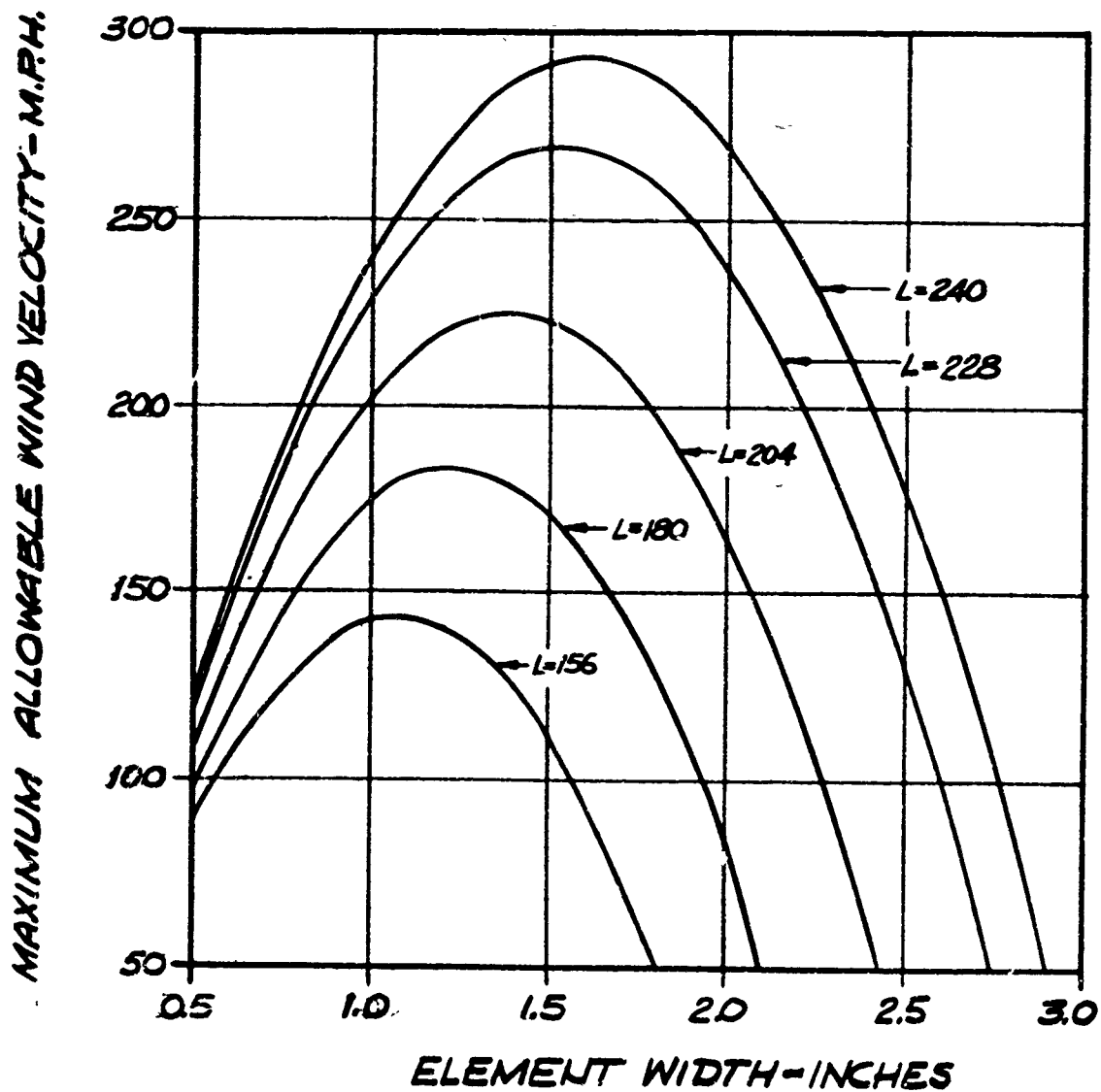


FIG. 5

COMPARISON OF GENERAL AND LOCAL  
BUCKLING DESIGN CONSTRAINTS  
ON ALUMINUM ELEMENTS OF  
150 FT DIA. RADOME

GENERAL BUCKLING -----  
LOCAL BUCKLING \_\_\_\_\_

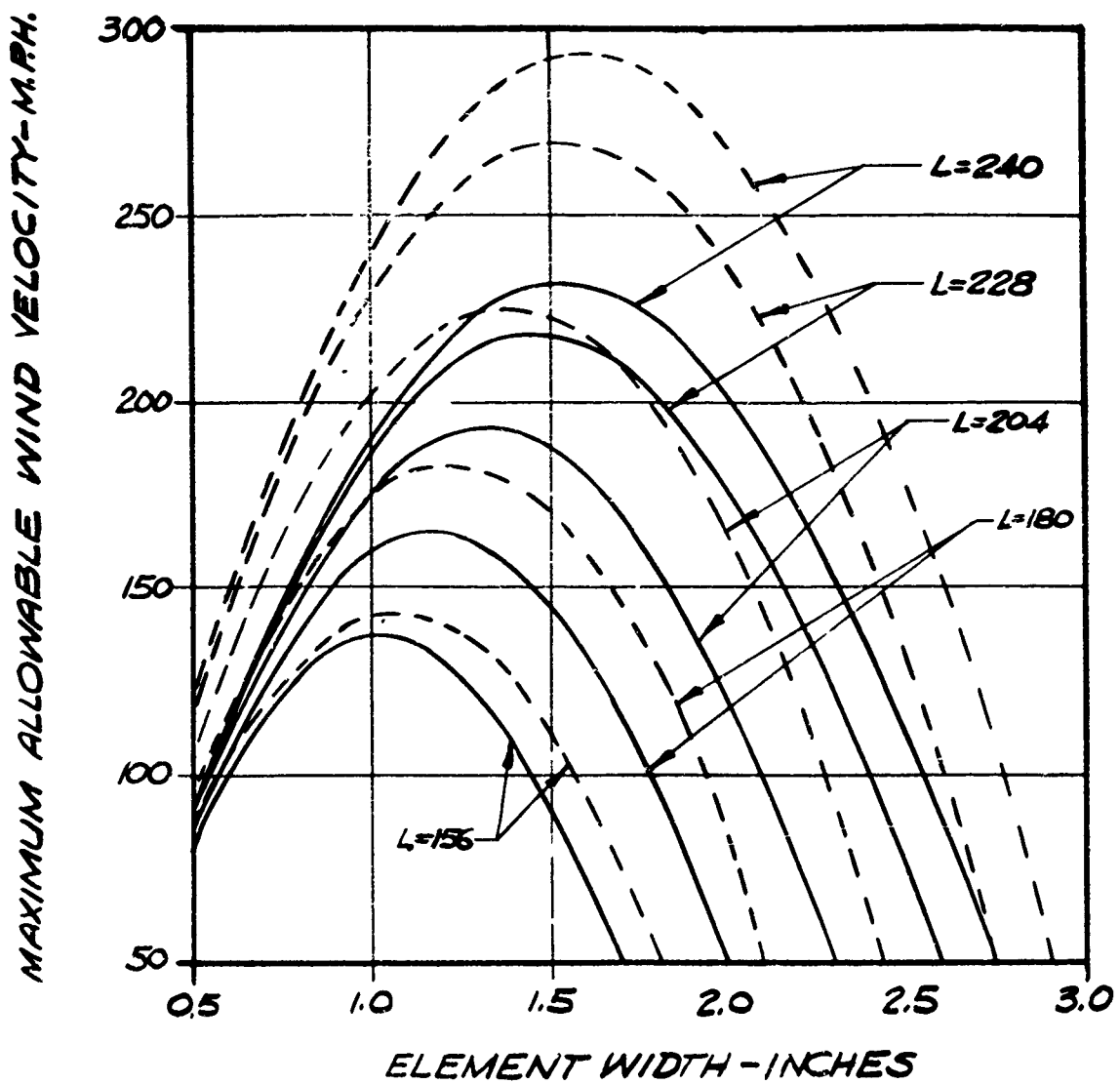


Fig. 6

The total differential of the structural constraint is written

$$(56) \quad dF = \frac{\partial F}{\partial L} dL + \frac{\partial F}{\partial w} dw + \frac{\partial F}{\partial d} dd = 0 .$$

The differentials of L, w, and d can not all be independent. Arbitrarily specifying the differentials of L and w as independent the remaining differential (dd) is solved for from equation (56) by setting

$$(57) \quad dd = - \frac{\left( \frac{\partial F}{\partial L} dL + \frac{\partial F}{\partial w} dw \right)}{\frac{\partial F}{\partial d}}$$

provided  $\partial F / \partial d$  is not equal to zero. By substituting equation (57) into equation (55) the dependent differential is eliminated and the resulting equation is

$$(58) \quad \frac{\partial G}{\partial L} dL + \frac{\partial G}{\partial w} dw - \lambda \left( \frac{\partial F}{\partial L} dL + \frac{\partial F}{\partial w} dw \right) = 0$$

where for brevity  $\partial G / \partial d / (\partial F / \partial d)$  is defined as  $\lambda$ . Equation (58) can be written by collecting like terms as

$$(59) \quad \left( \frac{\partial G}{\partial L} - \lambda \frac{\partial F}{\partial L} \right) dL + \left( \frac{\partial G}{\partial w} - \lambda \frac{\partial F}{\partial w} \right) dw = 0 .$$

Since the differentials of L and w were defined as independent, the coefficients must vanish in order to satisfy equation (59). In this manner a system

of four independent equations in four unknowns ( $L, w, d, \lambda$ ) are obtained, the simultaneous solution of which will yield the element dimensions that cause the transmission loss to be an extremum. The transmission loss must be evaluated for each unique set of element dimensions to determine if a minimum exists. The system of equations to be solved is

$$(60) \quad \frac{\partial G}{\partial L} - \lambda \frac{\partial F}{\partial L} = 0$$

$$(61) \quad \frac{\partial G}{\partial w} - \lambda \frac{\partial F}{\partial w} = 0$$

$$(62) \quad \frac{\partial G}{\partial d} - \lambda \frac{\partial F}{\partial d} = 0$$

$$(63) \quad F(L, w, d) = 0 .$$

A direct extension of this procedure would consist of imposing an additional constraint on the method of Lagrangian Multipliers. The additional constraint would conceivably be placed on the maximum weight of the space frame. In such a case five independent equations in five unknowns, the three element dimensions and two Lagrangian Multipliers  $\lambda_1$  and  $\lambda_2$ , would be solved

simultaneously. A complete description of the method of Lagrangian Multipliers can be found in ref [11] or most any text on advanced calculus.

An alternative optimization procedure based on the reduction of the structural weight subject to an electrical and structural constraint was developed and is essentially graphical in complexion. The method description is first precluded by the formulation of the required equations. The structural constraint will be the severest design condition imposed by either the general or local buckling equations. The electrical constraint is established by substituting a value for the minimum allowable transmission loss into the gain equation,  $G = G(L, w, d)$ . The electrical constraint equation is plotted in Figure 7 for constant lengths and a maximum transmission loss of 0.5db. The remaining equation to derive is the expression for the total element weight in terms of element dimensions. This equation was written by taking the product of the total volume and the weight density of the structural elements. The total volume is equal to the element cross sectional area times the collective length of the elements. The weight equation was, then, expressed as:

$$(64) \quad W = \rho w d \sum_i^N L_i$$

where the summation of element lengths has been shown to be equal to

**AVERAGE LENGTH OF ELEMENT  
DUE TO ELECTRICAL CONSTRAINT  
FOR TRANSMISSION LOSS (0.5db)**

$$L = 79W + 7d + 18 \frac{d}{W}$$

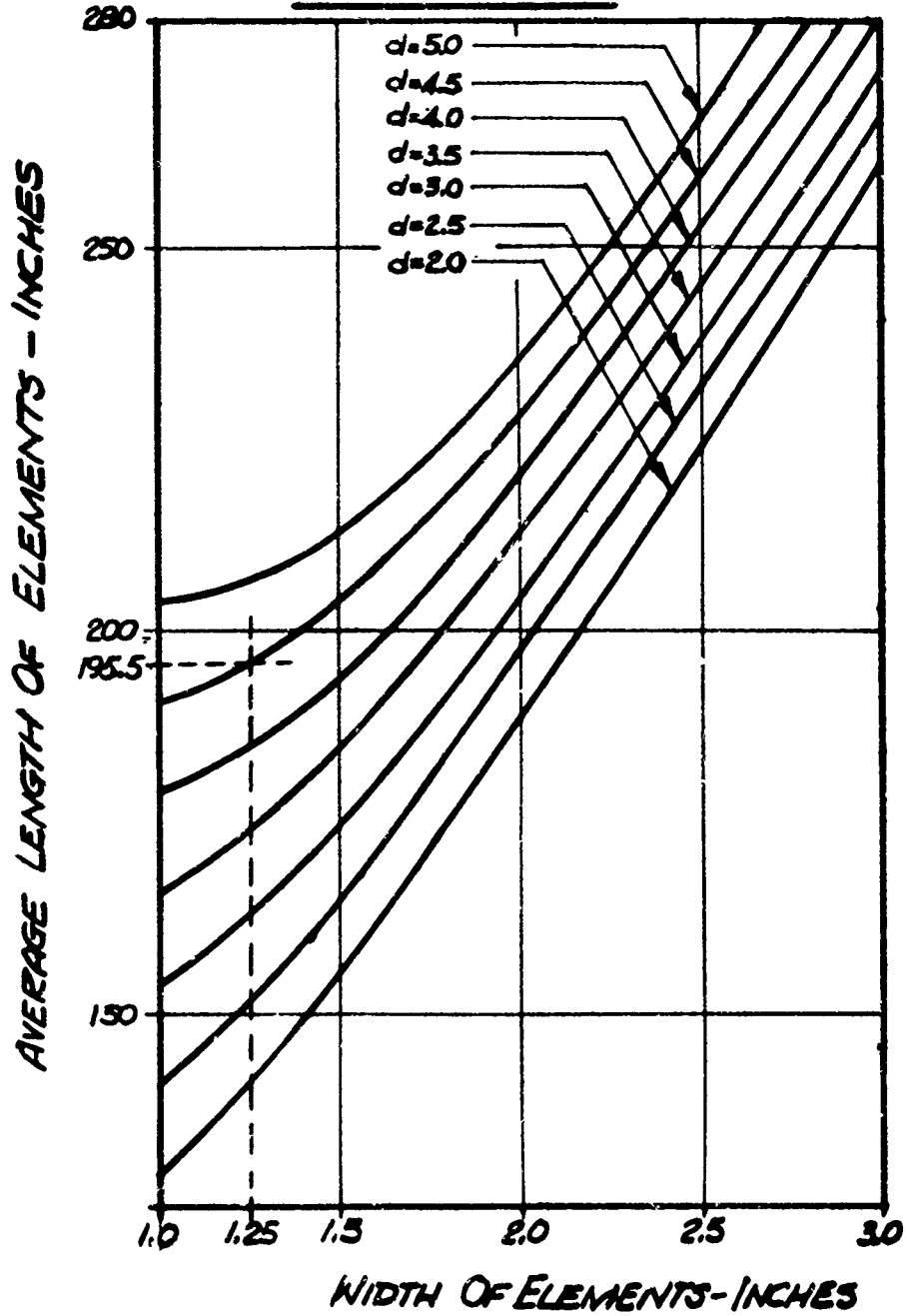


**FIG. 7**

$$(10) \quad NL = \frac{24\pi R^2 k}{\sqrt{3L}} .$$

Substituting equation (10) into equation (65) gives

$$(65) \quad W = 13.85\pi R^2 k \rho \frac{wd}{L} .$$

A graphical examination of the three equations, electrical and structural constraints and the structural weight, provides, perhaps a less direct approach to the optimum selection of element dimensions. However, the necessary solution of a system of equations, which may be tedious and cumbersome, is avoided.

The objective of the graphical approach was to generate a set of curves which display the behavior of the weight and constraint equations for a practical range of element dimensions and arrive at a design decision by graphical examination. The curves generated for the example design were: (1) the maximum wind velocity permitted by the local buckling equation, (2) the maximum wind velocity permitted by the general buckling equation, (3) a comparison of local and general buckling, (4) the electrical constraint equation for constant lengths, (5) the weight of aluminum elements for a range of widths which satisfy both an electrical and structural constraint, (6) the weight of aluminum elements for a range of lengths which satisfy both an electrical and structural constraint, (7) the exponential decay function for the bending moments due to the radome boundary conditions.

## SAMPLE RADOME DESIGN

An example design of a 150 foot diameter space frame radome was performed to provide an illustration and detailed description of the optimization design procedures. The design calculations were based on the following radome and environmental specifications:

1. Radome diameter - 150 feet.
2. Structural description - triangulated space frame of regular (snub-dodecahedral) or random (icosahedral) geometry.
3. Truncation base diameter - 130 feet.
4. Structural material - 6061 T6 aluminum.
5. Maximum wind velocity - 150 mph sustained.
6. RF band - 200-500 mc.
7. Maximum transmission loss - 0.50db.

The general radome design equations developed in the preceding sections are:

1. Transmission loss - gain equation

$$G = \frac{79w^2 + 7wd + 18d}{2Lw}$$

2. General buckling, Tsien-VonHarman equation

$$P_{cr} = \frac{3KE\mu(1-\cos \phi_b)}{2\sqrt{3}\mu R^2} \frac{wd^2}{L}$$

3. Local buckling criterion

$$\frac{\sqrt{3}P_0 L^3}{16\sigma_{yp} wd^2} + \frac{2\sqrt{3}(P_0 R - \sqrt{\mu} \rho_s Rd)L^3}{\pi^2 E(1-\cos \phi_b)wd^3} \leq 1$$

4. Total weight of elements

$$W = 13.85\pi R^2 k \rho \frac{wd}{L}$$

These equations become specific design formulas upon substitution of the appropriate parameters which are:

1.  $E_R = 10^7$  psi
2.  $K = 0.50$
3.  $k = 0.75$
4.  $\phi_b = 120^\circ$
5.  $R = 900$  inches
6.  $\sigma_{yp} = 40,000$  psi
7.  $\rho = 0.098$  pcf
8.  $Q = 0.004$  pcf
9.  $P_0 = 0.3125$  psi
10.  $G = .5$ db

The design formulae are equal to

$$(66) \quad Lw = 79w^2 + 7wd + 18d$$

$$(67) \quad P_{cr} = 4.64 \frac{wd^2}{L}$$

$$(68) \quad (1.316 + 0.0832d)L^3 \times 10^{-5} = wd^3$$

$$(69) \quad W = 2643 \frac{wd}{L} \quad (\text{kips})$$

The sample design description includes the method of Lagrangian Multipliers to minimize the transmission loss subject to one constraint and a graphical method to reduce the total weight of elements subject to an electrical and structural constraint.

In both illustrations it is necessary to eliminate one of the structural design formulae by determining which dictates the most severe restriction on the element dimensions. Figures 4 and 5 are plots of equations(67) and (68). Figure 6 is a comparative plot of equations (67) and (68) and displays the fact that for all element widths and lengths over one inch and 14 feet, respectively, the local buckling design restriction is most severe. Since a width of one inch

or less is impractical for the size radome considered in the example design, the local buckling equation was selected as the structural constraint.

The method of minimizing the transmission loss subject to a single constraint was previously outlined where equations (53) and (54) take on the form:

$$(53) \quad F = (1.316 + 0.0832d)L^3 \times 10^{-5} - wd^3 = 0$$

$$(54) \quad G = \frac{79w^2 + 7dw + 18d}{2Lw}$$

The system of equations to be solved for the element dimensions which minimize the transmission loss are obtained by performing the appropriate differentiation. The equations in terms of the four unknowns L, w, d, and  $\lambda$  are:

$$(55) \quad 39.5w^2 + 3.5dw + 9d + 3\lambda w [1.316 + 0.0832d] L^5 \times 10^{-5} = 0$$

$$(56) \quad 39.5w^2 - 9d + \lambda w^2 d^3 L = 0$$

$$(57) \quad 3.5w + 9 - \lambda w [0.0832L^3 - 2wd^2] L \times 10^{-5} = 0$$

$$(58) \quad [1.316 + 0.0832d] L^3 \times 10^{-5} - wd^3 = 0.$$

The method of Lagrangian Multipliers, which requires the simultaneous solution of the above equations, is a direct analytic approach to the evaluation of the element dimensions consistent with minimum transmission loss. The above system of equations was developed as an illustration of technique only, and the solution was not attempted. However, attention is directed to the degree of algebraic complication involved in obtaining a complete solution which would be increased by the addition of a second constraint. Therefore, emphasis was centered on a graphical approach which although less analytically direct, is more favorable to hand calculation and visual interpretation.

The graphical method was instrumented by the generation of a set of curves, Figures 4 through 9. The total weight versus element width curve, Figure 8, clearly defines a consequential design objective which parallels the reduction of weight, which is the minimization of width. However, it is necessary to establish a minimum width below which the advantage of suppressed structural weight is totally masked by unmanageable mechanical design difficulties. The total weight versus element length curve, Figure 9, provides a cue to the selection of a minimum element width. The weight equation is not a single valued function and displays a point of minimum element length which satisfies the electrical and structural constraints. The element width which corresponds to the minimum element length is of a practical magnitude and is defined as the goal for the ensuing mechanical design. Therefore, the requirements for structural integrity during sustained 150 mph winds, minimum transmission loss of

WEIGHT OF ALUMINUM ELEMENTS OF 150 FT. DIA. RADOME WHICH DIMENSIONALLY SATISFY THE ELECTRICAL CONSTRAINT (0.5 db LOSS) AND THE STRUCTURAL CONSTRAINT (150 M.P.H. WIND)

$$W_T = 2643 wd/L$$

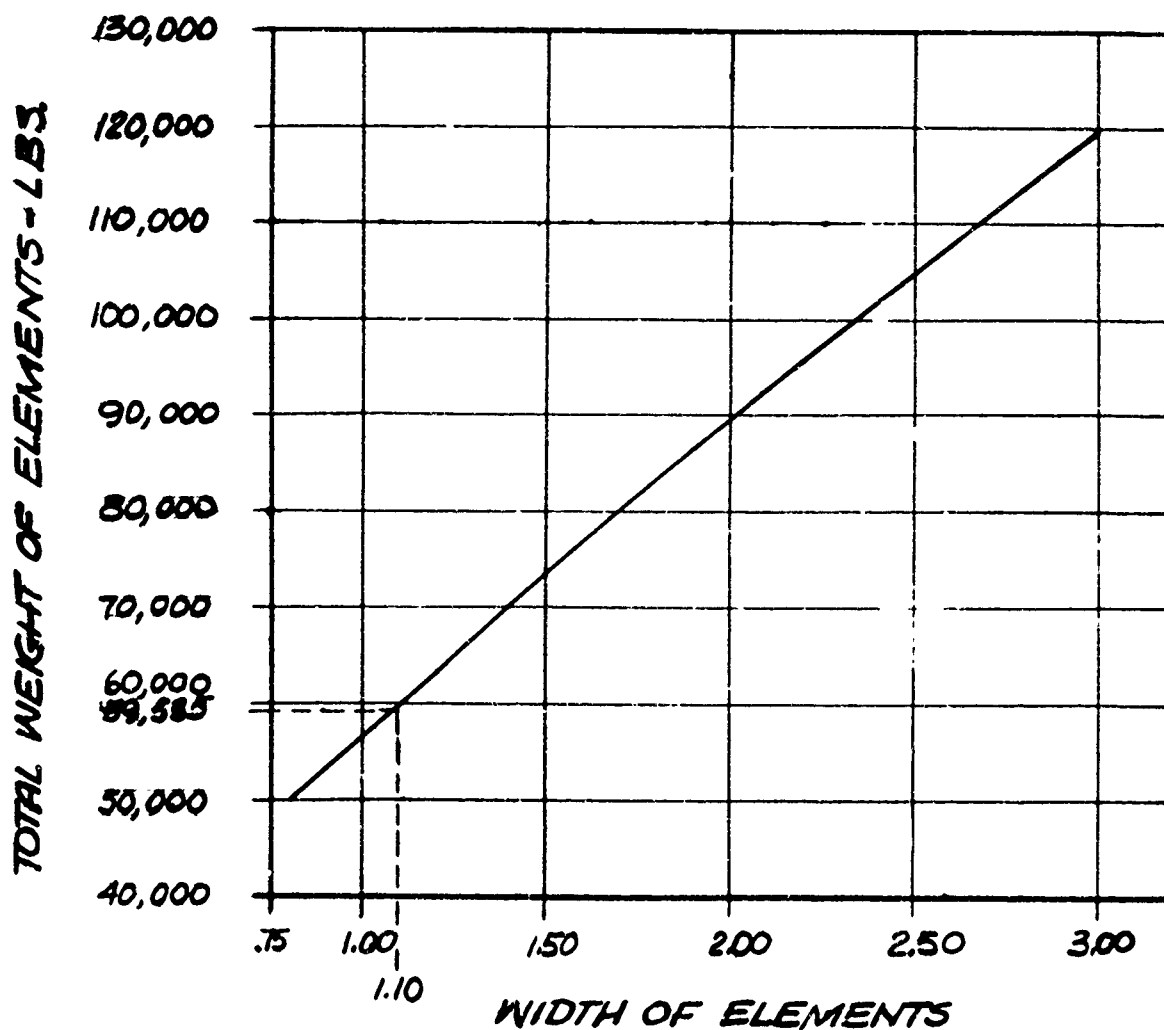


FIG. 8

WEIGHT OF ALUMINUM ELEMENTS OF 150 FT. DIA.  
 RADOME WHICH DIMENSIONALLY SATISFY THE  
 ELECTRICAL CONSTRAINT (0.5 db LOSS) AND  
 THE STRUCTURAL CONSTRAINT (150 M.P.H. WIND).

$$\underline{W_T = 2643 \omega d/L}$$

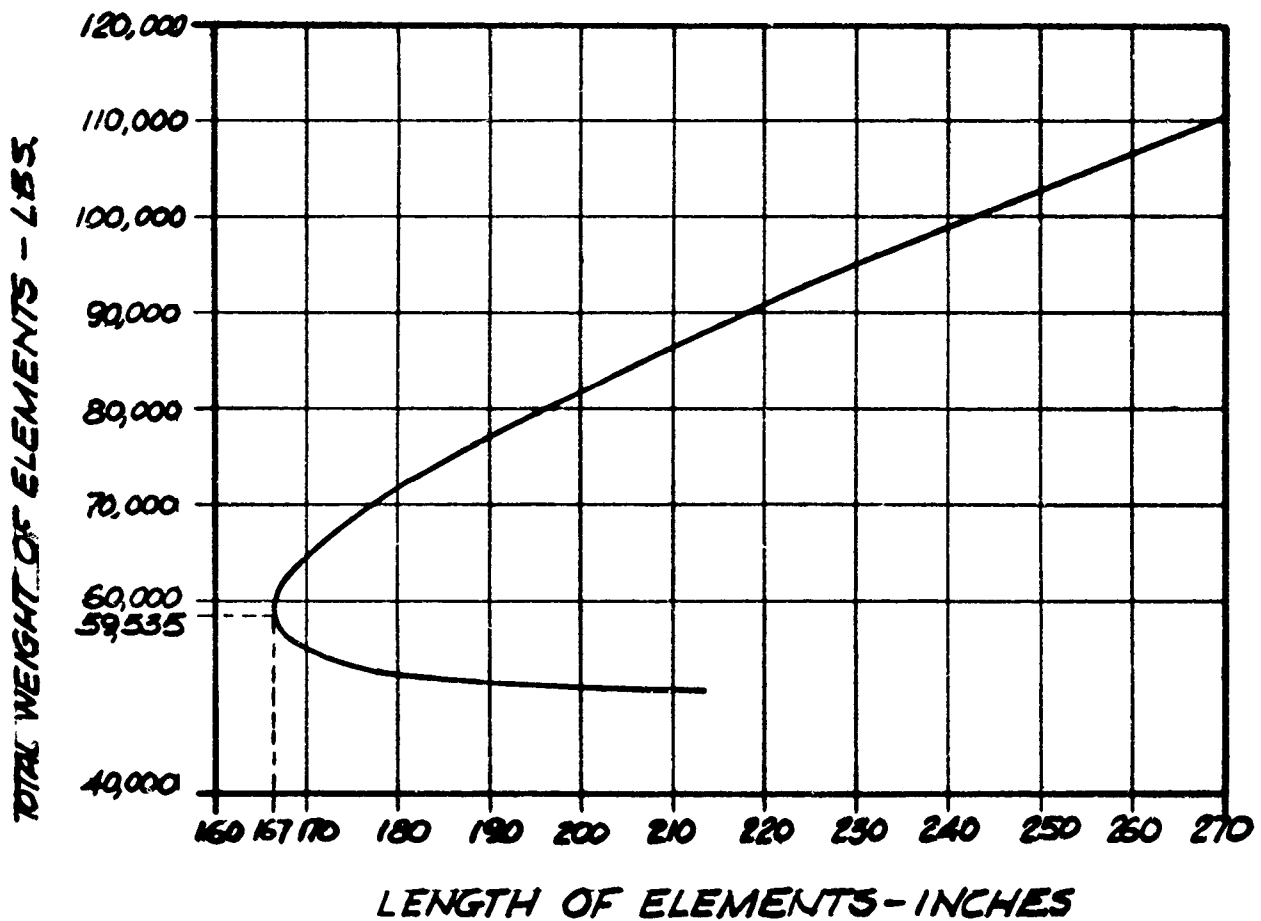


FIG. 9

0.50db, minimum element length, and minimum total weight of elements within practical limitations are satisfied for a structural element of the following dimensions:

$$w = 1.10 \text{ inch}$$

$$d = 3.42 \text{ inches}$$

$$L = 167 \text{ inches}$$

The remaining design consideration concerns the reinforcement of the standard element. The reinforcement calculation involved the evaluation of the shell displacement and derivatives at the radome base and substitution into the bending moment equations (48) and (49) which gives for the resultant moment at the base:

$$(70) \quad M_{\phi_0} = \frac{P_0 R d}{4 \sqrt{\frac{3(1+\mu)}{\mu(1-\mu)}}}$$

The bending moment applied to the elements at the base are then equal to the resulting moment  $M_{\phi_0}$  times the effective spacing (s).

$$(71) \quad M_{\phi_0} s = 15.95dL.$$

The standard element was modified such that the maximum flexure stress of the reinforced elements was maintained equal to the maximum flexure stress of the standard element. This requirement was formulated by equating

the flexure stress of the two elements, one of standard cross section and the other of modified cross section.

$$(72) \quad \frac{\sqrt{3} P_0 L^3}{16wd^2} = \frac{\sqrt{3} P_0 L^3}{16(w+\Delta w)(d+\Delta d)^2} + \frac{6M_b s}{(w+\Delta w)(d+\Delta d)^2} .$$

Equation (72) was solved explicitly for the incremental width  $\Delta w$  and equals

$$(73) \quad \Delta w = \frac{wd^2}{(d+\Delta d)^2} + \frac{(1530 + 90d)wd^3}{\sqrt{3} P_0 L^2 (d+\Delta d)^2} - w .$$

The most convenient manner to reinforce the element is to maintain a fixed element depth and increase only the width. By fixing the element depth for the entire space frame the requirement for special transition hubs or adapters is avoided. The reinforcement equation is simplified by letting  $\Delta d$  vanish and reduces to:

$$(74) \quad \Delta w = (2830 + 167d) \frac{wd}{L^2} .$$

The requirement in element width for the sample design equals 0.459 inch and the reinforced element dimensions become

$$w = 1.559 \text{ inch}$$

$$d = 3.42 \text{ inch}$$

$$L = 167.0 \text{ inches}$$

The number of elements requiring reinforcement was determined by examining the rate at which the bending moment at the radome base damps out at points away from the base. The percent reduction in the moment was plotted as a function of meridian angle ( $\alpha$ ) receding from the base as dictated by the exponential term of equation (50). Figure 10 shows that for the sample design the moments are reduced by 98% at an angular displacement of  $10^\circ$  from the base. An equation for the number of reinforced elements was derived in the following manner:

Let  $A_r$  be the total area of the radome composed of reinforced elements. Then  $A_r$  is equal to:

$$(75) \quad A_r = 2\pi R^2 a \sin\left(\phi_b - \frac{a}{2}\right).$$

The number of reinforced panels ( $M_r$ ) equals the area divided by the unit panel area and equals

$$(76) \quad M_r = \frac{8\pi R^2 a \sin\left(\phi_0 - \frac{a}{2}\right)}{\sqrt{3} L^2}$$

and the number of elements corresponding to  $M_r$  panels is

$$(77) \quad N_r = \frac{3}{2} M_r$$

PERCENT REDUCTION OF SHELL BENDING  
MOMENTS DUE TO RADOME BOUNDARY  
CONDITIONS IN REGRESSION FROM THE BASE.

$$\underline{M\phi = M\phi_0 e^{-\beta x}}$$

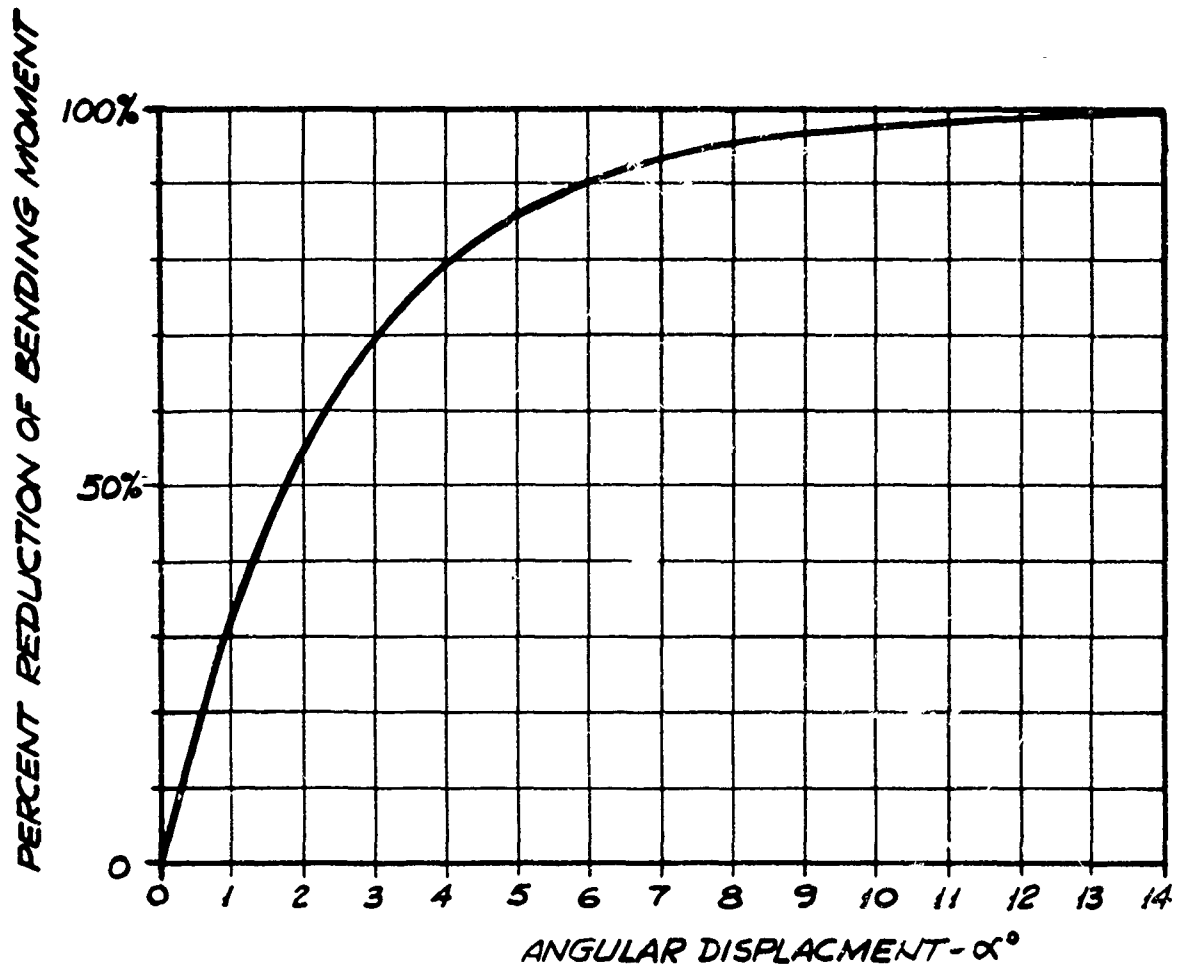


FIG. 10

or

$$(78) \quad N_r = \frac{12\pi R^2 a \sin(\phi_b - \frac{a}{2})}{\sqrt{3} L^2}$$

The value of  $N_r$  for the sample design and a 98% reduction of shell induced bending becomes 66 elements. The total number of elements of both cross sections is determined by substituting the element length into equation (11), which gives

$$N = 977.$$

The complete specification of the elements of the sample design is

1. Standard Element

Number - 911  
Width - 1.10 inches  
Depth - 3.42 inches  
Length - 167.0 inches  
Weight - 55,400 lbs

2. Reinforced Elements

Number - 66  
Width - 1.48 inches  
Depth - 3.42 inches  
Length - 167.0 inches  
Weight - 5,594 lbs

## MECHANICAL DESIGN OBJECTIVES

There are numerous mechanical design deficiencies existing in many of the large radomes which have been built in the recent past. This fact was made apparent during consultation with the personnel of several prominent manufacturers of large space frame radomes as well as by the inspection of the Haystack Installation. The most blatant deficiency seems to be in the area of dielectric panel to element attachment. A result of manufacturing panels of reinforced plastics within reasonable tolerances seems to be a condition of relative slack in the individual panels' membranes after assembly. Such a condition allows considerable furling of the panels due to wind pressure fluctuation. Fatigue failures of the panels frequently occur at the panel vertices which require undue and excessive maintenance. A possible solution or suppression of this type problem would be effected if an attachment design was generated which produced a pretension in the panel during installation. Such a design objective is complicated by the optimum design conclusion that minimum element width is desirable. A design concept is depicted in Figure 11 which has the merit of simplicity and warrants development consideration. The extruded V-slot in the edge of the element would cam the reinforced panel taut during depression of the panel into the slot by the cover plate. The camming action would induce a prestress on the panel dependent on the pitch of the slot and depth of depression.

A second deficiency seems to exist in obtaining and maintaining adequate weather seals. The panel to element seal could be significantly improved if and when prestressed panels become reality due to the increased bearing pressure and area of contact at the seal. The panel to hub seal is generally the most difficult to obtain. By providing a panel-hub engagement slot in the hub a forced and continuous attachment of the panel to the element and hub is possible. Therefore, direct contact of a hub cover plate and the panel would allow for generous surface for a continuous weather seal. Figure 12 schematically illustrates such a panel-element-hub attachment scheme.

The preceding recommendations are intended only as conceptual proposals which could be evaluated for design feasibility and refinement. A multitude of design improvements in the mechanical design of radomes all of which require considerable analysis. Some of the areas for improvement include erection procedures, reduction of manufacturing tolerances to a minimum for mating radome components, elimination of superfluous assembly hardware, and the aforementioned panel pretension and weather seals each of which requires individual and special attention.

PANEL-ELEMENT ATTACHMENT

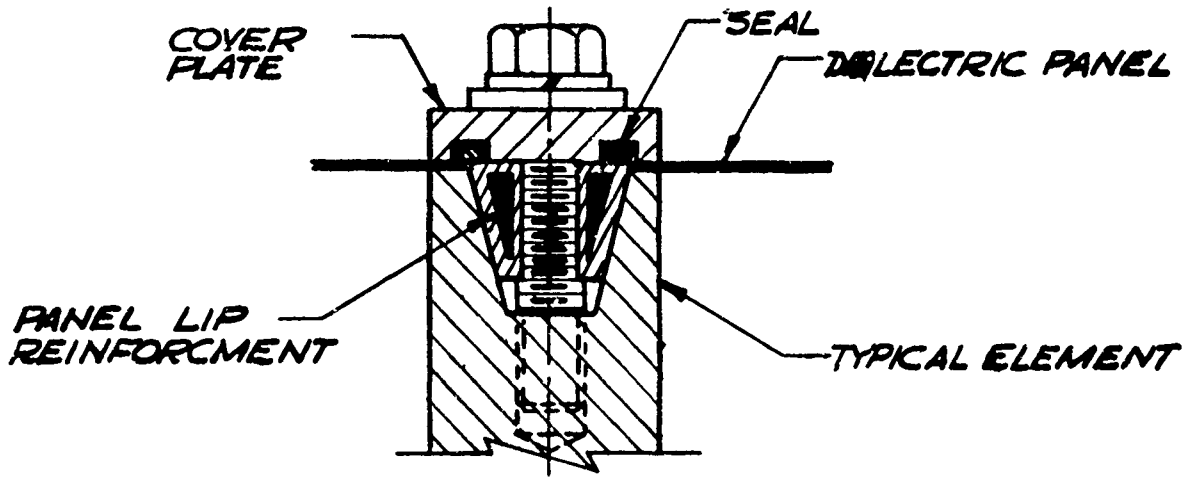


FIG. 11

PANEL-ELEMENT-HUB ATTACHMENT

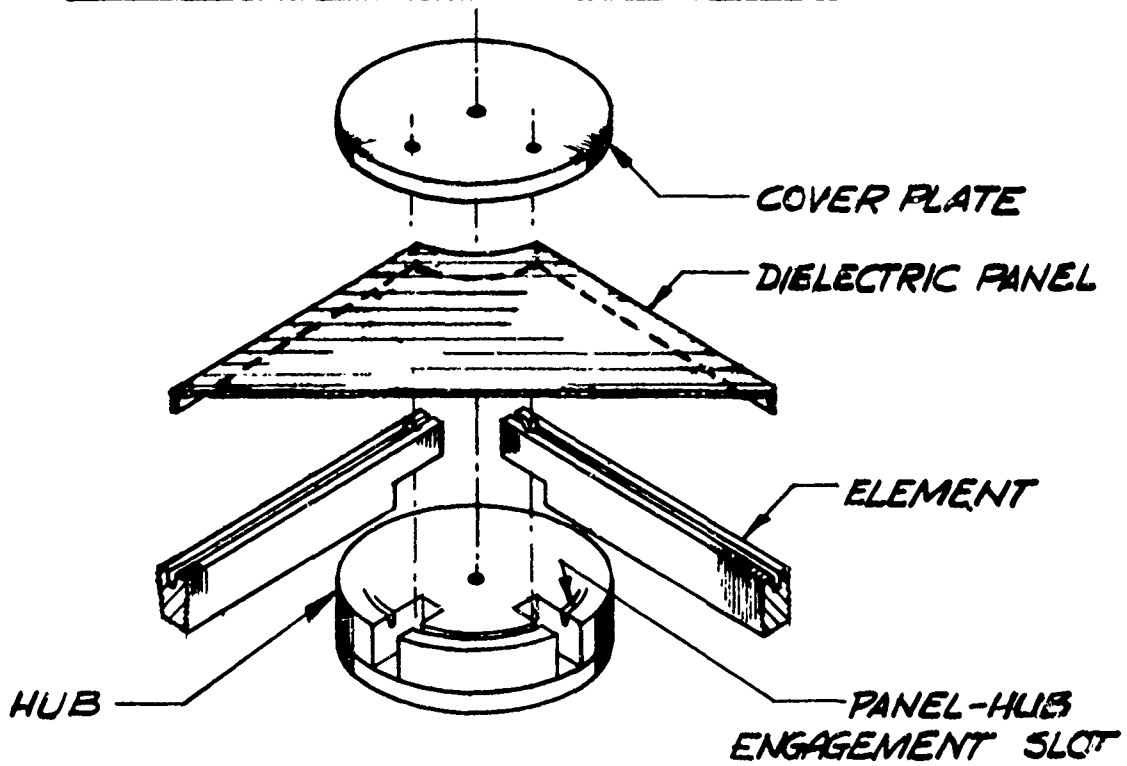


FIG. 12

## PART I

### REFERENCES

1. A. F. Kay, "Electrical Design of Metal Space Frame Radomes," TRG, Inc. August 20, 1963. Revised version March 23, 1964 accepted for publication by the TRANS of IEEE in November 1964 or January 1965 issue.
2. P. D. Kennedy, "An Analysis of the Electrical Characteristics of Structurally Supported Radomes," OSU Report on Contract AF30(602)-1620, dated November 15, 1958.
3. K. Mei and J. Van Bladel, "Low Frequency Scattering by Rectangular Cylinder," PGAP, January 1963, pp. 52-56.
4. M. G. Andreasen and A. F. Kay, "Scattering by Conducting Rectangular Cylinders," FR-220-2, November 9, 1962, BTL Contract DA-30-069-ORD-1955, P. O. D-605006. Paper submitted to PGAP, approved for publication in January 1964 issue.
5. A. F. Kay, "Application of Fresnel Zone Theory to Microwave Antenna Design," SR-3, November 15, 1962, AFCRL Contract AF19(604)-8057.

## PART II

### REFERENCES

1. H. S. Tsien, "A Theory of the Buckling of Thin Shells," *Journal of the Aeronautical Sciences*, Vol. 9, No. 10, August 1942.
2. T. VonKarman, and H. S. Tsien, "The Buckling of Spherical Shells by External Pressure," *Journal of the Aeronautical Sciences*, Vol. 7, No. 2, December 1939.
3. Timoshenko, "Theory of Plates and Shells," McGraw-Hill Book Company, Inc., New York, 1959.
4. W. Flügge, "Stresses in Shells," Springer-Verlag, Berlin/Göttingen/Heidelberg, 1962.
5. R. Curtis and Vaccaro, "Survey of Ground Radomes," RADC TR-61-52, May 1961, AD 258776.
6. R. Curtis, "Guide to the Structural Design of Truncated Spherical Rigid Ground Radomes," RADC TR-61-84, June 1961.
7. A. F. Foerster, "Stress Distribution and Stability Criteria of Spherical Ground Radomes Subjected to Wind Loads," *Proc of the OSU-WADC Radome Symposium*, WADC TR-58-272, Vol. 1, June 1958.
8. R. A. Muldoon, "Dynamic Buckling of Space Frame Radome Models," Lincoln Laboratory, MIT, February 1962.
9. "Ground Radome Study," Philco Corporation, Western Development Laboratories, WDL-TR-1936, December 1962.
10. H. D. Hauf and H. A. Pfisterer, "Design of Steel Structures," John Wiley and Sons, Inc., New York, 1956.
11. P. Franklin, "Methods of Advanced Calculus," McGraw-Hill Book Co. Inc., New York, 1944.

## APPENDIX

### DERIVATION OF EXPECTED SIDE LOBE LEVEL DUE TO RADOME

From equation (24) of [1] we may write the far field pattern in the presence of a space frame as

$$(A1) \quad F(u) = \int_0^{2\pi} d\eta \int_0^a r dr (1 + g_{av} \rho(r, \eta)) f(r, \eta) e^{j u r \cos \eta}$$

where  $f(r, \eta)$  is the antenna aperture illumination,  $\rho(r, \eta)$  is the blocking area ratio considered as a function of the polar coordinates  $r, \eta$  (see p. 12 of [1]) and  $u = k \sin \theta$  where  $\theta$  is the pattern observation angle. We shall now find the expected value of the power pattern  $|F(u)|^2$  under the assumption that  $\rho(r, \eta)$  is one of a large set of functions denumerated by a variable  $\alpha$  of known statistics approximating those of typical space frames. Hence we write  $\rho(r, \eta)$  as  $\rho(r, \eta, \alpha)$ . The average value of  $\rho(r, \eta, \alpha)$  is the average blocking area ratio  $\rho$  so that

$$(A2) \quad \int \rho(r, \eta, \alpha) d\alpha = \rho, \quad \text{where} \quad \int d\alpha = 1$$

and the integrals are over all admissible  $\alpha$ , normalized according to (A2).

We may then write the expected value of the power pattern from (A1) as

$$\int |F(u)|^2 da = |1 + g_{av}\rho|^2 |F_0(u)|^2$$

(A3)

$$+ |g_{av}|^2 \int_0^a p dp \int_0^{2\pi} d\eta \int_0^a r dr \int_0^{2\pi} d\phi I f(r, \eta) \overline{f(p, \phi)} e^{ju(r \cos \eta - p \cos \phi)}$$

where  $F_0(u)$  is the unperturbed pattern and the inner integral

$$(A4) \quad I = \int da \rho(r, \eta, a) \rho(p, \phi, a)$$

may be computed for any given space frame statistics. On the basis of some detailed computations a good approximation is believed to be Gaussian with the scale length, the width of the element. It is quite obvious that two points more than  $W$  apart are not highly correlated.

$$(A5) \quad I \simeq (\rho - \rho^2) e^{-|\bar{r} - \bar{p}|^2 / W^2} + \rho^2 \simeq \rho e^{-|\bar{r} - \bar{p}| / W^2}$$

where  $|\bar{r} - \bar{p}|^2 = r^2 + p^2 - 2rp \cos(\phi - \eta)$ .

If we make the further reasonable assumption that in the neighborhood of appreciable correlation,  $|\bar{r} - \bar{p}| < \sim W$ ,  $f(r, \eta)$  is virtually constant, we may explicitly integrate the last term in (A3) to obtain

$$(A6) \quad \int |F(u)|^2 da = |1 + g_{av}\rho|^2 |F_0(u)|^2 + \pi\rho W^2 |g_{av}|^2 e^{-(uW/2)^2}$$

$$\int_0^{2\pi} d\phi \int_0^a r f^2(r, \phi) dr.$$

The increase of pattern in the neighborhood of the first few side lobes, where

$$(A7) \quad e^{-(uW/2)^2} \simeq 1,$$

relative to the peak is given then by

$$(A8) \quad \frac{\pi\rho W^2 |g_{av}|^2 \int_0^{2\pi} d\phi \int_0^a r f^2(r, \phi) dr}{\left| \int_0^{2\pi} d\phi \int_0^a r f(r, \phi) dr \right|^2}$$

The expression (28) in the text is an approximation to (A8) using (2) and typical values of  $f(r, \phi)$ .

## DERIVATION OF EQUATION (1) Part 1

The far field  $F_0$  of an aperture antenna may be written as the Fourier transform of its aperture illumination  $f(r, \eta)$ :

$$(A9) \quad F_0 = F_0(\bar{\theta}) = \iint_{A_0} f(r, \eta) e^{jkr \cdot \bar{\theta}} r \, dr \, d\eta$$

when  $\bar{\theta}$  is a unit vector in the direction of observation,  $\bar{r}$  is a vector from the origin to the integration point,  $k$  is the wave number, and  $r$  and  $\eta$  are polar coordinates in the aperture.

The induced field ratio IFR of a set of scatterers in the antenna beam (1) whose mutual coupling can be neglected and (2) whose dimensions projected into the antenna beam are small compared to variations in  $f(r, \eta) e^{jkr \cdot \bar{\theta}}$  and are non-overlapping, can be defined as  $g(r, \eta)$ , equal to either the IFR of the scatterer projecting to  $(r, \eta)$  or equal to zero if no scatterer projects to  $r, \eta$ . In this case the scattered far field may be written as

$$(A10) \quad F_s = F_s(\bar{\theta}) = \iint_{A_0} g(r, \eta) f(r, \eta) e^{jkr \cdot \bar{\theta}} r \, dr \, d\eta.$$

If all of the scatterers have the same IFR,  $g$ , a constant, then (A10) becomes

$$(A11) \quad F_s = \rho g \iint_{A_0} f(r, \eta) e^{jkr \cdot \bar{\theta}} r \, dr \, d\eta$$

where  $\rho$  is the ratio of the projected area occupied by the scatterers to the total area of the beam, or the blocking area ratio. From (A9) and (A11) we may write the total far field as

$$(A12) \quad \mathbf{F} = \mathbf{F}_0 + \mathbf{F}_s = (1 + \rho \mathbf{g}) \mathbf{F}_0.$$

In the forward direction (2) above is satisfied for all practical space frames and the relative power loss due to the radome is

$$(A13) \quad G = \left| \frac{\mathbf{F}}{\mathbf{F}_0} \right|^2 = |1 + \rho \mathbf{g}|^2.$$